ANALYSIS ON WIND SOLAR HYBRID SYSTEM FOR STAND –ALONE POWER GENERATION IN SRI LANKA

A dissertation submitted to the
Department of Electrical Engineering, University of Moratuwa
In partial fulfillment of the requirements for the
Degree of Master of Science

by

HETTI PATHIRANEHELAGE HEMANTHA KUMARA KARUNASEKARA

Supervised by Prof. Lanka Udawatta
Eng. W. D. Anura S. Wijayapala

Department of Electrical Engineering
University of Moratuwa, Sri Lanka

February 2011

DECLARATION

The work submitted in this dissertation is the result of my own investigation, except where otherwise stated.

It has not already been accepted for any degree, and is also not being concurrently submitted for any other degree.

H.P.H.K. Karunasekara

Date 10/02/2011

We/I endorse the declaration by the candidate.

Prof. Lanka Udawatta

Eng. W. D. Anura S. Wijayapala

CONTENTS

Abstract

The 100W wind home power generation system fabricated and installed by the NERDC at Nikavatiya in Kurunagala district is facing insufficient power generation within few months due to monsoon wind changes. The researcher was motivated to develop a hybrid wind solar power generation system to overcome this challenge. The power consumption of a rural house was evaluated and metrological data (wind speed and solar irradiance) were measured during year 2008 as part of this study. According to the metrological data, 3.92 m/s wind speed and 5.44 kWh/m^2/day solar potential could be obtained from the site annually.

The dynamic behavior and simulation results in a stand – alone hybrid power generation system of wind turbine, solar array and battery storage are presented by this analysis. This study is to review the state of the simulation, optimization and control technologies for the stand-alone hybrid solar–wind energy systems with battery storage. The hybrid system includes a 100W wind turbine, 150W solar array, 70Ah Lead -acid battery, AC/DC rectifier and DC/AC inverter.

The NACA 4415 two bladed wind rotor performance was analyzed theoretically by using blade elementary and momentum theory and the parameters of this analysis were found by using C++ program. The performance of a Fuzzy Logic Maximum Power Point Tracker (MPPT) controller (hill climbed) was applied for variable – speed, fixed –pitch NERDC small-scale wind turbines as wind speed sensor less application. More 35 % of extra energy absorb from the system by using Fuzzy Logic controller than fixed voltage method. The maximum power point tracking (MPPT) method based on perturbation & Observation (P&O) searching algorithm was applied to stand – alone solar photovoltaic system. The P&O algorithm was tested with actual irradiance data provided by simulations, using sunny day and cloudy day two sets of irradiation data. The simulation result shows the efficiency of 96.2% for P & O algorithm. The 70Ah lead – acid batteries were used in for the analysis and the same type is used for the hybrid solar–wind power generation system. Lead – Acid battery model was developed and simulated with Simulink software platform. Also laboratory testing was done according to the SLS 1126 test procedures.

MATLAB Simulink™ 7.2 / Simpower system software environment was used to simulate individual wind and PV dynamic models of hybrid system. HOMER has being used extensively to optimize the hybrid system size, sensitivity analysis with case study data in stand-alone areas in Sri Lanka. The 60 W solar PV array and NERDC 100W wind turbine with 70Ah four battery bank is proposed as hybrid power system and battery state of charge (SOC) is close to 100 % present level annually. Correct modeling of the dynamic and non linear systems is an important area of the study, but various difficulties remain in the current study. Some approaches of analysis are limited with use of commonly available simulation software.

Physical implementation of the system with power electronics remains for future research. The author suggests that solar home power system is suitable below the wind speed of 3.5 m/s , solar and wind hybrid system for the wind speed between 3.5m/s to 4.5 m/s and the wind turbine home power generation system for the wind speed above of 4.5 m/s to fulfill the rural energy requirement .

Acknowledgment

First I would like to thank Prof. Lanka Udawata and Eng. W. D. Anura S. Wijayapala for guiding me to successfully complete this research within the time frame. As search supervisors, they directed me to find all necessary literature and to do the research work to the standard.

My sincere thanks go to the officers in Post Graduate office Faculty of Engineering, University of Moratuwa, Sri Lanka for helping in various ways to clarify the things related to my academic works in time with excellent cooperation and guidance. Sincere gratitude is also extended to the people who serve in the Department of Electrical Engineering office.

I extend sincere gratitude to the National Engineering Research & Development Centre of Sri Lanka for providing me necessary founds laboratory facilities and other resources during my academic period.

Lastly, I should thank many individuals, friends and colleagues who have not been mentioned here personally in making this educational process a success. May be I could not have made it without your supports.

List of Figures

List of Tables

Chapter 1

Introduction

The energy crisis is one of the major issues in the world which is badly affected every aspect of the man's life tending. Energy is crucial for the progress of a nation and it has to be consumed in a most efficient manner. Not only the technologies should be developed to produce energy in a most environment-friendly manner from all varieties of fuels but also enough importance should be given to conserve the energy resources in the most efficient way. Energy is the ultimate factor, which is responsible for both industrial and agricultural development. It seems that conventional energy sources such as hydroelectric power, fossil fuels and nuclear power will not fulfill the demand of the future. And the fossil fuels that are depleting energy sources have being consumed rapidly and are expected to be exhausted within several decades. As results of consumption of fossil fuels, environmental pollution and global warming occurs and these pheromones affect seriously not only mankind but also all the living organism of the earth.

Hydropower is main power generation method in early Sri Lanka but identified water resources are limited for hydropower generation. Small-scale micro and Pico hydropower generation sites can be utilized as off – grid community systems. Establishment of the nuclear power plants in Sri Lanka has more issues and sufficient technologies and required lands are not available. According to the present energy scenario in Sri Lanka, 65% of electricity is generated from fossil fuel. Use of generators run on diesel the consumption of fossil fuels also has environment impacts with the release of carbon dioxide (CO_2) into the atmosphere. The cost of extension of the national grid for installation and services of distribution lines is considerably higher in remote areas. Also there will be a substantial increase in transmission line losses in addition to poor power supply reliability. In most of the remote and non-electrified sites, extension of utility grid lines experiences a number of problems such as high capital investment, high lead-time, low load factor, poor voltage regulation and frequent power supply interruptions.

The use of renewable energy technology to meet the energy demands has been steadily increasing for the past few years, however, the considerable drawbacks associated with renewable energy systems are their inability to guarantee reliability and their lean nature. There is a growing interest in harnessing renewable energy sources since they are naturally available, pollution free and inexhaustible. Special attention and hence concentrated efforts are continually provided in implementing standalone PV and wind integrated systems at sites that have a large potential of either solar, wind or both.

Gross electricity generation of Ceylon Electricity Board (CEB) from Hydro, Thermal and Renewable energy power plant Figure 1.1. And grid connected capacities of the power plants are shown in Figure 1.2.

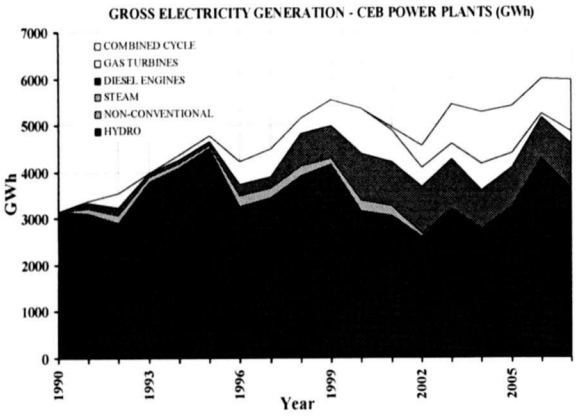

Figure 1.1: Gross Electricity Generation in Sri Lanka

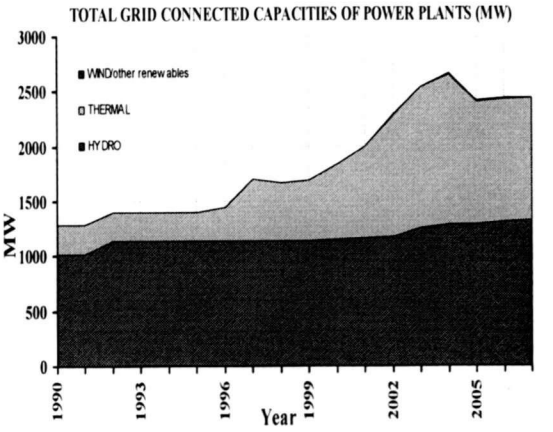

Figure 1.2: Total Grid Connected Capacities of Power Plant

Fossil fuels as thermal power generation are the easiest selection to increases the power generation for the demand of the public of the country shown in Figure 1. 3 and 38.9% of the energy for domestic purposes and 36% of the energy for industrial purposes are spent from the total power generation in Sri Lanka shown in Figure 1. 4.

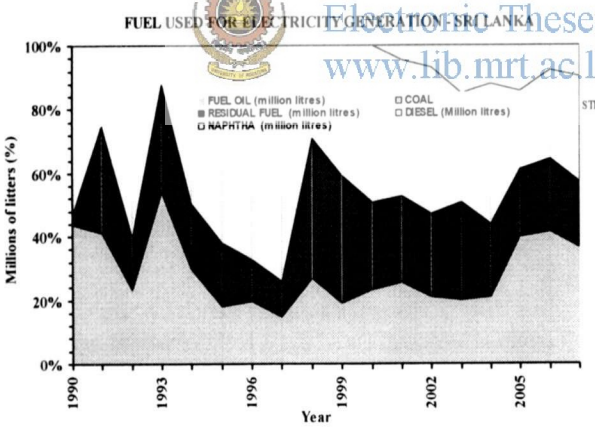

Figure 1.3: Fuel used for Electricity Generation is Sri Lanka

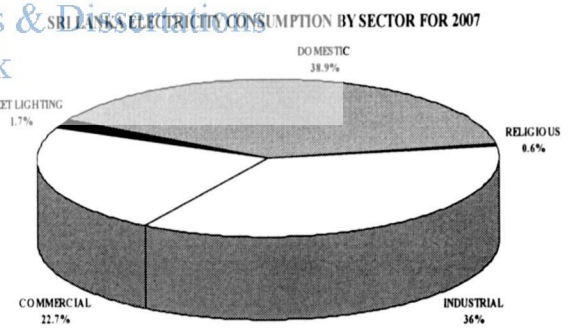

Figure 1.4: Electricity consumption by sector for year 2007 – Sri Lanka

1.1 Rural Electricity Generation

Rural electrification is identified as a catalyst for enhancing rural economic and social development. While conventional grid extension has made good progress connecting nearly 63 percent of Sri Lankans on average to grid electricity, accessibility differs widely among regions. The more developed Western Province has over 80 percent coverage, but other Provinces such as Uva has less than 30 percent coverage. According to the available data in year 2003, status of electrification is shown in Table1.1.

Total number of households	4,576,554
Urban households	23 %
Rural households	77 %
Number of electrified households	3,000,721
Number of non-electrified households	1,575,833

Table 1.1: Status of electrification in Sri Lanka

Electric energy requirement of 23% of rural households in Sri Lanka has being not catered by the main grid electricity supply due to high costs and lack of energy generation capacity. Harnessing of renewable energy is a possible option to accomplish the rural electric energy demand. Present status of off-grid rural energy supply is as given in Table 1.2.

Type of power plant	**No. of systems**							
	2000	2001	2002	2003	2004	2005	2006	2007
Total Village Hydro	78	102	112	127	141	167	176	195
Total Estate Hydro	32	32	32	32	32	32	32	32
Solar PV	10,000	20,906	34,285	52,862	76,166	97,105	114,883	128,527
Wind Battery Charging			25	25	25	25	25	25
Wind						1	1	1
Biomass						1	1	1

Table 1.2: Status of Off – Grid rural Energy Supply systems

Type of power plant	**Capacity (kW)**							
	2000	2001	2002	2003	2004	2005	2006	2007
Total Village Hydro	421.90	641.85	712.75	867.78	1,007.15	1,210.85	1,358.15	1,506.15
Total Estate Hydro	3,226.24	3,226.24	3,226.24	3,226.24	3,226.24	3,226.24	3,226.24	3,226.24
Solar PV	400.00	836.24	1,371.40	2,207.40	3,258.38	4,264.19	4,978.49	5,805.99
Wind Battery Charging			8.20	8.20	8.20	8.20	8.20	8.20
Wind						1.00	1.00	1.00
Biomass						1.00	1.00	1.00
Total	4,048.14	4,704.33	5,318.59	6,309.62	7,499.97	8,711.48	9,573.08	10,548.5

Table 1.3: Statistic data of Generation Capacity for Rural Electrification

According to the present status of off-grid rural electricity supply only small scale solar and wind systems are being used as home power systems. A home power system is the small power system that can be used for fulfilling a single house electricity requirement. Micro hydro plants are commonly used as community based power systems and few community base dendro power schemes are operated to fulfil the electric energy requirement in off-grid rural communities.

1.2 Rural Electric Energy Demand in Sri Lanka

At present under the World Bank/GEF project an exercise titled "Renewable energy for rural economic development (RERED)" has been undertaken to develop renewable energy resources based electricity generation in Sri Lanka. Therefore most of the renewable energy based rural electric energy supply schemes were developed under these projects, especially solar home systems and small hydropower generating systems.

No.	Appliance	Rated (Wattage)	Daily use (Hours)	Total
1	Compact fluorescent lamp for kitchen	11W	3hr	33Wh/day
2	Compact fluorescent lamp for the living room	11W	4hr	44Wh/day
3	Compact fluorescent lamp for out side the house or one bedroom.	11W	2hr	22Wh/day
4	Black & white Television (12" screen)	20W	3hr	60Wh/day
5	AM/FM radio stereo	15W	7hr	105Wh/day
	Total Load (per day)			264Wh/day

Table 1.4: Minimum Daily Energy Demand for a typical Rural House in Sri Lanka

Biomass (fire wood) is the main source of domestic energy supply in a rural house in Sri Lanka. Normally, in off-grid areas kerosene lamps are being commonly used for lighting purposes and dry cells are being used for radio and hand lantern or torches. Solar or wind power home systems have been identified as a possible options to fulfil the electricity requirement for illumination purposes, television and radio. Quality illumination of houses is the benefit of using solar/wind power systems when compare to the use of kerosene oil lamps. Added advantage is that, other appliances like televisions and radios can be powered by the solar/wind power systems. Then the basic electricity requirement of a typical rural house is only for lighting, television and radio.

The daily energy demand for a typical rural house in Sri Lanka is shown in Table 1.4. Daily electric demand pattern is shown in Figure 1.5. Total electric net power requirement is around 264Wh/day. Efficiency of electrical equipment used in home power generation is shown in Table1.5. If average efficiency of electrical equipment is 69%, the daily gross electric energy requirement is 382Wh and monthly gross electric energy requirement is approximately 10 kWh for a rural house in Sri Lanka.

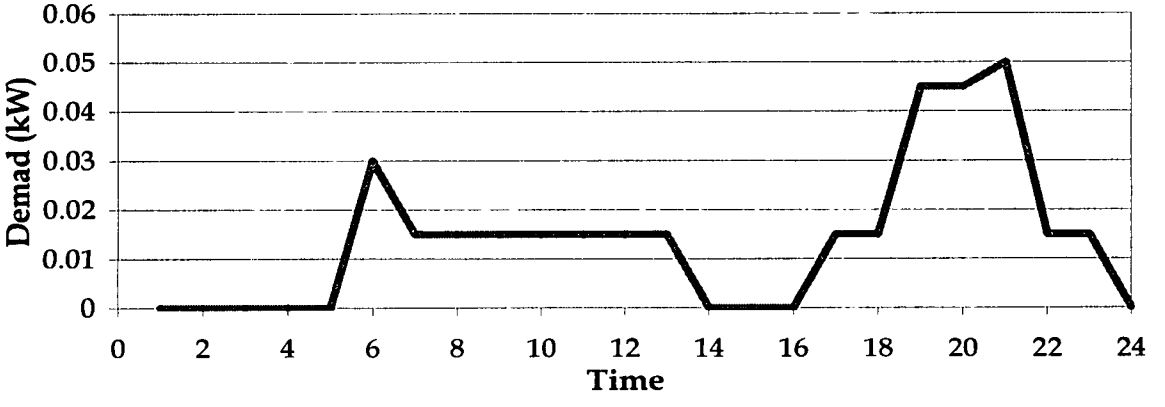

Figure 1.5: Daily electric demand pattern of rural house in Sri Lanka

1.3 Renewable Energy for Power Generation

1.3.1 Wind Power Home Systems

There are only few types of wind home systems (WHS) those are being used in Sri Lanka. Wind turbine generator capacities of 100W and 200W are commonly used for off-grid wind power home systems in Sri Lanka. Wind potential in Sri Lanka is seasonal hence continuous and reliable firm power supply could not obtain by wind power home systems. This may be a one reason of Solar Home Systems are much popular than use of wind home power system. Wind energy is used to small scale battery charging power generation in off grid areas (More than 20 wind home systems and two community system installed in rural areas in Sri Lanka)

1.3.2 Solar Photovoltaic Home Systems

At present solar home systems (SHS) are using in 3% of non-electrified houses in Sri Lanka and it is the major component of home power systems in Sri Lanka. Installed solar home systems at year 2007 are shown in Table 1.3. Under the UNEP/GEF project titled "Solar and Wind Resources Assessment (SWERA)" 10-km solar map and 1-km wind map was developed for Sri Lanka. According to the 10-km solar map, solar potential tilted at latitude of most part of the Island is existed within 4kWh/m^2/day to 5kWh/m^2/day.

Photovoltaic technology has become relatively cost effective method for rural areas. In the technology solar energy is converted to direct current (DC) directly and it is completely solid state self contained. But varying the intensity of solar energy on earth surface over the time and depending on environment conditions (temperature, irradiation ect.) is a challenge for having continues electricity generation by the system. Both wind and solar PV battery charger controllers do not consider battery feed back conditions. Most of the storage batteries are damage due to none controlling of charging rate of the system. When electrifying remote areas it will be difficult and extending the grid. To fill this gap, a hybrid system offers an off – grid energy supply and is a combination of PV and wind power generators incorporating battery storage. The cost effective, reliable design and appropriate operation of these systems is important. Reliable and proper charger controlling system is the main issue for promoting PV, wind battery charging hybrid system for rural electrification. Figure 1.6 shows the off – grid power generation pattern growth in Sri Lanka.

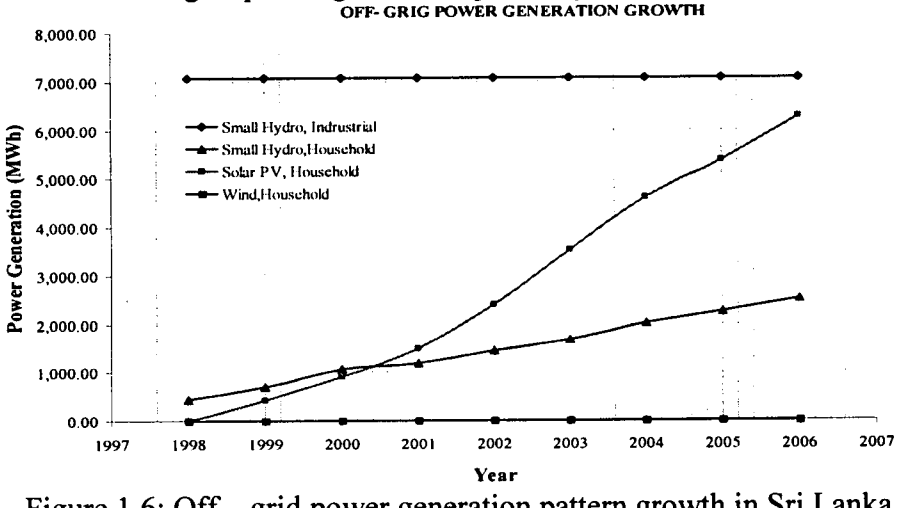

Figure 1.6: Off – grid power generation pattern growth in Sri Lanka

1.4 Literature Review

More than 200 million people, live in rural areas without accessing to the grid – connected power [23]. At present, standalone solar photovoltaic and wind systems have been promoted around the globe on a comparatively large scale [41]. Utilization of solar and wind energy has become increasingly significant, attractive and cost – effective and, since the oil crises of early 1970. Among the renewable energy resources, wind power has had the fastest growth in the world (at the rate of 3% annually) in many developed and developing countries over the last 20 years [1].

PV systems are highly reliable and are often chosen because they offer the lowest life – cycle cost, especially for applications requiring less than 10kW, where grid electricity is not available and where internal – combustion engines are expensive to operate [24]. With the complementary characteristics between solar energy and wind energy for certain locations, the hybrid solar – wind power generation systems with storage banks offer a high reliable source of power [2], which is suitable to electrical loads that need higher reliability.

For the stand- alone hybrid solar – wind power generation systems, because the design and sizing of the photovoltaic (PV) array, the wind turbine, and the battery capacity strongly depend on the performance of the batteries, an adequate prediction of the lead – acid battery's behavior is essential [3]. Despite the fact that batteries are widely used, the behavior of their electrochemical reactions hides an unexpected complexity. At present, many models for battery behavior simulation are available [3-10], and different models can be found to have different degrees of complexity and simulation quality.

The first attempt to study MPPT was made by Dang [16] of California Polytechnic State University, Pomona. Variable – pitch aerodynamically controlled win turbines are more costly and complex. Therefore, variable – speed fixed – pitch approach is becoming more popular for low cost construction and is most common scheme for small wind turbines. In this scheme, MPPT control mechanism is used to control the restoring torque of the electric generator for optimum operation of the wind turbine system [22].

The generator output frequency and power or torque mapping technique is used to track the MPP [33]. Another way for MPP tracking is the use of 'searching' method, which is a suitable strategy for small wind turbines [20 -50].

A lot of work has been done on analysis of the environmental factors that influence the PV module/ arrays performance [30-31]. Radziemska and Klugmann [45] presented the influence of temperature on the parameters of silicone photocells. Borowy an Salameh [7] gave us one simplified model with which the maximum power output could be calculated for one certain PV module once solar radiation on the PV module and ambient temperature were found. Simulation programs are the most common tools for evaluating performance of the hybrid solar – wind systems. HOMER has been used extensively in previous renewable energy case studies [31, 57] and in renewable energy system validation test [18].

Windy lands in Sri Lanka support more than 24,000MW of potential installed capacity [21].

1.5 Scope of Study

The NERDC has being already installed four number of 100W turbines at Nikawaratiya area in Sri Lanka. Main problem that wind power generation is not enough to fulfill the energy requirement in rural house at several months.

The main objective of this study is to develop dynamic moles for the wind turbine, PV system and storage battery systems. Wind rotor performance analyze by theoretically. A photovoltaic system combined with wind generation system is suggested to reduce the zero – power intervals. Sunny days are usually quit and not windy but it is windy on cloudy days and at night. Therefore this hybrid power system (HPS) will avoid shortcomings above mentioned.

In this analysis, dynamic models for each wind and photovoltaic system with the zero power intervals storage battery system individually suggested to develop. The operating point at where the maximum power can be supplied to the load is called the maximum power point (MPP). It is a single best point and the path of this point has a non – linear variation with solar irradiation and the cell temperature. The perturbation & observation (P&O) algorithm for the tracking of (MPP) with panel data in the PV system is used in this analysis.

For the controlling the restoring torque of the electrical generator for optimum operation of the wind turbine system an MPPT control mechanism, which is based on a fuzzy logic searching method for small wind turbine system, is used.

Second objective of this project is simulating above mathematical models with MATLAB Simulink™ 7.2 / Simpower system software environment. And used to carry out to simulate individual wind and PV dynamic models of hybrid system and HOMER has being used extensively in optimized the hybrid system with feasibility analysis and meteorological data in stand-alone areas in Sri Lanka.

Chapter 2

Wind Power Generation

All renewable energy (except tidal and geothermal power), and even the energy in fossil fuels, ultimately comes from the sun. The sun radiates 100,000,000,000,000-kilowatt hours of energy to the earth per hour. In other words, the earth receives 10 to the 18^{th} power of watts of power. About 1 to 2 per cent of the energy coming from the sun converts into wind energy. That is about 50 to 100 times more than the energy converted into biomass by all plants on earth. The wind rises from the equator and moves north and south in the higher layers of the atmosphere. Around 30° latitude in both hemispheres the Coriolis force prevents the air from moving much farther. At this latitude there is a high-pressure area, as the air begins sinking down again. As the wind rises from the equator there will be a low-pressure area close to ground level attracting winds from the North and South. At the Poles, there will be high pressure due to the cooling of the air.

2.1 Wind Energy Resources in Sri Lanka

National Renewable Energy Laboratory (NREL), USA has developed a 1km high-resolution wind map by using the Wind Resource Assessment Model WRAM. The WRAM is used to produce a wind resource map of girded wind power density values with a 1-km^2 resolution and it was developed with powerful ArcInfo GIS software package. This model allows more consistent application of analysis techniques in a regional assessment, more detailed analysis of the wind resource, and it produces high quality maps.

According to the WRAM wind resource map in Sri Lanka [21] there is nearly 5000km^2 of windy areas with good-to-excellent wind resource potential. The amount of land area of good-to-excellent wind resources at 50m is shown in Table 2.1. National park, reserves, archaeological and cultural sites were excluded in this land coverage. WRAM wind resource map is shown in Figure 2.1.

Wind resources utility scale	Wind class	Wind power at 50m (W/m^2)	Wind speed at 50m (m/s)	Land area km^2	Lagoon area km^2	Total area km^2	Percentage of windy land %	Total capacity installed MW
Good	4	400-500	7.0-7.5	2,341	664	3,005	3.6	15,000
Excellent	5	500-600	7.5-8.0	788	41	829	1.2	4,150
Excellent	6	600-800	8.0-8.8	517	0	517	0.8	2,600
Excellent	7	>800	>8.8	501	0	501	0.8	2,500
Total				4,147	705	4,852	6.4	24,250

Table 2.1: windy areas with good-to-excellent wind resource potential in Sri LAnka

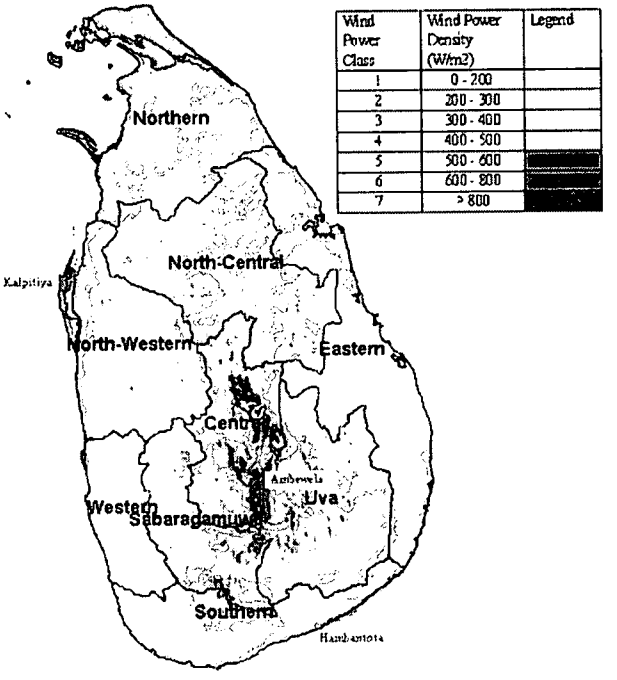

Figure 2.1: WRAM wind resource map in Sri Lanka

2.2 Small Scale Wind Turbine Technology

Small-scale wind turbines are generally rated from 50W to 10kW power with diameter ranging from 1m to 10m. Most of the commercially available units are horizontal axis type having two or three bladed [2-39]. Small scale turbines generally operate at variable speed, variable frequency (VSVF) and in constant pitch angle with yaw regulated in wind direction, a tail rudder aligns the rotor against the wind. A passive controlling mechanism allows the rotor body to furl away in case of high winds against the rotor. These mechanisms are essential in regulating the power extracted by the system and reducing structural stresses on the machine parts and the tower [39].

2.2.1 Operation of the Wind Turbine

The main aim of wind turbine technology is converting wind energy to electricity. To assure a proper operation the wind turbine has to adapt to any wind conditions, which is in the first order to adjust itself according to the wind direction. It also needs to protect itself from the violence of wind greater than the rated wind speed. All this must happen automatically.

2.3 NERDC Wind Turbines

National Engineering Research & Development Centre has been involving design and fabrication of 100W battery charging wind turbines for rural electrification. The 100W battery charging wind turbine operates with constant pitch variable wind condition. The wind turbine system consists of fiberglass wind rotor with two blades, 100W permanent magnet generator (PMG) and stay supported 20m height tilt up tower. The specification of the NERDC wind turbine is given Table 2.2. And operating schematic diagram is shown in Figure 2.2.

1	Rotor Diameter	2.21m
2	Hub Diameter	0.210m
3	Tower height	20m
4	No. of blades	2
5	Design tip-speed ratio	6.5
6	Design wind speed	6m/s
7	Cutting wind speed	3m/s
8	Cut-off wind speed	12m/s
8	Rated power output	100W
9	Maximum power coefficient	0.42
10	System efficiency	13%
11	Control mechanism	Inclined hinged Tail Vane
12	Blade Profile	NACA4415

Table 2.2: Specifications of NERDC 100W wind turbine

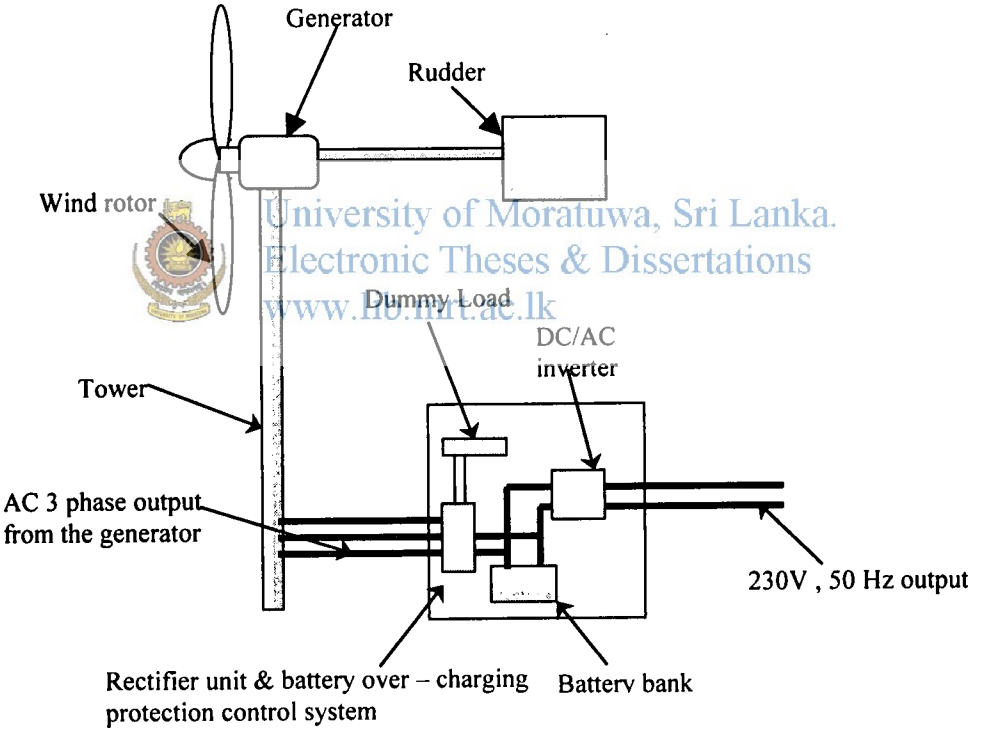

Figure 2.2: Schematic diagram of NERDC 100W Battery charging wind turbine system

2.3.1 Control Systems

Main objective of the passive control system for Small-scale Horizontal Axis Wind Turbines is, wind rotor automatically face to the wind direction and out of direction while higher wind blowing through the rotor. Larger wind turbines have computer driven control systems, which operate servomotors, hydraulic motors, and all sorts of paraphernalia. Small wind turbines need simple passive controls where possible. Tilt –up rotor system shown in Figure 2.3 and Gravity operated furling tail with offset wind rotor shown in Figure 2.4 are the most commonly utilized passive controlling systems for the small scale horizontal axis wind turbines.

Figure 2.3: Tilt –up rotor passive control system

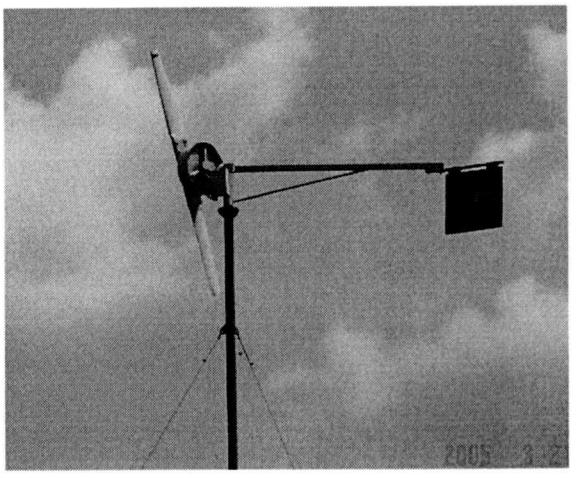

Figure 2.4: Gravity operated furling tail with offset wind rotor passive control system

NERDC 100W small-scale wind turbines are designed with inclined hinged tail vane with side vane passive control system as shown in Figure 2.5. This system is simple and with minimum maintenance than the other passive controlling systems. The Tail vane is mounted with the base by means of inclined hinge and the side vane is fixed perpendicular to the rotor axis as shown in Figure 2.6 and Figure 2.8 shows torque act on the side and tail vanes of the system.

Figure 2.5: inclined hinged tail vane with side vane passive control system

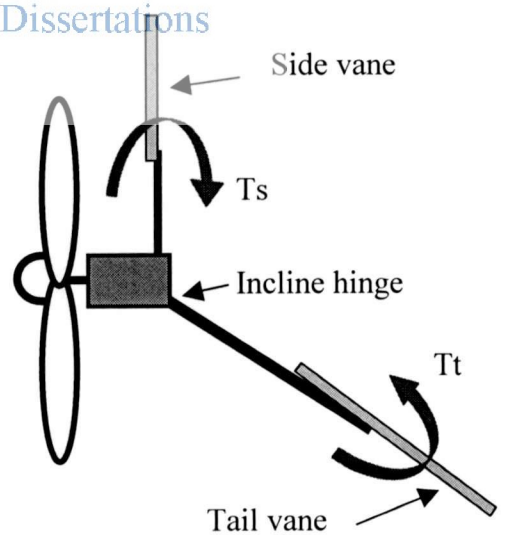

Figure 2.6: Arrangement of inclined hinged tail vane with side vane passive control system

T_s – Torque on the side vane
T_t – Torque on the tail vane
T_h - Torque on the incline hinge

Torques on Tail Vain and Side Vane

Torque on tail vain due to incline hinge give in equation 2.1

$$T_h = mL \tan\phi \tan\theta \tag{2.1}$$

m = weight of the tail vane
L = distance from the hinge point and center of gravity of the vane
ϕ = Hinge angle
θ = Angle of rotation from the original position

When the wind blowing is at operational wind speed (6 m/s) angles of side and tail vans are controlled with above parameters. When the wind speed reaches around cut- off speed (12 m/s), side and tail vanes are close together and system controlled by the rotor yawing out of the wind direction as shown in Figure 2.7.

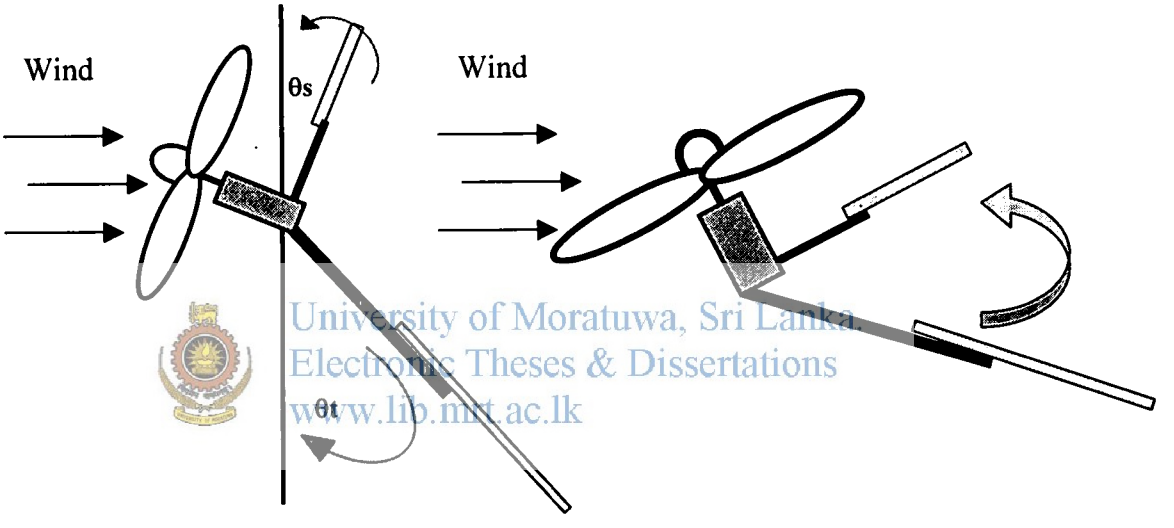

Figure 2.7: Schematic diagram of operation inclined hinged tail vane with side vane passive control system

Aerodynamic Torque on tail vain is given in equation 2.2

$$T_t = \frac{1}{2} W^2 \rho A_t L_t \left[c_l \cos\alpha + c_d \sin\alpha\right] \tag{2.2}$$

Lt = Effective length of the tail vane

At = Area of the tail vane

α = Angle of attack

Aerodynamic Torque on side vain is given in equation 2.3

$$T_s = \frac{1}{2} W^2 \rho A_s L_s \left[c_l \cos\alpha + c_d \sin\alpha\right] \tag{2.3}$$

L_s = Effective length of the tail vane,

A_s = Area of the tail vane

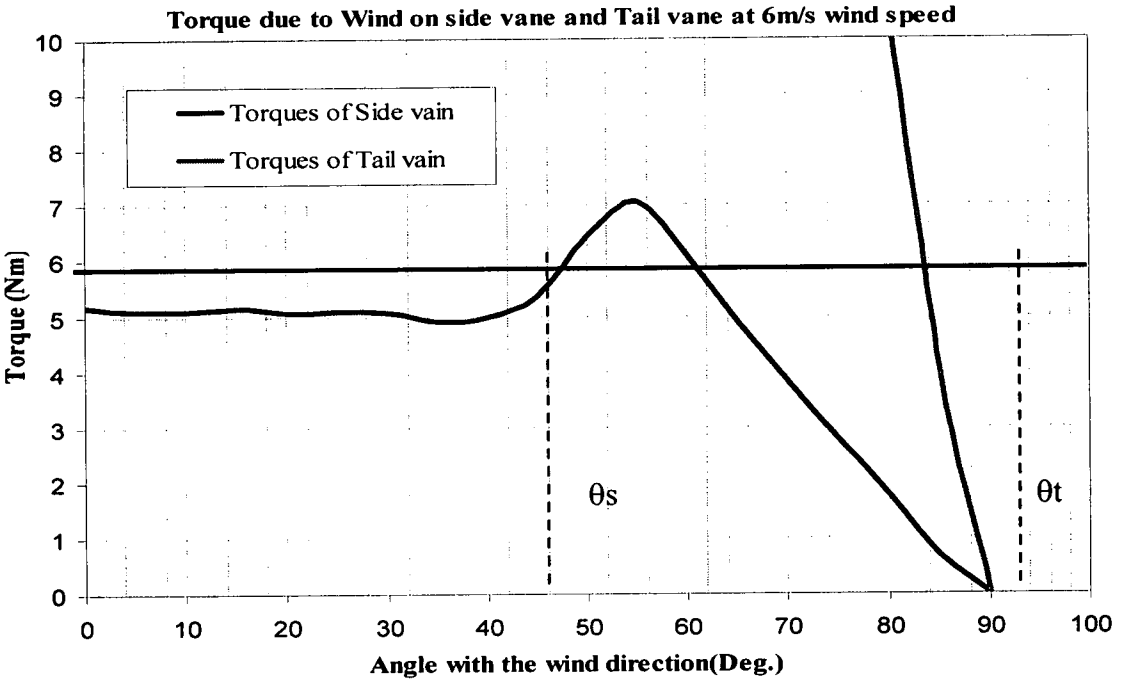

Figure 2.8: Torque against wind on the side vane and tail vane at operating wind speed (6 m/s)

2.4 Analgize of NERDC 100W Wind Turbine Performances

2.4.1 Wind Rotor Geometry

The rotor has being improved to extract more energy from low wind-speeds, since it is necessary to reduce the cut-in wind speed. Low starting torque of wind rotors has being identified as a main restriction against the reduction of cut-in wind speed of wind turbine generators. Therefore, in certain instances, off-grid wind turbines must be designed to extract energy from low wind-potential sites to fulfill the energy requirement.

NERDC wind rotor is fabricated by fibreglass material with NACA 4415 aerodynamic profile as shown in Figure 2.9. Rotor diameter is 2.21m with a hub. 6mm thick fibber resin with mat composite structure shows better flexibility and durability when exposed to the turbulent wind and atmospheric impacts. Cross-section of the rotor is hollow, and it reduces material usage and weight of the rotor.

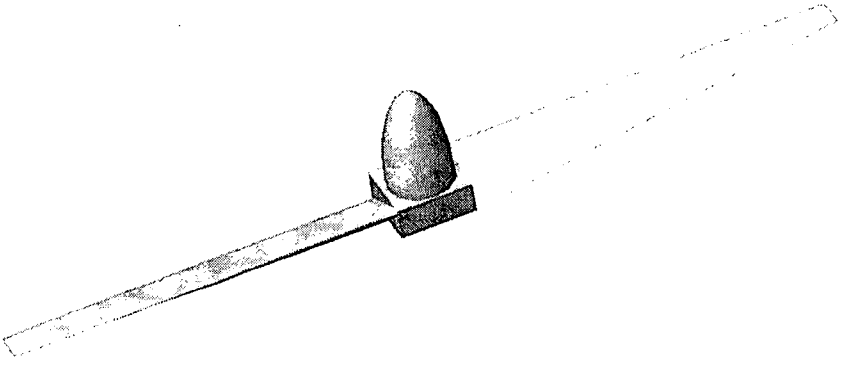

Figure 2.9: Geometry of NACA 4415 wind rotor used for NERDC 100W wind turbines

Section	Radius (mm)	Chord length (mm)	Blade angle(β) (Degrees)
1	155	189.2	22.0
2	255	177.7	19.5
3	355	166.2	17.1
4	455	154.7	14.7
5	555	143.2	12.3
6	655	131.7	9.8
7	755	120.2	7.4
8	855	108.7	5.0
9	955	97.2	2.6
10	1055	85.7	0.2

Table 2.3: Geometrical parameters of NERDC 100W wind rotor

2.4.2 Wind Rotor Performance

In the analysis of the characteristic performance of a wind-rotor, the main parameters are thrust force on the rotor, torque generated by the rotor, and rotational speed of the rotor. These parameters should be found at different values of wind speeds in order to analyze the characteristic performance of the wind- rotor. A wind-rotor, in general, is designed so that optimum energy conditions are satisfied at a given specific tip-speed ratio. But in practice wind rotors do not always function at optimum conditions. It may run at various other tip-speed ratios.

In this study, power output of this wind rotor should be evaluated for different wind speeds. The main objective here is to theoretically find out the C_p values for different λ_0 values of the NERDC wind-rotor. Geometry of wind rotor blade is shown in Figure. 2.9. Geometrical parameters of the rotor are presented in Table 2.3. Performance of the existing wind-rotor can be analyzed by using the blade element theory (BET) and momentum theory (MT) [17]. This rotor consists of ten blades with arc shape Profile. The radius of the rotor is 1055 mm, and the hub radius is 210 mm.

Blade Element Theorems and Momentum Theorem

Energy extracted from the wind is transmitted through the rotor in the form of torque, and the air is acted upon with a reactive torque that makes wakes which rotate opposite to the rotor motion. This implies that the downstream air consists of rotational kinetic energy, which is not included in the axial momentum theory. Indeed, this energy component represents a part of energy in air, which could not be absorbed by the rotor. Therefore, a more realistic value for C_{pmax} can be derived by the inclusion of wake-rotational effect.

It should be noted that the wake-rotational effect is the main case for low C_p values in low-speed wind-rotors. These rotors impart higher reactive torques in the wind, than high-speed rotors, which result in higher wake-rotations leading to higher losses. Figure 2.10 shows the basic configuration of the flow through a wind-rotor with wake-rotation. The rotor speed is denoted by ω, and rotational speed of the wake given by Ω varies along the radius r.

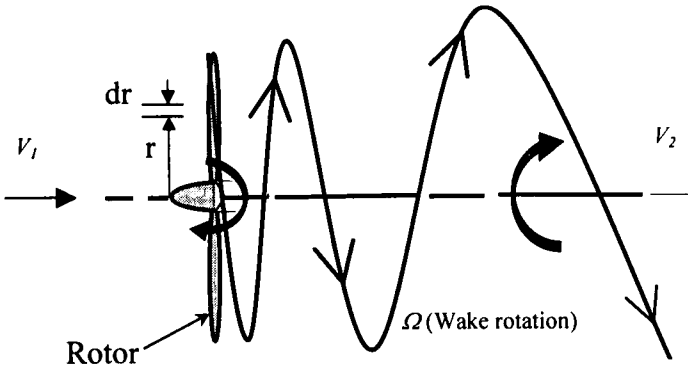

Figure 2.10: Flow behind the rotor with wake-rotational effect

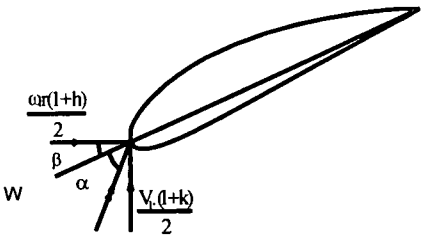

Figure 2.11: Velocity diagram of a blade element

Flow behind the rotor with wake – rotation as shown Figure 2.10

Downstream of the rotor, the rotational speed of the wind flow Ω is given in equation 2.4

Hence, $\Omega = h\omega$ (2.4)

h - Radial flow interference factor

The axial speed through the rotor can be derived.

Let, $V_2 = k\, V_1$

k - Axial flow interference factor.

Velocity diagram of a blade element shown in Figure 2.11 is used for calculations given in equations 2.5 – 2.7

$$\phi = \alpha + \beta \tag{2.5}$$

$$\cot\phi = \frac{U}{V} = \frac{\omega r.(1+h)}{V_1.(1+k)} \tag{2.6}$$

$= (\omega r/V).\ (1+h)/\ (1+k)$

$= \lambda.\ (1+h)/\ (1+k)$ (2.7)

Let; $\lambda = \dfrac{\omega r}{V}$

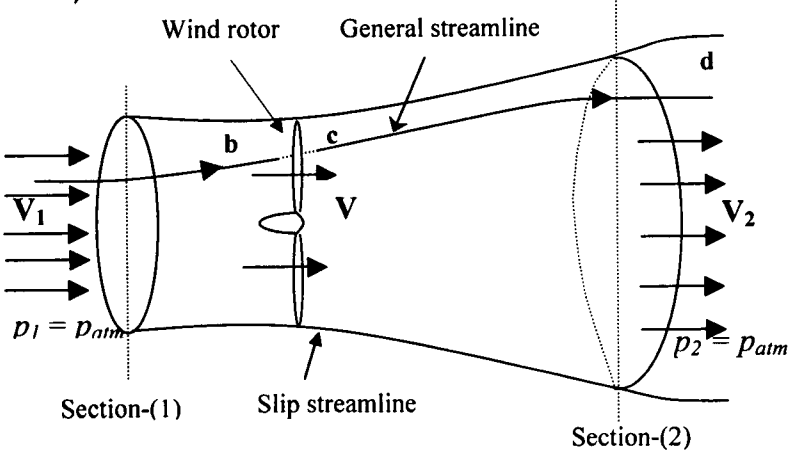

Figure 2.12: Control volume used for a wind turbine

Aerodynamic Performance

The performance of the wind rotor is theoretically predicted by considering the wake-rotation of the wind-rotor by using blade element theory and momentum theory, where the geometrical parameters (β, C) of the existing blade are used. The characteristic performance of a wind-rotor is usually given by the variation of power coefficient (C_p) with respect to tip-speed ratio (λ_0).

Calculation of axial thrust and torque

Considering the blade element theory, axial thrust dF is given by equation 2.8

$$dF = b.d.F_v = \frac{\frac{1}{2}.\rho.l.W^2.b.C_l.\cos(\phi-\varepsilon).dr}{\cos\varepsilon} \tag{2.8}$$

Aerodynamic torque, dM, is given by equation 2.9

$$dM = r.b.dF_u = \frac{\frac{1}{2}.\rho.l.r.W^2.C_l.\sin(\phi-\varepsilon).dr}{\cos\varepsilon} \tag{2.9}$$

Where,

Tan $\varepsilon = C_d/C_l$

The above two values, dF and dM, can be determined by the general dynamics theory. Consider the axial momentum of the flow through the annulus with control volume as shown in Figure 2.12.

Thrust = (rate of mass flow, m, through the element) x (change in the axial velocity).

Then,

Axial thrust, $dF = \rho.\ \pi.r.dr.V_1^2.(1\text{-}k^2)$ (2.10)

Aerodynamic torque,

$$dM = \rho.\pi.\ r^2.\ dr.\ V_1.\ (1+k)\ \Omega$$
$$= \rho.\pi.r^3.dr.\omega.V_1.(1+k).(h\text{-}1) \tag{2.11}$$

Comparing the expression for dF derived by blade elementary theory with that derived by momentum consideration given in equations 2.8 and 2.10 leads to, after substituting for ω,

$$C_l.b.l = \frac{2.\pi.r.V_1^2.(1-k^2).\cos\varepsilon}{W^2.\cos(\phi-\varepsilon)} = \frac{8.\pi.r.(1-k).\cos\varepsilon.\sin^2\phi}{(1-k).\cos(\phi-\varepsilon)}$$

Similarly, comparing dM given in equation 2.9and 2.11

$$C_l.b.l = \frac{2.\pi.r.V_1.(1+k).(h-1).\cos\varepsilon}{W^2.\sin^2(\phi-\varepsilon)} = \frac{4.\pi.r.(h-1).\sin 2\phi.\cos\varepsilon}{(h+1).\sin(\phi-\varepsilon)}$$

After rearrangement to get the following given in equation 2.12 and 2.13

$$\frac{1-k}{1+k} = \frac{C_l.b.l.\cos(\phi-\varepsilon)}{8.\pi.r.\cos\varepsilon.\sin^2\phi} \tag{2.12}$$

$$\frac{h-1}{1+h} = \frac{C_l.b.l.\sin(\phi-\varepsilon)}{4.\pi.r.\sin 2\phi.\cos\varepsilon} \tag{2.13}$$

The wind rotor is divided in to 10 equal sections and C_p value for each section was calculated by using the iterative search procedure given in Equations 2.14 – 2.16. C++ program was developed to obtain required C_{pr} Values for each blade elements (Appendix A). The curve of coefficient of lift (C_l) and coefficient of drag (C_d) verses the angle of attack (α) of the blade profile NACA 4415 was used for this calculation [17]. Mathematical relationships of C_l and C_d with α were determined by using the curve fitting methods. Then, coefficient of performance of the wind rotor (C_p) with respect to different tip speed ratios (λ_0) was calculated. Finally NERDC 100W wind rotor performance curve was plotted with various wind speeds as shown in Figure 2.13.

$$C_{Pr} = \frac{dP_u}{\rho.\pi.r.dr.V^3} = \lambda^2.(1+k).(h-1) \tag{2.14}$$

$$P = \int_r^R C_{Pr}.\rho.\pi.r.dr.V_1^3 = \tfrac{1}{2}.C_p.\rho.\pi.R^2.V_1^3 \tag{2.15}$$

$$C_p = \frac{2}{R^2}.\int_r^R C_{Pr}.r.dr \tag{2.16}$$

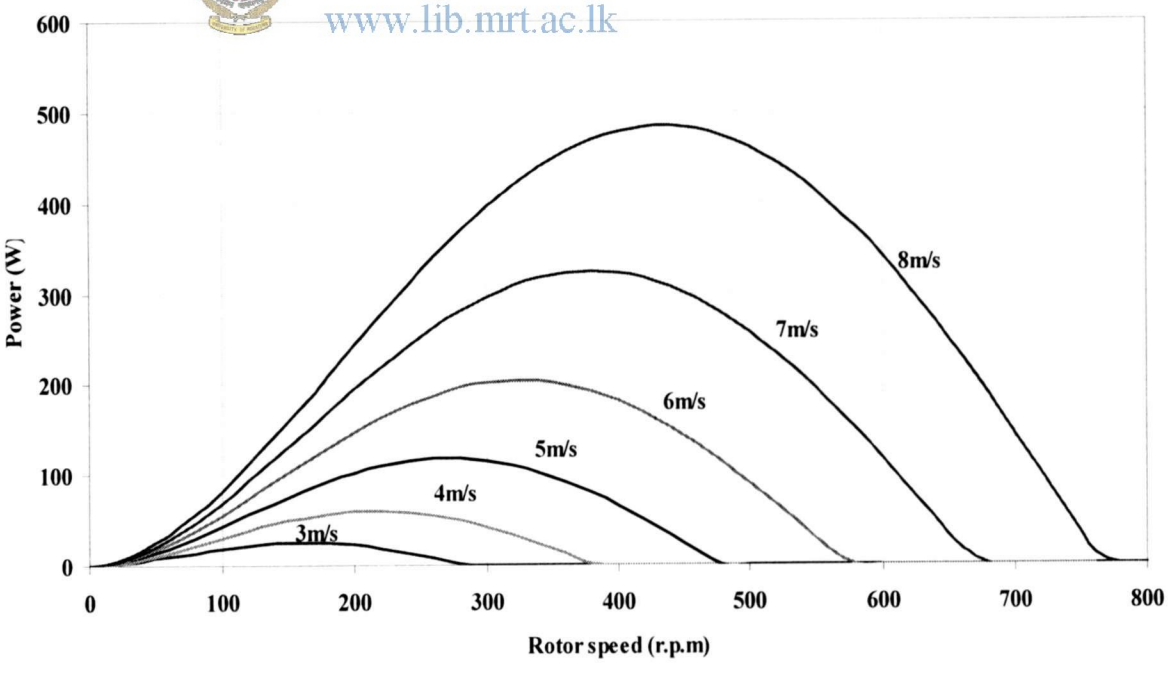

Figure 2.13: NERDC wind rotor performance variation with wind speeds

2.5 Electrical Generators used for Wind Turbines

The generator converts mechanical energy generated by the wind rotor to electrical energy. Types of generators used in grid connected wind energy application include induction (asynchronous) generators, synchronous generators and multi-pole-permanent-magnet generators. In grid connected wind power generation, not only the power generation but also the rotational speed of rotor is very important. Since rotational speeds of medium- or large-scale wind-rotors are very low compared with speeds generators. A gearbox should be used to match the rotational speeds. In different multi-pole generators can be operated at low rotational speed and can be directly coupled with wind rotors.

2.5.1 Wind Turbine with Multi-Pole Permanent Magnet Generators

Permanent magnet generators (PMGs) consist of stator winding and magnets mounted rotor. In this system, required electrical magnetic force (EMF) of generator is developed by its permanent magnets and thus it does not require external excitement. PMG can generate power efficiently in wider range of rotational speed [34]. Then system of multi-pole permanent magnet generators with and AC/DC rectifier and a DC/AC inverter could be operated at optimum energy absorption condition. Pitch-control system is used to control the power output by regulating rotational speed of the rotor. As such, this system can be operated at variable rotational speeds. Main advantages of these systems are, the generator is self-excited, power output can be controlled, and wind rotor and generator can be directly coupled. Disadvantages are complex in construction as generated power should be converted to DC, then reconverted to AC with correct grid frequency and synchronised with grid.

2.5.2 Generators Used for Small Scale off - Grid Wind Turbines

Off-grid wind turbines are mainly used to fulfill the energy requirement of the rural community. Hence, these systems should be of low cost, simple construction and low maintenance requirements. Therefore, direct drive variable speed systems with passive control mechanisms are identified as appropriate option. The most suitable generator type for such systems is permanent-magnet generator (PMG). At present, almost all off-grid wind turbines are equipped with AC out put generators, which supply an electric output with variable voltage and variable frequency. However, in few cases, DC generators are used for special applications.

Magnetic flux of PMG remains constant, but other types of generators magnetic flux may increase when generating power. Due to less electro magnetic force (EMF), PMG need more winding to generate required power. As resistance of winding of PMG is high, efficiency is less than that of other type of generators.

2.6 Performances of the Permanent Magnet Generator Developed By NERDC

Development of a suitable electric generator has been a long felt need for micro scale electricity generation using wind for rural electrification. Any generator that can be used with small-scale wind power generation should perform satisfactorily within two constraints namely low starting torque and low rotational speed, which are imposed by the wind rotor inherent characteristics.

NERD Centre has involved in the research & development work on PMG since 1981. Initially NERDC manufactured a pancake type PMG for small-scale power generation applications [34]. Ferrite type speaker magnets were used for this generator. This type of generators has very low EMF, and therefore the efficiency is low. Another disadvantage of this generator is the difficulty in keeping a constant air gap.

Subsequently, NERDC modified this system to plate type permanent magnet generator, which has better EMF, as it includes a proper magnetic path. This is new evolution of pancake type permanent magnet generator, however maintaining of a constant and small air gap was difficult. Further, the magnets were subjected to shear during operation due to physical contact under heavy centrifugal forces.

With these experiences, NERDC decided to develop PMG with different configuration and came up with a cylindrical type permanent magnet generator. This type has satisfactory performance in small-scale applications and the air gap is maintained as smaller as possible at a constant level.

NERDC has developed a 100W permanent magnet generator considering two of the principle constraints imposed by small wind turbines are low starting torque and low rotational speed. Anyhow certain types of wind turbines can be designed to have higher starting torque but as a result speed will be further reduced and will make it not suitable for the application. Records of the wind speeds in Sri Lank show that the wind received during larger period of the year by many areas in the low speed ranges. Design of wind turbine rotor blade profile also has shown the difficulty of obtaining high wind rotor speeds under above conditions. Therefore it was clearly identified that 100W PMG can be used with small scale wind power generation in any sites in Sri Lank. Figure 2.14 shows the NERDC 100W Permanente magnet generator

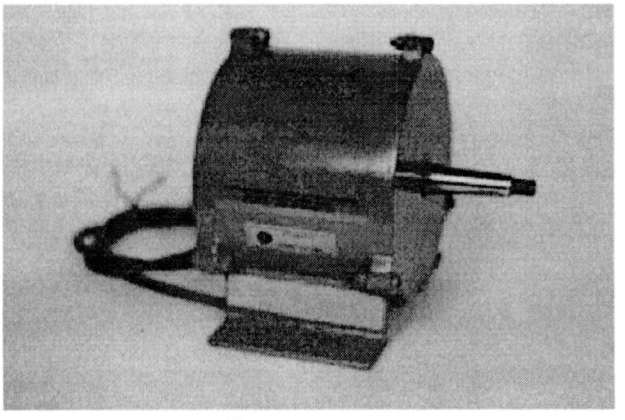

Figure 2.14 NERDC 100W Permanente magnet generator

Specifications of NERDC 100W PMG

Rated power	100W at 500r.p.m
Output voltage at rated speed	16V DC or 26 VDC (Through rectifier)
Number of phase	3
Number of poles	8
Method of excitation	permanent magnet
Rating	continuous
Rated maximum current (continuous)	5.5A DC
Maximum operating speed	800 r.p.m
Totally enclosed	foot mounting
Brushless	
Shaft	Tapered with left hand screw at the end or parallel shaft with key way

2.6.1 Characteristics of NERDC Permanent Magnet Generator

Characteristic performance of the PMG was predicted by experimental measured in the NERDC laboratories. Power absorption by the PMG with different rotational speeds was measured by using a current brake dynamometer. The 100W PMG was tested with hydro turbine and generator testing ring in Renewable Energy Department of NERDC. The PMG was mounted on turbine testing bed and coupled to the current brake dynamometer by means of a flexible coupling. The current brake dynamometer has both absorption and regenerative testing facility. The PMG rotate by means of brake dynamometer.

PMG output three phase terminals connected to the rectifier unit and DC output terminals connected to the 12V battery bank. Out put voltage and current were measured while rotating particular rotating speed set by dynamometer. Also the PMG input power is measured by measuring dynamometer rotational speed and dynamic torque as shown in Figure 2.15.

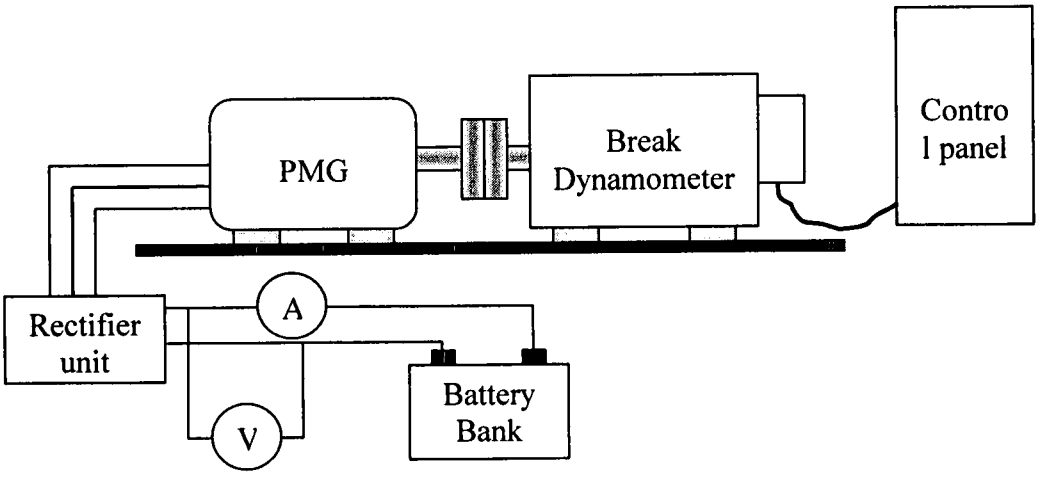

Figure 2.15: Schematic diagram of PMG performance test arrangement

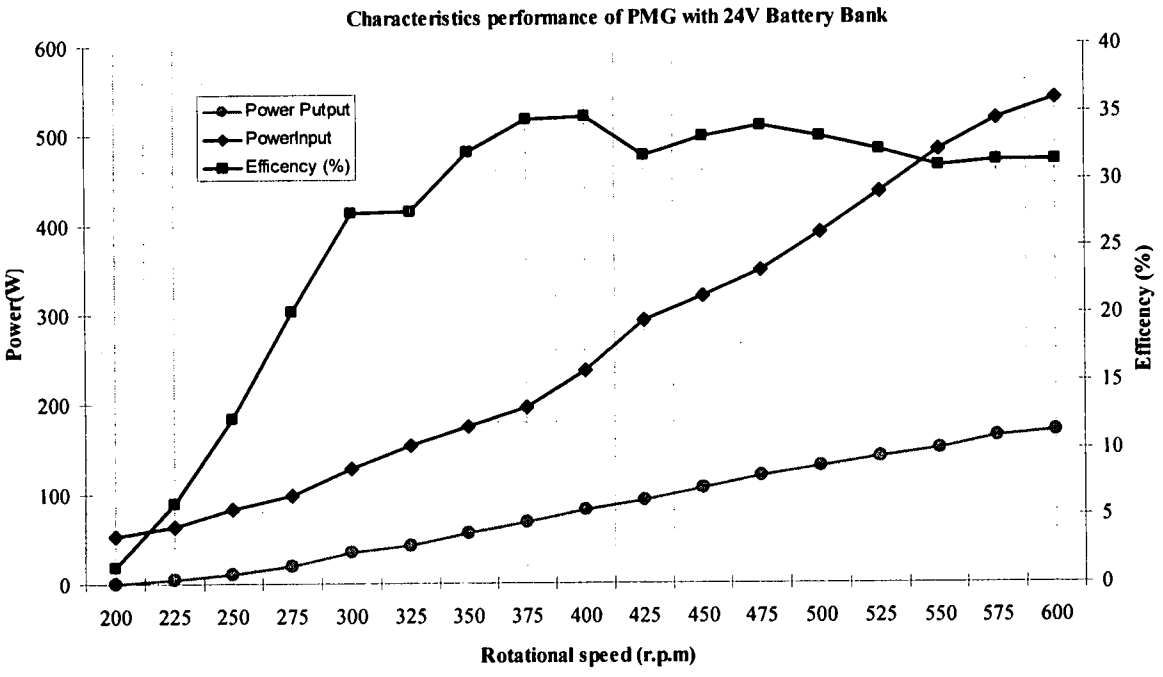

Figure 2.16: NERDC 100W PMG performance test result

According to the characteristics performance of NERDC PMG, its maximum efficiency is given when the rotational speed is above the 375 rpm and its rated power 100W is generated at the 438 rpm. Power generation starts at a relatively low rotational speed of 200 rpm, when it is coupled to a 24V battery-bank. Performance of NERDC PMG is shown in Figure 2.16. Also PMG performance plotted with NERDC wind rotor performance curve against varying wind speeds as shown in Figure 2.17.

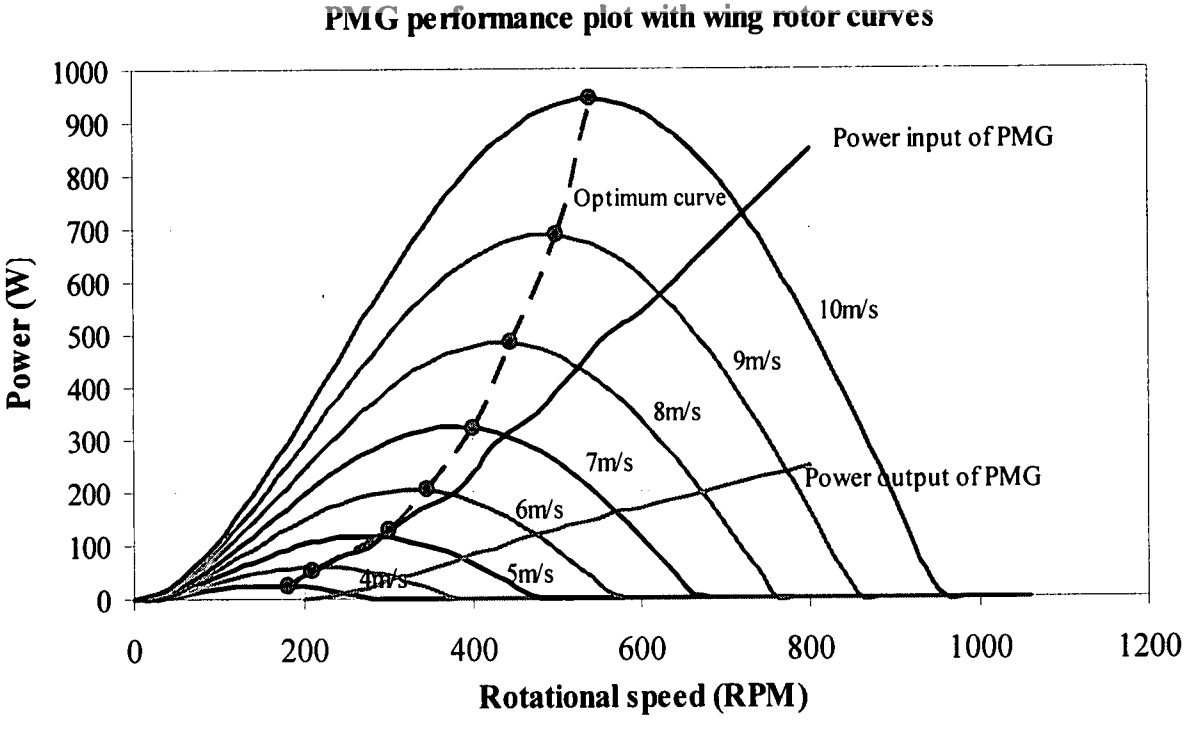

Figure 2.17: NERDC 100W PMG performance plot with wind rotor performance curve

Chapter 3

Case study of Nikavaratiya 100W Wind Turbine Site

A case study was attempted at a place called Nikavaratiya ($7^0$44" 26.28"N 80^0 06" 53.79" E), in Kurunagala district, Sri Lanka. Four number of 100W wind turbines were installed in Nikavaratiya area as wind power home systems as shown in Figure 3.1. This project is NERDC and practical action collaborative project and started and commission at year 2005. As feasibility study the wind data of Nikavaratiya area was predicted from Putthalum metrological station by using a Wasp7 micrositing software tool. These four locations are selected as the best wind speed and feasible places. After commissioning the wind turbines the power generation was not enough to fulfill the electricity requirement of the householders. Site locations of four wind turbine in Nikavaratiya area as Table 3.1 and Figure 3.2shows the site locations on digitized map in Nikavaratiy area.

Figure 3.1: Shows the 100W wing turbines installing at Nikawaratiya site

100W wind Turbine	X [m]	Y [m]
Turbine site 1	120414	283844
Turbine site 2	120471	283682
Turbine site 3	119737	282976
Turbine site 4	118548	282775

Table 3.1 shows the locations of 100W wing turbines at Nikawaratiya site

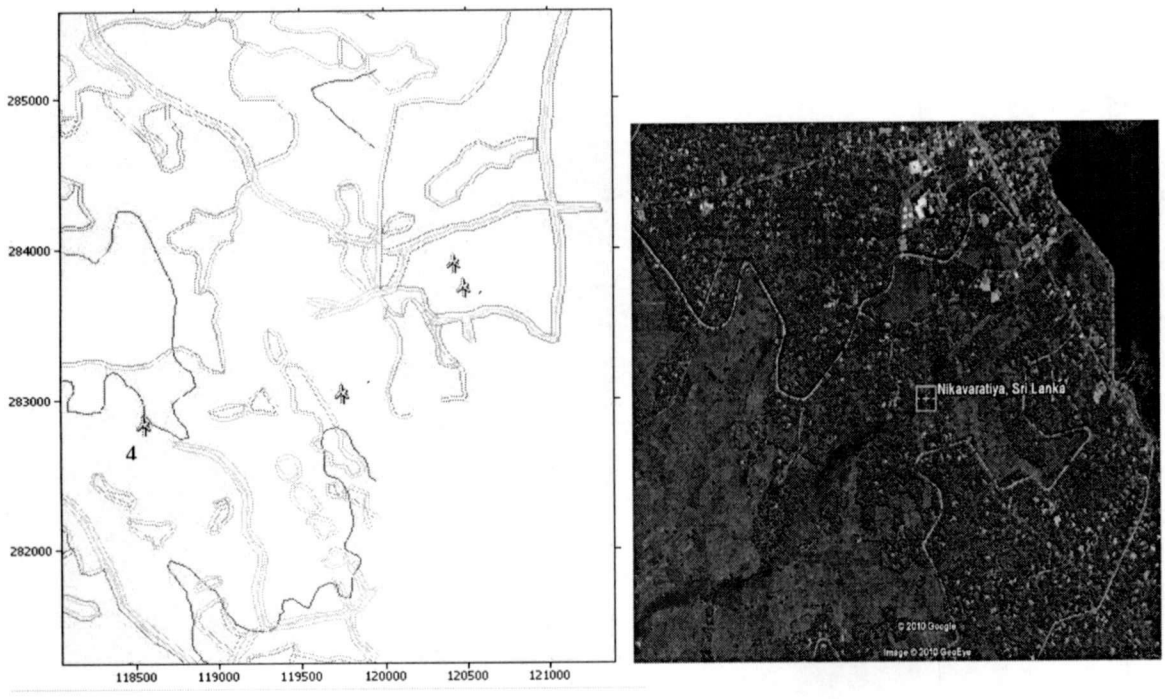

Figure 3.2: Shows the locations of 100W wing turbines on digitized map at Nikavaratiya

As a part of this study monthly energy production (kWh) of NERDC 100W wind turbine at four different places was obtained in Nikavaratiya site as shown in Table 3.2.

			Jan	Feb	Mar	Apr	May	Jun	Jul	Aug	Sep	Oct	Nov	Dec
Site ID	X [m]	Y [m]												
Turbine site 1	120414	283844	10.43	3.26	7.28	10.24	26.74	26.18	18.19	25.73	25.24	20.18	9.38	10.95
Turbine site 2	120471	283682	10.39	3.26	7.39	10.80	26.66	26.44	18.30	25.39	25.61	20.51	9.34	10.80
Turbine site 3	119737	282976	10.95	3.64	6.64	9.53	25.46	23.51	18.23	26.96	23.85	17.89	9.49	12.08
Turbine site 4	118548	282775	10.80	3.41	6.34	9.00	26.14	24.68	18.56	26.96	23.36	17.18	9.15	11.18

Table 3.2: Shows the monthly energy generation of 100W wing turbines locations

The NERDC 100W small-scale wind turbine system consists of numerous devices such as DC/AC invertors (300W), Battery charger regulator and Lead – acid battery (70 Ah) as shown in Figure 3.3. The efficiency of electrical equipment used in wind power generation as follows

DC to AC inverter	85 to 95 %
Battery charge regulator (includes losses due to cables)	90 to 95 %
Battery	75 to 90 %
Overall efficiency of the electrical system	57 to 81 %

Required energy generation by a wind turbine per day for rural home is 382 Wh and considering the equipment efficiency of the system required energy generation by a wind turbine per month is around 11.5 kWh. According to the Table 3.2, monthly energy generation is satisfactory in May to October. And in other six months energy generation cannot fulfil the electric requirement in above four locations.

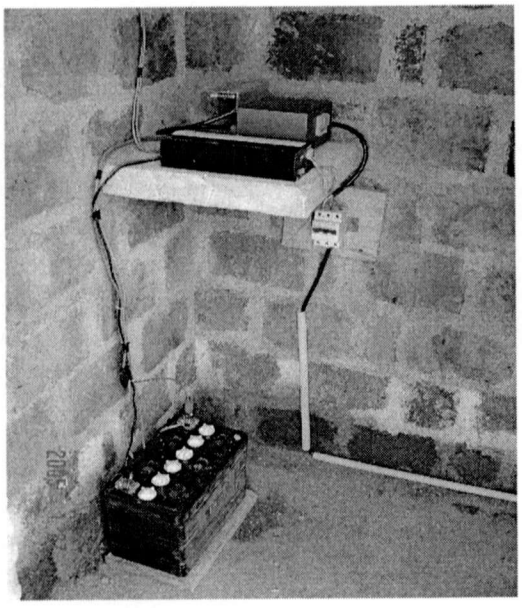

Figure 3.3: Shows the electrical components of 100W wing turbines system

3.1 Wind data measurement

According to this study, wind data was measured in one station of the Nikavaratiya 100W wind site. The three cup anemometer with data logger shown in Figure 3.4 is used to measure a wind speed *V (m/s)* data. The measured hourly average and daily average wind speed at 20m height at [X(m)120471,Y(m) 283682] for all the months of the year 2008 were as shown in Figure 3.5 and Figure 3.6 respectively .

Figure 3.4: Shows the three-cup anemometer used to measure wind speed

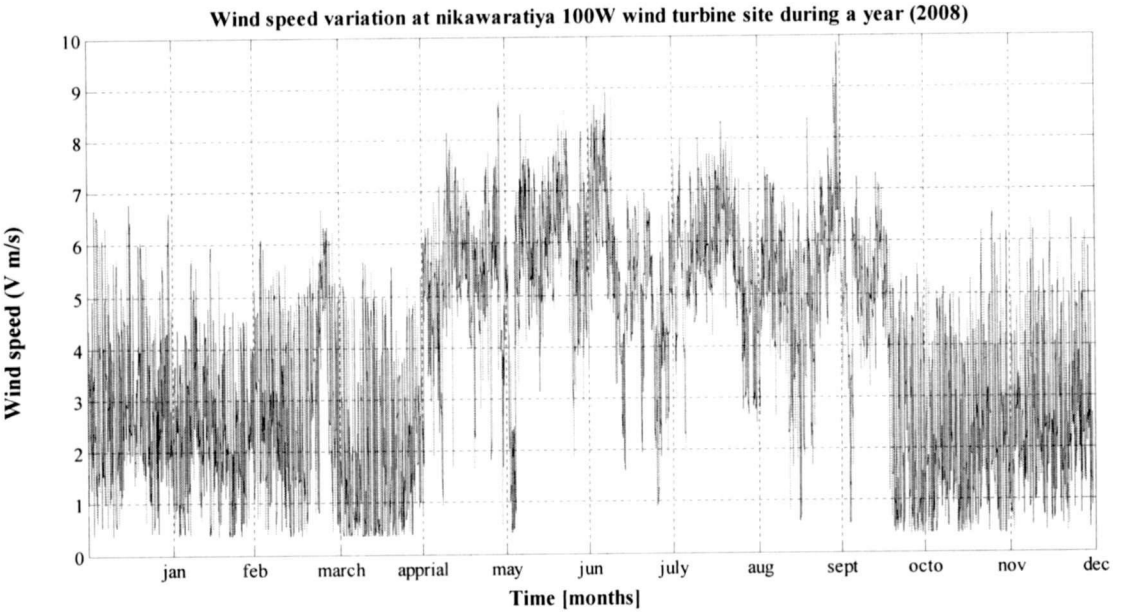

Figure 3.5: Hourly average wind speed variation throughout the year 2008

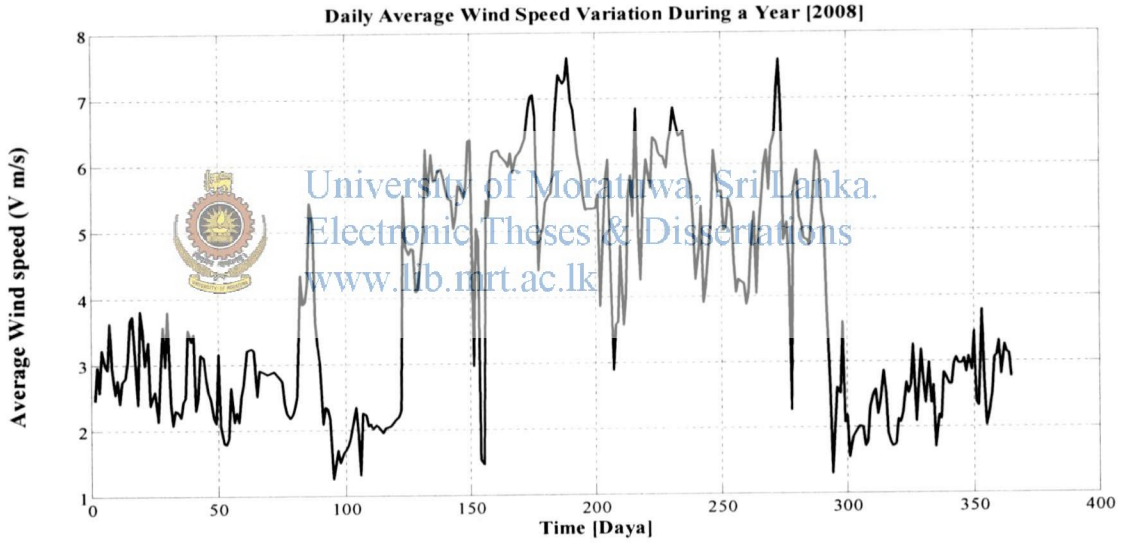

Figure 3.6: The daily average wind speed variation throughout the year 2008

3.2 Solar Irradiation Measurement

Also hourly average total solar irradiance $G(W/m^2)$ impinging on a horizontal plane for a random period of one hour duration in year 2008 was measured at the same place by installing weather monitoring system with data logger . The Solar irradiation measurement throughout the year 2008 was as shown in Figure 3.7.

In the existing 100W wind site location of [X(m)120471,Y(m) 283682] at Nikawaratiya area the annually average wind speed at 20 m height is 3.92m/s and the solar potential of the same location measured round 30 ~ 32 ^{0}C environment temperature is 5.44 kWh/m^2 /day.

Required energy generation by a wind turbine for rural home is 382 Wh/day and wind system parameters like cut – in –speed of 3m/s, rated wind speed is 6m/s and cut-off-speed is 12m/s.

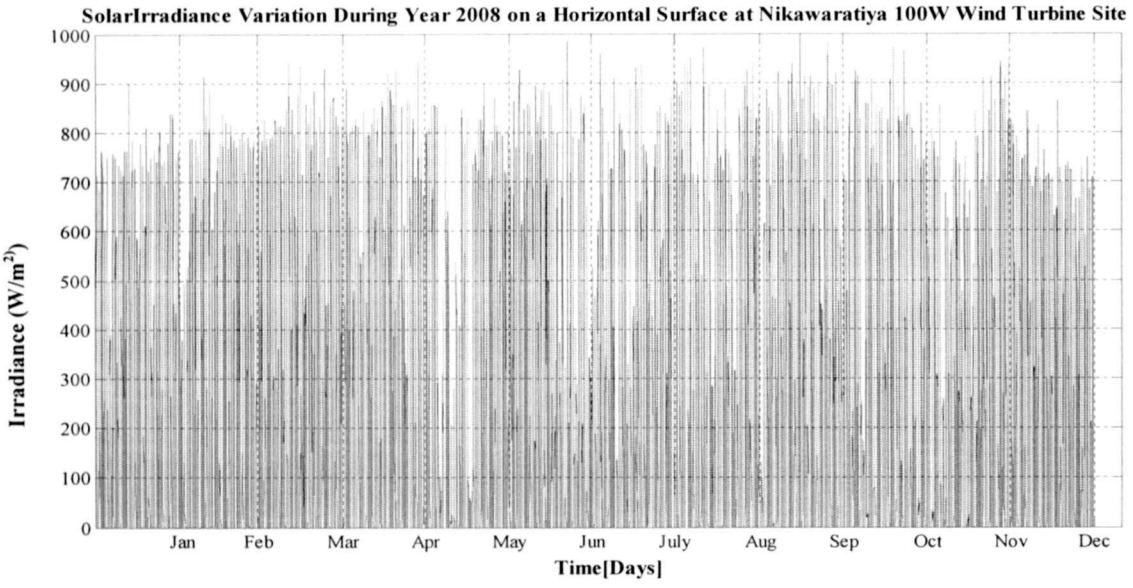

Figure 3.7: Hourly average solar irradiation variation throughout the year 2008

According to the monthly power generation data as shown Table 3.2 the NERDC 100W wind turbine system cannot fulfil the energy requirement at least even in one place of above site locations in Nikawaratiya area. The environmental conditions and annual monsoon wind direction changes are the main reasons for this situation. However, the wind and solar resources suffer from their intermittent nature and thus are not predictable in a deterministic sense, since frequently undergo rapid fluctuation.

The hybrid system proposed consists of a 100W NERDC wind turbine and photovoltaic array as main energy sources with possibility to incorporate this site condition.

Chapter 4

Wind Turbine Model & MPPT Controller

Variable – speed wind turbines are generally characterized as having higher efficiency than fixed – speed wind turbines and hence are becoming more popular, particularly for small wind turbines. Normally, variable – speed wind turbines are aerodynamically controlled, usually by using power electronics to regulate the torque and speed of the turbine in order to maximize the output power. Variable – pitch aerodynamically controlled wind turbines are more costly and complex.

NERDC 100W wind turbine has being designed for variable wind conditions with constant pitch as a passive controlled machine. Therefore, variable – speed fixed approach is becoming more popular for low cost construction and is the most common scheme for small wind turbines. In this scheme, a MPPT control mechanism is used to control the restoring torque of the electrical generator for optimum operation of the wind turbine system [22]. The performance of variable – speed fixed – pitch wind turbines could be optimized without a need of a complex aerodynamic control. These turbines are normally operated on the relevant optimum points of wind rotor curve and electrical generator curve coincide, as shown in Figure 4.1. Therefore, in order to obtain maximum output power from the turbine, it is necessary to drive it at an optimal rotor speed for a particular wind speed.

4.1 Control Strategies

The maximum power point tracking (MPPT) control mechanism is used to control the restoring torque of the electrical generator for optimum operation of the wind turbine system [22]. The performance of variable – speeds and fixed – pitch wind turbines could be optimized without a need of a complex aerodynamic control [43]. In these turbines the relevant optimum points of wind rotor curve which gives MPPT coincide, as shown in Figure 4.1.Therefore, in order to obtain maximum output power from the turbine, it is necessary to drive it at the optimal rotor speed for a particular wind speed.

The wind speed, the turbine rotational speed and the turbine rotor characteristics are the main factors that determine the maximum power point. The electrical generator characteristics may be used in order to control the restoring torque to track the optimum operation points. If the wind speed varies from V_1 to V_4, the rotor speed should change from ω_1 to ω_4 for optimum operation of the wind turbine. However, rotational speed of the wind turbine cannot change instantaneously. Usually, a controller that occupy wind speed sensor (anemometers) is used to control the wind turbine. In systems that employ wind speed sensor, the sensor provides the reference signal to the MPPT controller

[49]. This reference is compared with the power extracted from the wind energy converter. In a sensor less control technique no anemometer is used to provide the wind speed information [50]. Hence, it is essential to estimate the wind speed. The generator output frequency and power or torque mapping techniques are used to track the MPP [33]. Another way for MPP tracking is the use of 'searching' method, which is a suitable strategy for small wind turbines [20-51]. The output power is used as feedback signal for the perturbation & observation (hill climbed) algorithm, which is used to find the maximum power point of the system.

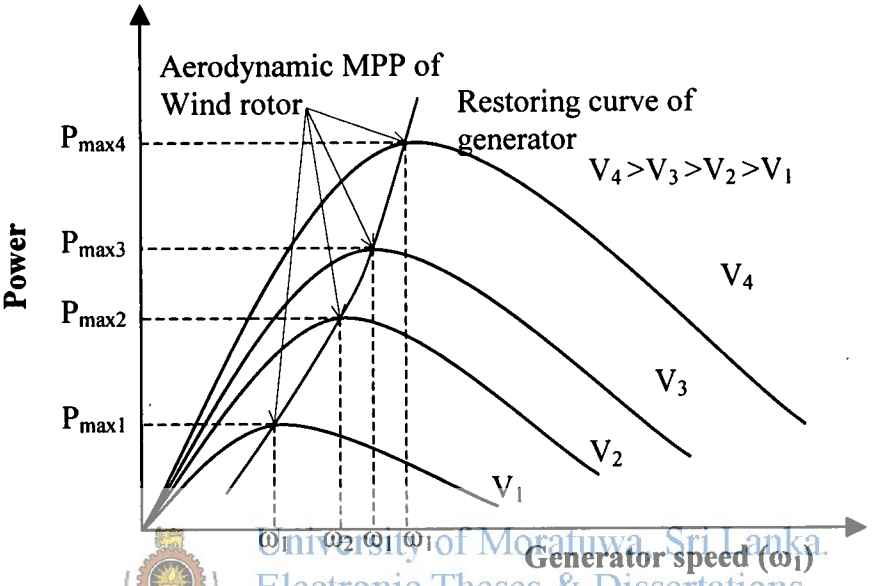

Figure 4.1: Operating point of the wind turbine with MPPT

4.2 Aerodynamic Characteristics of the Rotor

Based on the wind turbine rotor aerodynamic behavior, the turbine grasps only a part of the kinetic energy of the wind [17], shown in equation 4.1.

$$P_a = \frac{1}{2}\rho\pi R^2 v^3 C_p \tag{4.1}$$

Where P_a is captured power by the rotor, R is the radius of the rotor, ρ is the air density and v is the speed of the incident wind. The proportion of the useful power is defined by the power coefficient C_p, which is for a given wind rotor depending on the pitch angle of the rotor blades and the tip speed ratio (λ) defined as equation 4.2.

$$\lambda = \frac{\omega.R}{v_s} \tag{4.2}$$

Where, ω is the rotational speed of the wind rotor

The rotor aerodynamic characteristics are represented by the C_p - λ relationship. C_p has a maximum value at the optimal tip speed ratio value (λ_{opt}). Near the optimum tip speed ratio, the power extraction is maximal at any wind speed that results in the maximum power coefficient. When wind speed varies in variable speed wind turbines the rotor

speed should be adjusted proportionally to maintain optimum tip speed ratio for maximum power extraction. Using Equation 4.3 and 4.4 aerodynamic torque (T_a) from a wind rotor can be obtained as follows

$$T_a = \frac{1}{2}\rho\pi R^3 v^3 \frac{C_p}{\lambda} \tag{4.3}$$

$$T_a = \frac{1}{2}\rho\pi R^3 v^3 C_r \tag{4.4}$$

Where $\lambda = \frac{\omega.R}{v}$

Where C_T is the torque coefficient and T_a is aerodynamic torque of rotor.
The C_p & C_T - λ relationship of the wind turbine is shown in Figure 4.2.

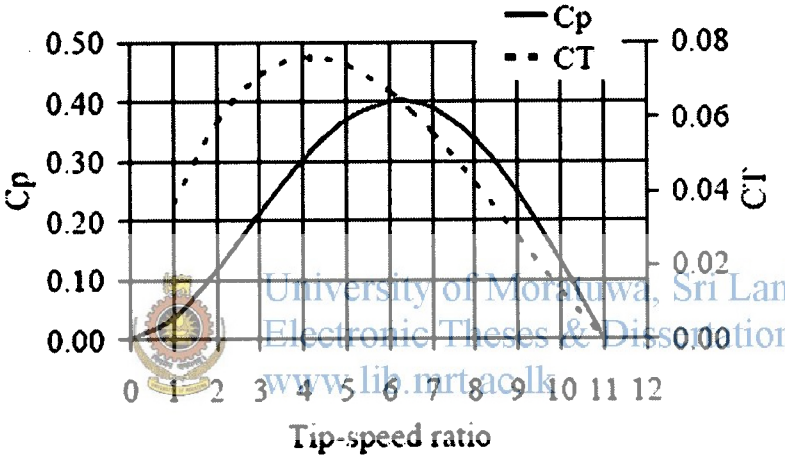

Figure 4. 2: Wind rotor characteristics

The aerodynamic torque of a wind turbine is function of wind speed (v) and rotational speed (ω) of the rotor as given in equation 4.5. For wind turbine-generator systems with a gearbox, the mechanical torque (the torque supplied to the generator) can be expressed as

$$T = K.f(v.\omega) \tag{4.5}$$

Where, K is the gear ratio of the gearbox.

NERDC 100W small-scale wind turbine generator with a fiberglass wind rotor is directly coupled with PMG and there is no gearbox and hence K=1.

4.3 Permanent Magnet Generator (PMG) Model

Small-scale variable speed wind turbines are equipped with a permanent magnet generator [46]. However DC motors are usually preferable due to their reliability, durability, low cost, voltage characteristics, positive convention coefficients between electrical and mechanical parts, sizing and design flexibility.

A permanent magnet DC motor converts electrical power provided by a voltage source to mechanical power provided by a spinning rotor by means of magnetic. The equitant circuit of a PMG is illustrated in Figure 4.3. The armature coil of the DC motor can be presented by an inductance (L_m) in series with resistance (R_m) in series with induced voltage (e_m), which opposes the voltage source [12]. A differential equation for the equivalent circuit can be derived by using Kirchoff,s voltage law around the electrical loop.

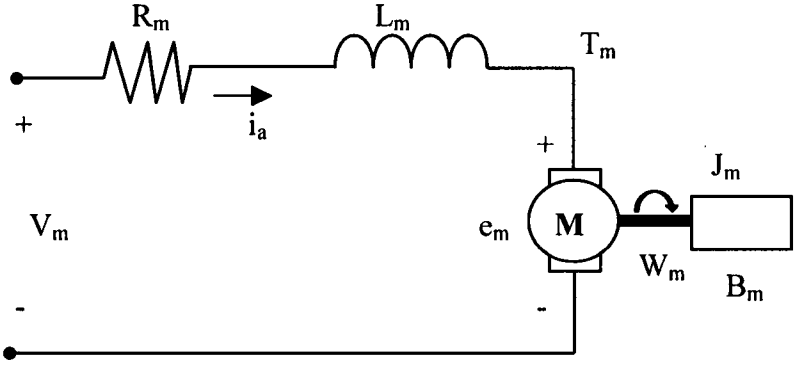

Fig 4.3: The equitant circuit of DC motor

The differential equations into state space form for the armature current and angular velocity can be written by equation 4.6.

$$\frac{d}{dt}\begin{bmatrix} i_a \\ \omega_m \end{bmatrix} = \begin{bmatrix} -\frac{R_m}{L_m} & \frac{K}{L_m} \\ \frac{K_t}{J} & -\frac{B}{J} \end{bmatrix}\begin{bmatrix} i_a \\ \omega_m \end{bmatrix} + \begin{bmatrix} \frac{1}{L_m} & 0 \\ 0 & -\frac{1}{J} \end{bmatrix}\begin{bmatrix} V_m \\ T_l \end{bmatrix} \quad (4.6)$$

The load torque is given by equation 4.7.

$$T_L = K_o + K_1\omega_m + K_2\omega_m^2 \quad (4.7)$$

The nonlinear inertia and viscous friction B have the following variable non-liner forms written by equation 4.8 and 4.9

$$B_m = B_o + B_1\omega_m + B_2\omega_m^2 \quad (4.8)$$

$$J_m = J_o + J_1\omega_m + J_2\omega_m^2 \quad (4.9)$$

Restoring Torque of the Generator

Restoring torque of an electric generator can be derived from the electromagnetic torque developed by the rotor shaft of generator. The generator torque (which is define as a negative motor torque) is a function of generator current *(I_G)*, magnetic flux linkage and number of pole pairs [37- 49]. For a particular generator, magnetic flux linkage and number of pole pairs are fixed parameters. Therefore, restoring torque of a generator *(Te)* can be varied by controlling the current.

4.4 Maximum Power Point Tracking Control Mechanism

Input mechanical power curve of the electric generator has to be adjusted with the maximum power point of the rotor curves by varying the effective electric load on the generator. The system output power is interlaced with the wind turbine aerodynamic power and rate of change in the mechanically stored energy. As the efficiency of the

electric generator is variable, searching method of estimation of the aerodynamic power from the electric output of wind turbine system is difficult for maximum power point tracking.

$$T_a = J.\dot{\omega} + T_e \tag{4.10}$$

Then,

$$P_a = J.\dot{\omega}\omega + \frac{P_e}{\eta} \tag{4.11}$$

(as $P_e = \eta.T_e.\omega$)

Where, J is moment of inertia of rotating parts, η is the efficiency of the electric generator, T_e and P_e are the restoring torque of a generator and power output of the generator respectively given in equation 4.10 and 4.11.

The function of Maximum power point tracker provides the required load on the generator for optimum operation of the system. A schematic diagram of the maximum power point tracker is shown in Figure 4.4.

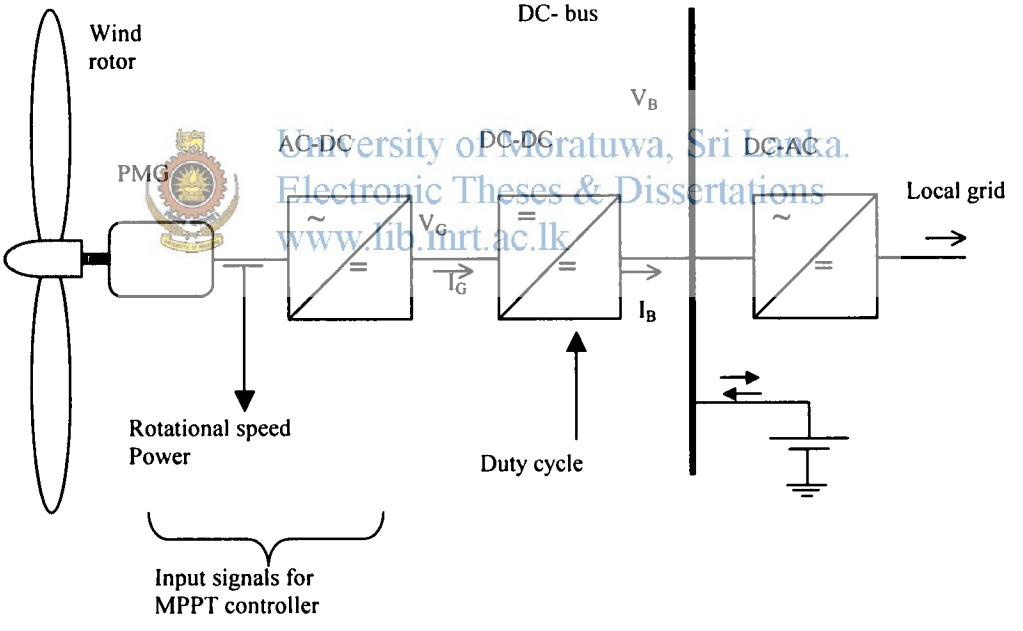

Figure 4 .4: Schematic diagram of small-scale wind power generation system

By considering the Buck/Boost DC-DC converter shown in Figure 4.4

Voltage ratio is given in equation 4.12

$$V_B = -V_G\left(\frac{D}{1-D}\right) \tag{4.12}$$

And the corresponding current is given in equation 4.13

$$I_B = -I_G\left(\frac{1-D}{D}\right) \tag{4.13}$$

Where,

$$D = \left(\frac{T_{on}}{T_{on} + T_{off}} \right) \tag{4.14}$$

V_B is voltage at DC bus, V_G is voltage at generator side, I_B is current flow towards the DC bus, I_G *is* current flow from the generator side Figure 4.4. Since the duty ratio "D" give in Equitation 4.14 is between 0 and 1 the output current and voltage can vary between lower and higher than the input voltage in magnitude. The negative sign indicates a reversal of the output voltage [43].

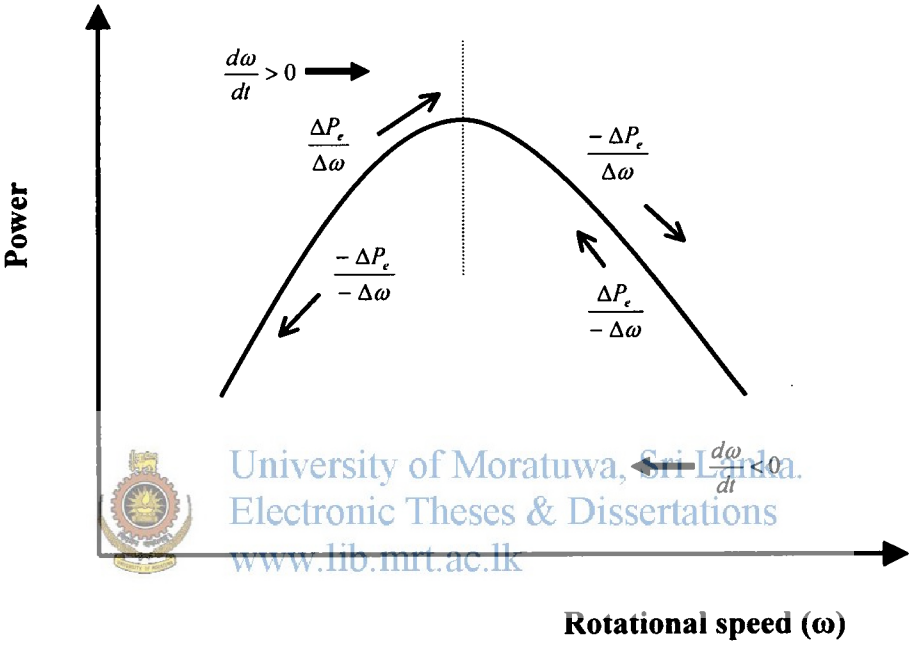

Figure 4.5: Generator restoring torque-controlling criteria

4.4 Fuzzy Logic Controller (FLC)

Fuzzy logic is derived from fuzzy set theory dealing with reasoning that is approximated rather than precisely deduced from classical predicate logic. It can be thought of as the application side of fuzzy set theory is dealing with well thought out real world expert values for a complex problem [55]. Degrees of truth are often confused with probabilities. However, they are conceptually distinct, fuzzy truth represents membership in vaguely defined sets, not likelihood of some event or condition [48] [15].

Fuzzy logic allows for set membership values between and including 0 and 1, and in its linguistic form, imprecise concepts like "slightly", "quite" and "very". Specifically, it allows partial membership in a set. It is related to fuzzy sets and possibility theory [57]. It was introduced in 1965 by Lotfi Zadeh at the University of California, Berkeley.

Fuzzy logic rules are used to control the restoring torque of the electric generator by considering and $dp_e/ d\omega$. The control criterion is demonstrated in Figure 4.5.The FLC adopted in this study is the Mamdani's type. Two inputs for the FLC is $d\omega/dt$, $dp /d\omega$ and the output of FLC is the Δd are considered. For the fuzzification, two input variables are

normalized first and triangular membership functions are used for easy implementation as shown in Figure 4.6.

For a particular wind speed, rotational speed and power output should be measured by considering time interval 't' and then varying the rate of change value of 'D' (Δd) by using defuzzfication of he FLC employs the centre o gravity method [43].

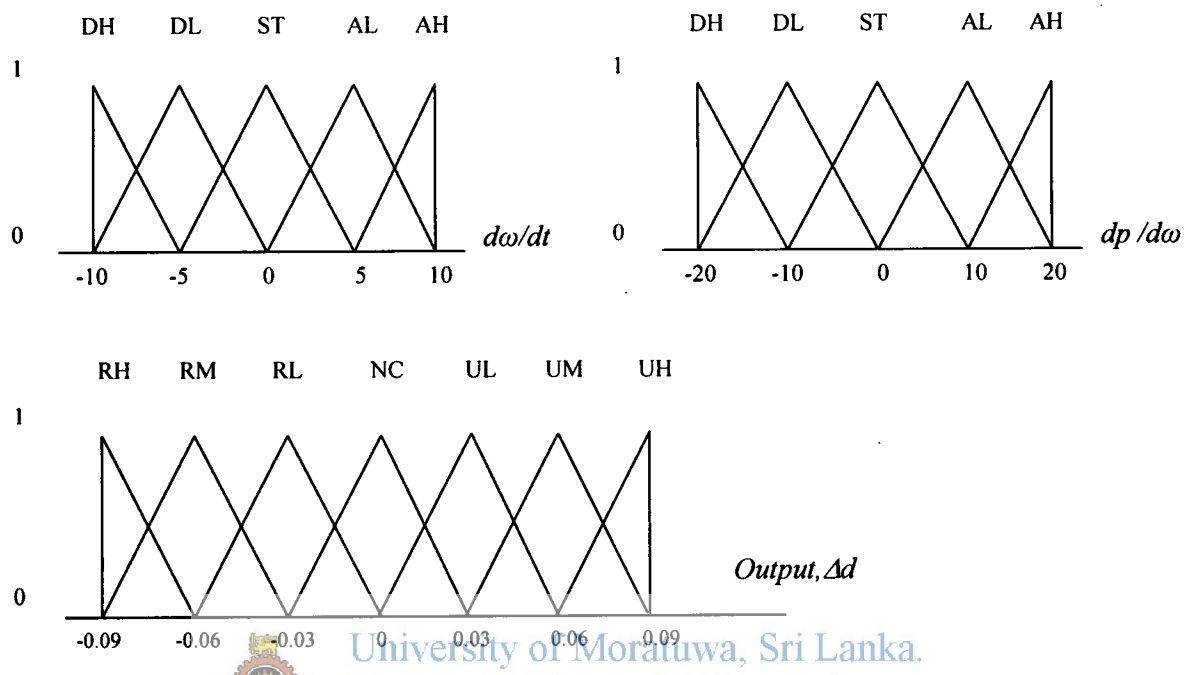

Figure 4.6: Fuzzy logic input and output membership functions

For the fuzzy inference engine, 'IF – THEN' rule with 'AND' logical operator are designed for the fuzzy variable process, and the 'MIN – MAX' method is employed for fuzzy rule implication as Shown in Table 4.1.

Input		Output
dω/dt	*dp/dω*	*Δd*
DH	DH	NC
DL	DH	UM
ST	DH	NC
AL	DH	UM
AH	DH	UH
DH	DL	UM
DL	DL	NC
ST	DL	NC
AL	DL	UL
AH	DL	UM
DH	ST	NC
DL	ST	NC
ST	ST	NC

Input		Output
dω/dt	*dp/dω*	*Δd*
AL	ST	NC
AH	ST	NC
DH	AL	RM
DL	AL	RL
ST	AL	NC
AL	AL	NC
AH	AL	RM
DH	AH	RH
DL	AH	RM
ST	AH	NC
AL	AH	RM
AH	AH	NC

Table 4.1: Fuzzy logic controller input and output rules

Where;
DH- Decelerate High RM- Reduce Medium
DL- Decelerate Low RL- Reduce Low
ST- Steady NC- Not Change
AL- Accelerate Low UL- Upgrade Low
AH- Accelerate High UM- Upgrade Medium
RH- Reduce High UH- Upgrade High
RM- Reduce Medium
RL- Reduce Low
NC- Not Change
UL- Upgrade Low
UM- Upgrade Medium
UH- Upgrade High

These input and output classes of linguistic rules are characterized by membership functions developed by using MATHLAB Fuzzy toolbox environment as shown if Figure 4.7 and Figure 4.8 shows the surface diagram of all 25 fuzzy rules for the design FLC.

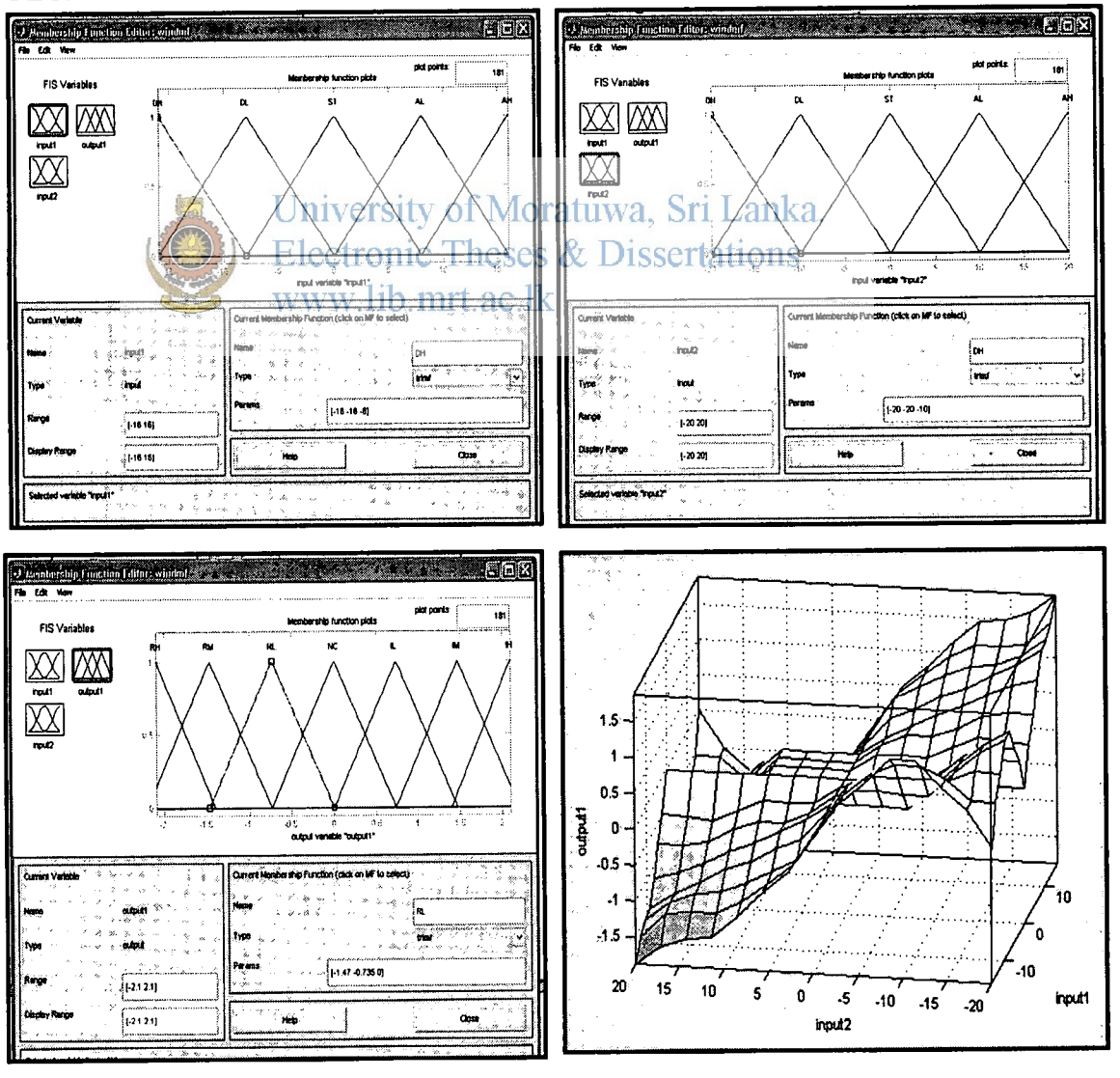

Figure 4.7: Membership functions for fuzzy variables

Figure 4.8: Rule surface of FLC

4.5 Simulink Model of MPPT Controller for Wind Turbine System

The entire 100W wind turbine system was modeled by the MATHLAB Simulik platform using dynamic formulas and component parameters as shown in figure 4.9. Wind speed data was stored with as a 'mat' file and the wind rotor performance enclosed with (2-D) lookup table as shown in Figure 4.10 for the simulation. The rotational speed of the rotor is another input parameter to the (2-D) lookup table. The corresponding torque values can be found from the lookup table while simulating the program [43].

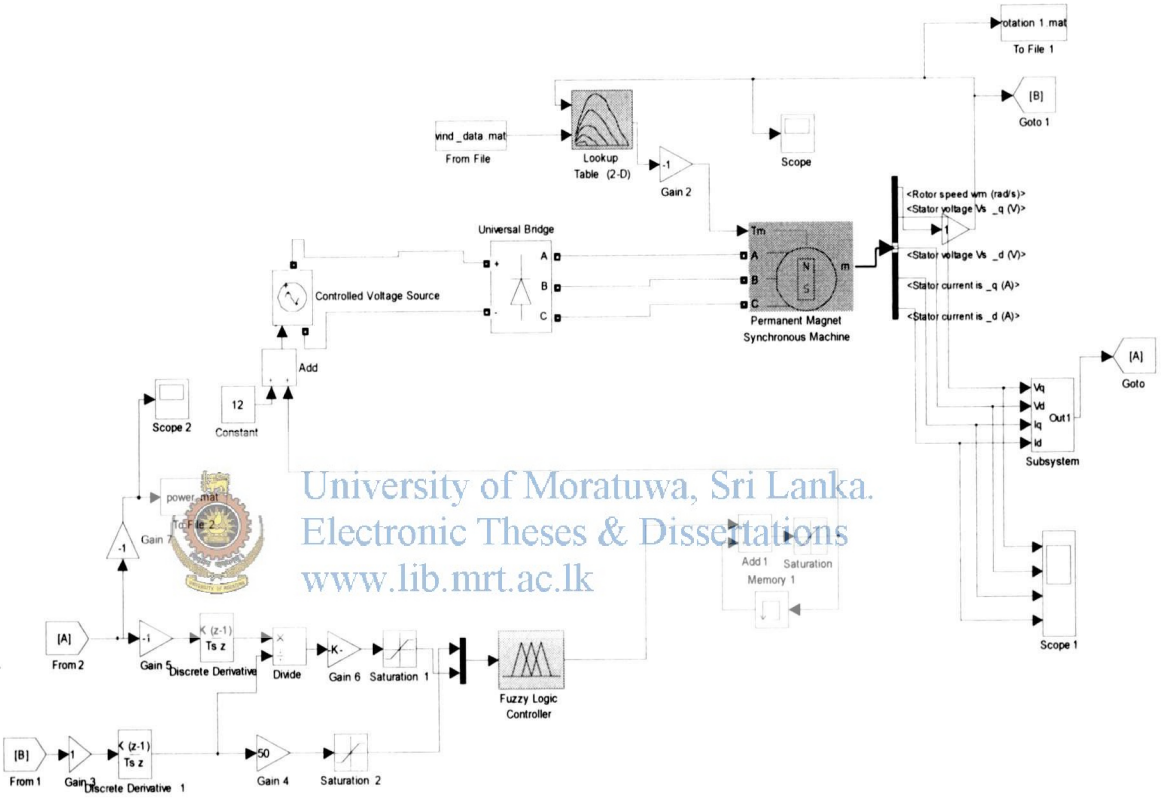

Figure 4.9. MATHLAB Simulink model of the 100W wind power generation system

The membership functions and fuzzy rules of the FLC developed by the MATHLAB are exported to the fuzzy logic block, which is used in simulink platform.

Fuzzy logic controller block membership function parameter of the MPPT controlling system was loaded from the 'FIS' file generated with MATHLAB flat form. Figure 4.11 shows the 'windmf' file loaded to the fuzzy logic controller of the system [4].

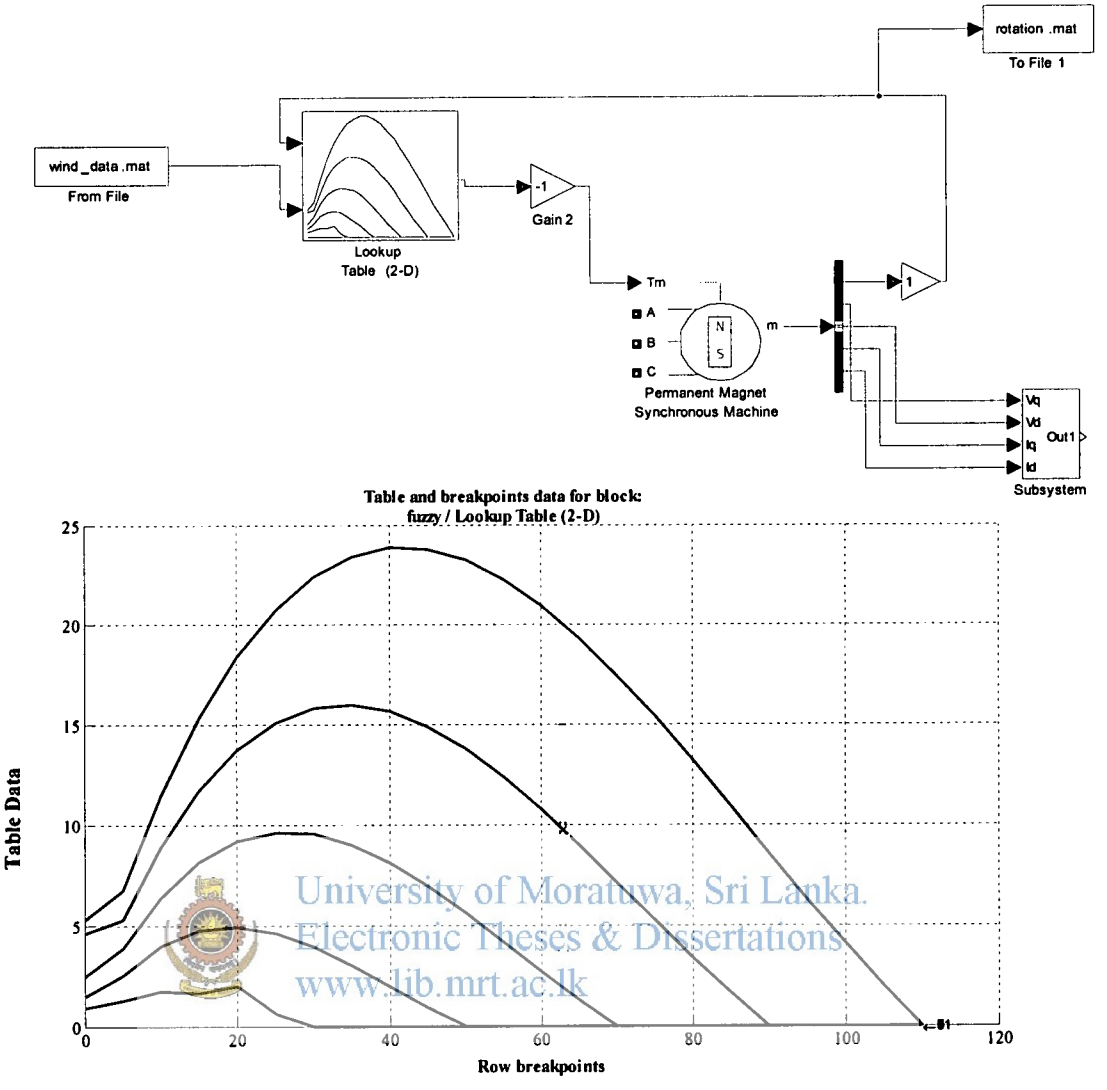

Figure 4.10: Simulink Block Parameters and Arrangement of (2-D) Lookup Table

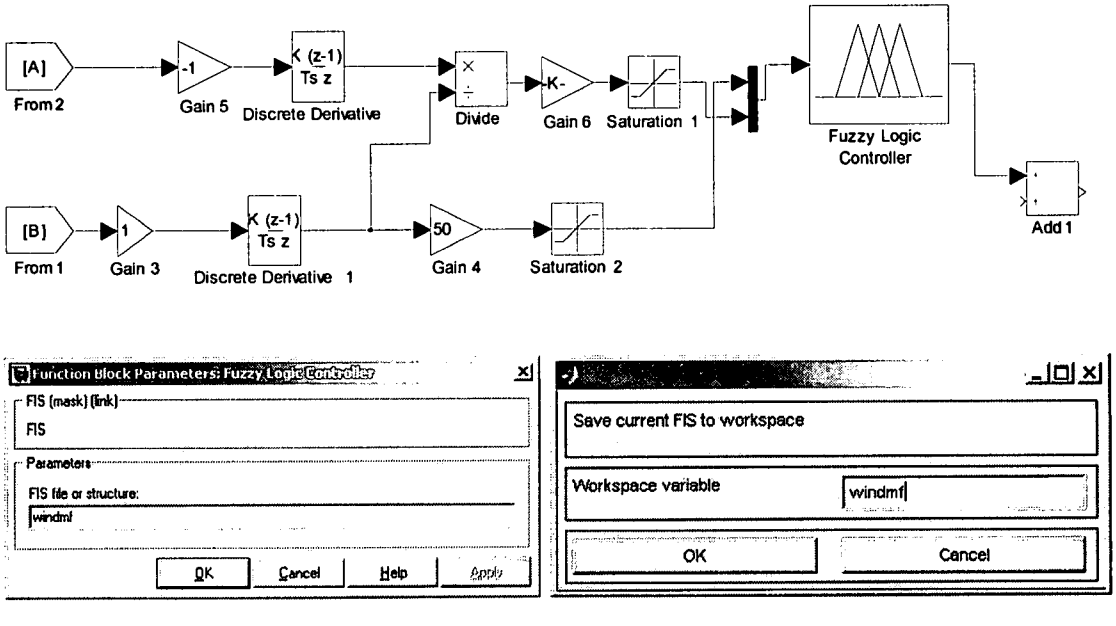

Figure 4.11: Fuzzy Logic Controller and Function Block Parameters

Synchronous machine block is used in simulink Simpower system toolbox as a permanent magnet generator (PMG) and the block parameter of permanent magnet Synchronous machine is shown in Figure 4.12 [44].

The simulation parameters of the Synchronous machine block were changed according to the NERDC 100W PMG specifications. Other simulink / simpower block parameters were changed by considering the operation of the small-scale 100W wind turning system.

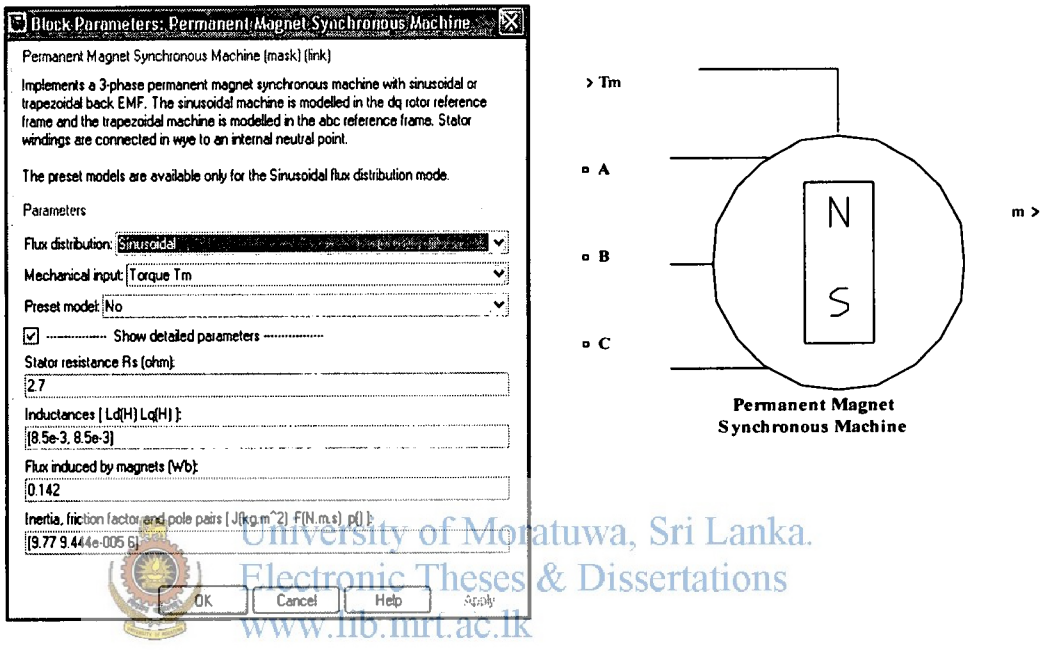

Figure 4.12: Block parameters of the permanent magnet generator (PMG)

A small wind turbine design at the National Engineering Research & Development Centre (NERDC) in Sri Lanka was simulated in MATHLAB / Simulink using measured wind speed data in a turbulent wind conditions. Performance of system with the Fuzzy Logic controller and fixed voltage system were compared. Simulated wind turbine system performances are shown in Figure 4.13 – 4.17.

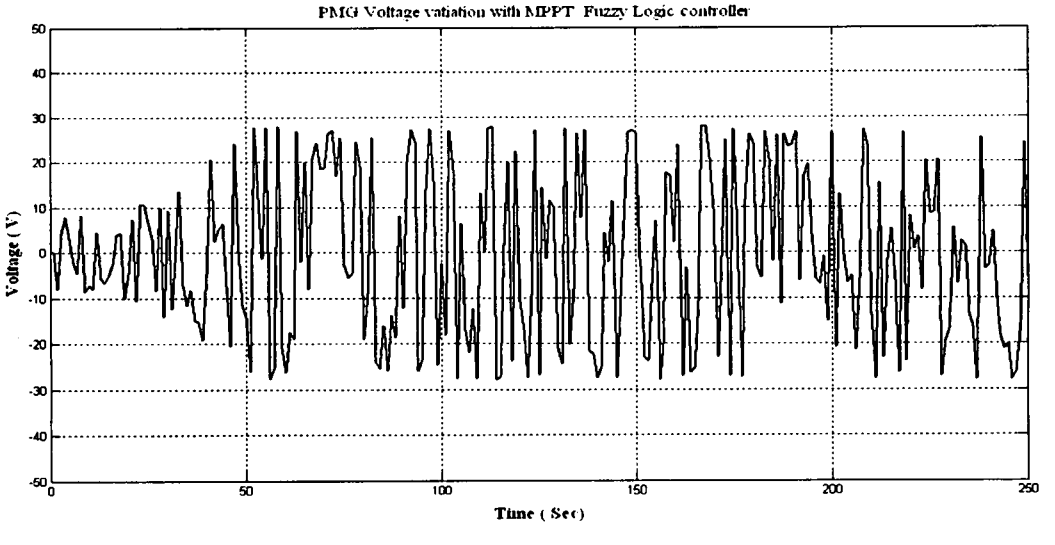

Figure 4.13: Shows PMG Voltage Variation with Fuzzy Logic Controller

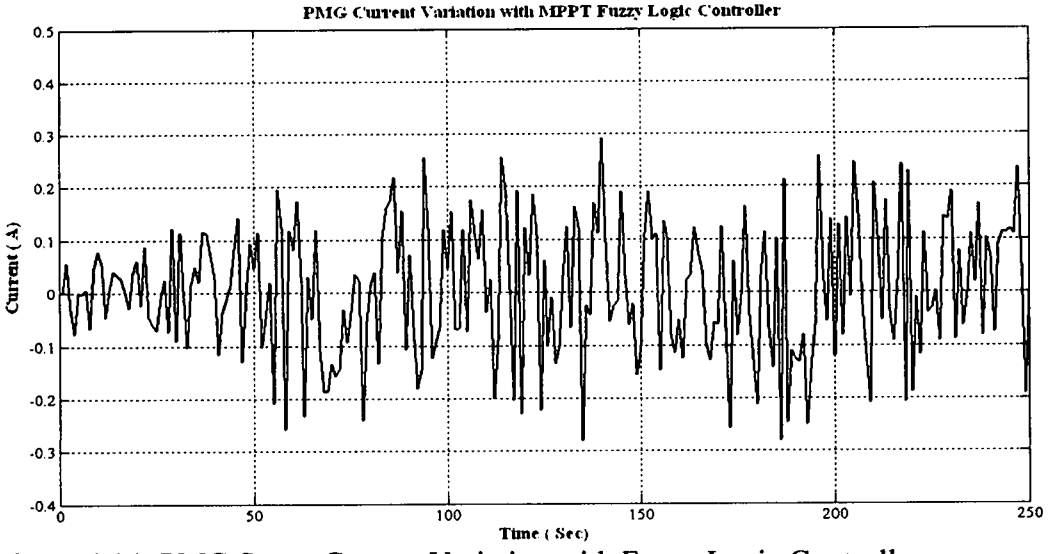

Figure 4.14: PMG Stator Current Variation with Fuzzy Logic Controller

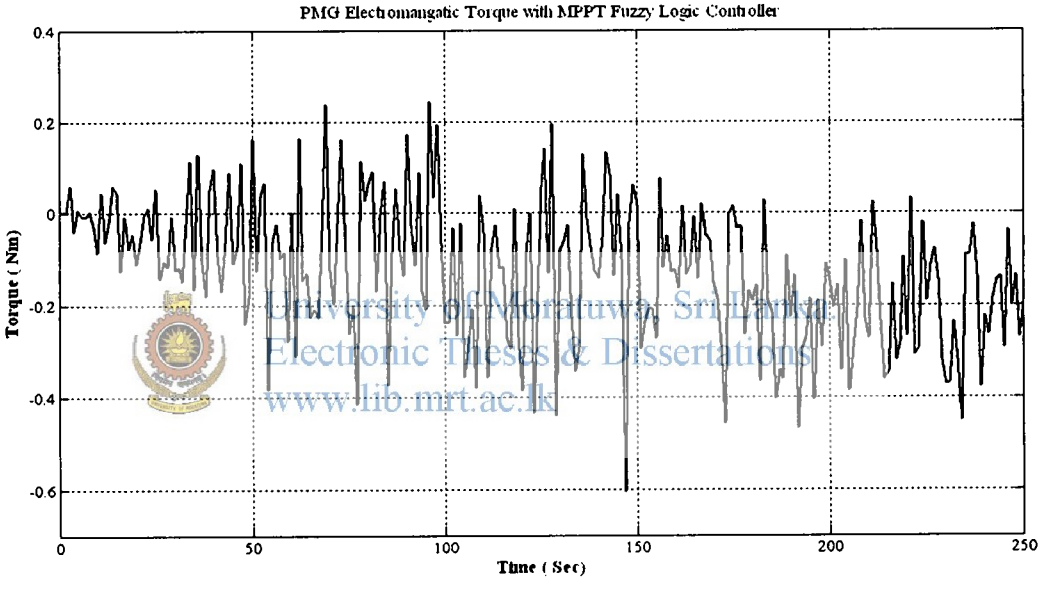

Figure 4.15: PMG Stator Current Variation with Fuzzy Logic Controller

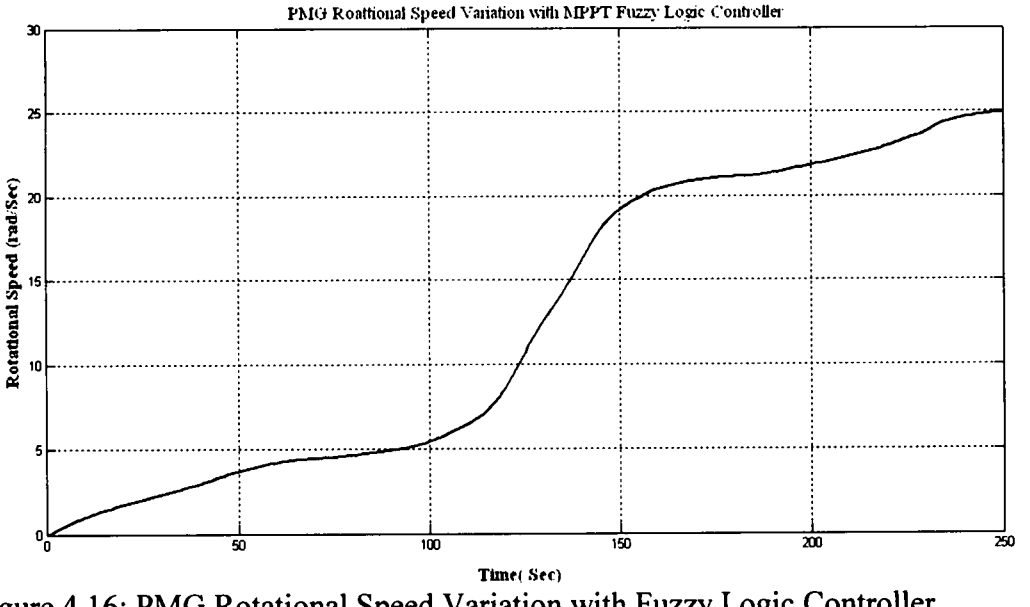

Figure 4.16: PMG Rotational Speed Variation with Fuzzy Logic Controller

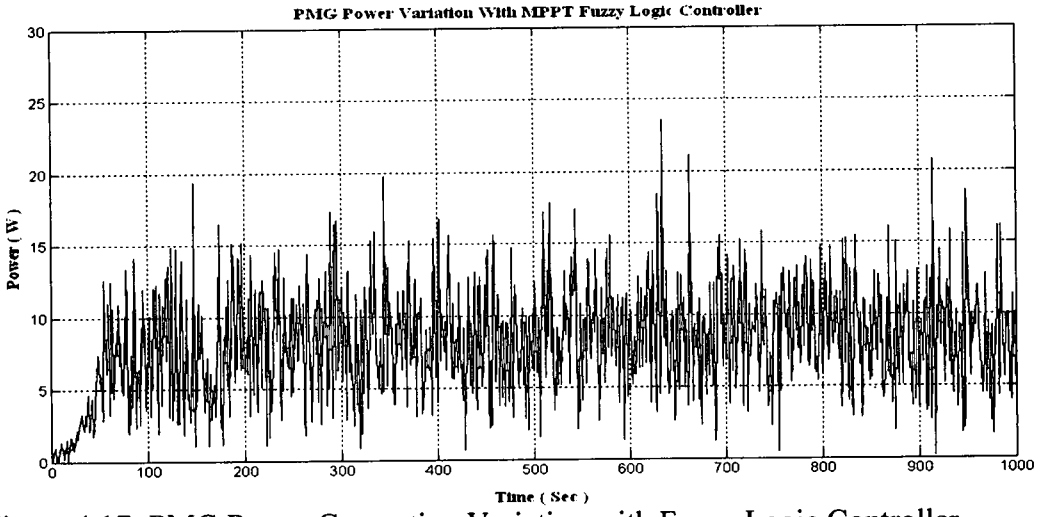

Figure 4.17: PMG Power Generation Variation with Fuzzy Logic Controller

Simulated results show that system with Fuzzy Logic controller performs better than that of with fixed voltage system. With the given wind speed data, energy output over 1000 s period is 1673.95 J with Fuzzy controller and 593.73 J with a fixed voltage controller. Figure 4.18 show that 35% more energy can be generated by the system with a Fuzzy controller.

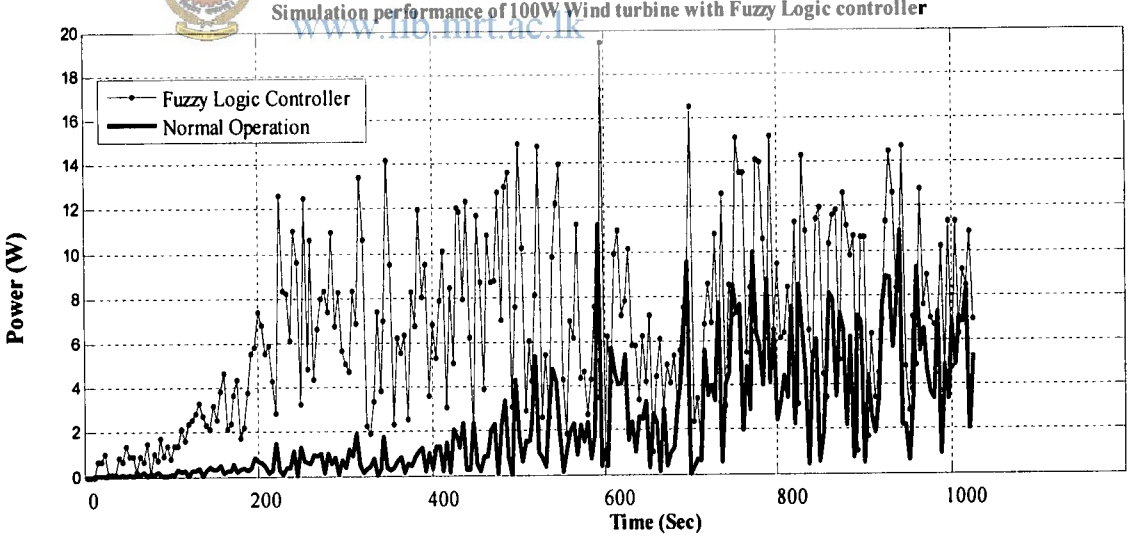

Figure 4.18: Shows the simulation characteristics of 100W wind turbine with Fuzzy controller

Chapter 5

Photovoltaic Module

The history of PV dates back to 1839 when a French physicist, Edmund Becquerel, discovered the first photovoltaic effect when he illuminated a metal electrode in an electrolytic solution [36]. Thirty-seven years later British physicist, William Adams with his student Richard Day, discovered a photovoltaic material selenium and made solid cells with 1~2% efficiency which was soon widely adopted in the exposure meters of camera [36].

In 1954 the first generation of semiconductor silicon-based PV cells was born with efficiency of 6% [13] and adopted in space applications. Today, the production of PV cells is following an exponential growth curve since technological advancement of late '80s that has started to rapidly improve efficiency and reduce cost.

This chapter discusses the fundamentals of PV cells and modeling of a PV cell using an equivalent electrical circuit. The models are implemented using MATLAB to study PV characteristics and simulated a real PV module [38].

5.1 Photovoltaic Cell

Photons of light with energy is higher than the band-gap energy of PV material that can make electrons in the material break free from atoms that hold them and create hole-electron pairs, as shown in Figure 5.1. These electrons however, will soon fall back into holes causing charge carriers to disappear. If a nearby electric field is provided, those in the conduction band can be continuously swept away from holes toward a metallic contact where they will emerge as an electric current. The electric field within the semiconductor itself at the junction between two regions of crystals of different type is called a *p-n* junction [36].

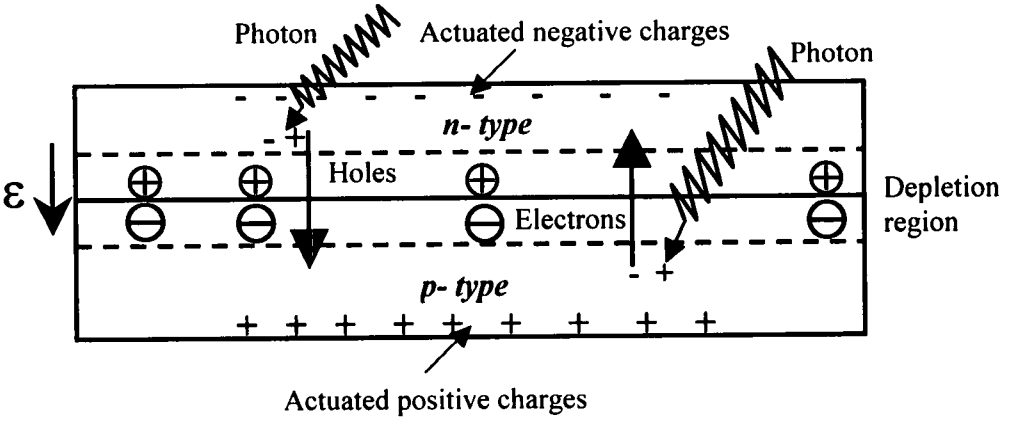

Figure 5.1: Illustration of the p-n junction of PV cell

The PV cell has electrical contacts on its top and bottom to capture the electrons, as shown in Figure 5.2. When the PV cell delivers power to the load, the electrons flow out of the *n-side* into the connecting wire, through the load and back to the *p-side* where they recombine with holes [36]. Note that conventional current flows in the opposite direction from electrons.

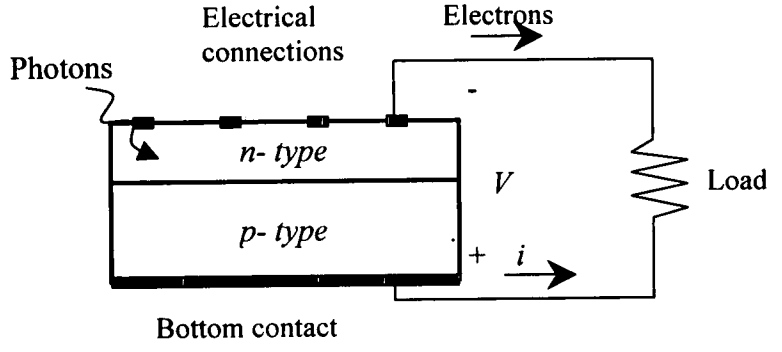

Figure 5.2: Side view of solar cell and the conducting current

5.2 Modeling a PV Cell

The use of equivalent electric circuits makes it possible to model characteristics of a PV cell. The method used here is implemented in MATLAB programs for simulations. The same modeling technique is also applicable for modeling a PV module.

5.2.1 The Simplest Model

The simplest model of a PV cell is shown in Figure 5.3.An equivalent circuit below that consists of an ideal current source in parallel with an ideal diode. The current source represents the current generated by photons (often denoted as I_{ph} or I_L), and its output is constant under constant temperature and constant incident radiation of light.

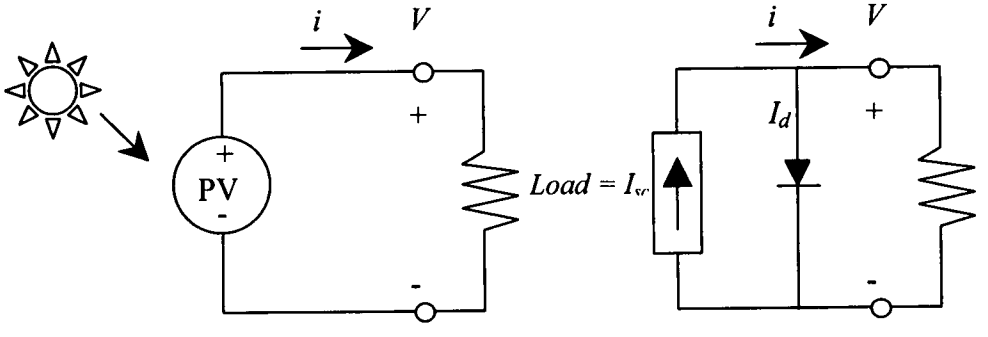

Figure 5.3 : PV cell simple equivalent circuit with load

There are two key parameters frequently used to characterize a PV cell. Shorting together the terminals of the cell, as shown in Figure 5.4 (a), the photon generated current will follow out of the cell as a short-circuit current (I_{sc}). Thus, $I_{ph} = I_{sc}$. As shown in Figure 5.4 (b), when there is no connection to the PV cell (open-circuit), the photon-generated current is shunted internally by the basic p-n junction diode. This

gives the open circuit voltage (V_{oc}). The PV module or cell manufacturers usually provide the values of these parameters in their datasheets.

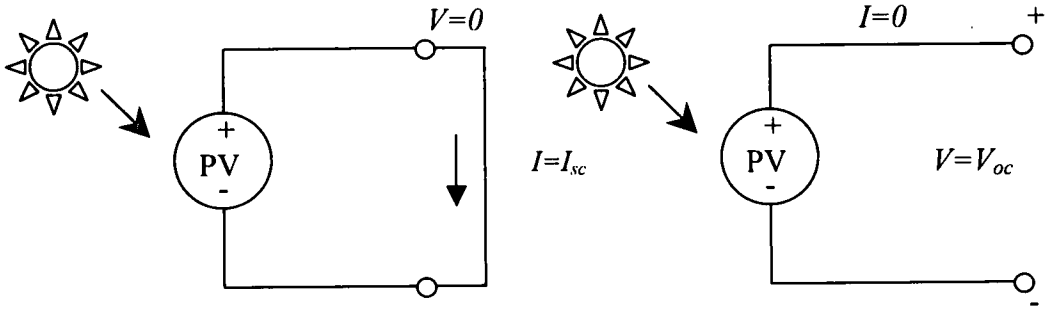

(a) Short - circuit current (b) Open – circuit voltage

Figure 5.4: Shows a short – circuit and an open – circuit PV cell condition

The output current (I) from the PV cell is found by equation 5.1 applying the Kirchoff's current law (KCL) on the equivalent circuit shown in Figure 5.3.

$$I = I_{sc} - I_d \tag{5.1}$$

Where: I_{sc} is the short-circuit current that is equal to the photon generated current, and I_d is the current shunted through the basic diode. The diode current I_d is given by the Shockley's diode equation 5.2

$$I_d = I_o(e^{qV_d/KT} - 1) \tag{5.2}$$

Where: I_o is the reverse saturation current of diode (A),
q is the electron charge ($1.602 \times 10^{-19}\ C$),
V_d is the voltage across the diode (V),
k is the Boltzmann's constant ($1.381 \times 10^{-23}\ J/K$),
T is the junction temperature in *Kelvin (K)*.

Replacing I_d of the equation (5.1) by the equation (5.2) gives the current-voltage relationship of the PV cell in equation 5.3.

$$I = I_{sc} - I_o(e^{qV/KT} - 1) \tag{5.3}$$

Where: V is the voltage across the PV cell, and I is the output current from the cell.

The reverse saturation current of diode (I_o) is constant under the constant temperature and found by setting the open-circuit condition as shown in Figure 5.4 (b). Using the equation (5.3), let $I = 0$ (no output current) and solve for I_o.

$$0 = I_{sc} - I_o(e^{qV_{oc}/KT} - 1) \tag{5.4}$$

$$I_{sc} = I_o(e^{qV_{oc}/KT} - 1) \tag{5.5}$$

$$I_o = \frac{I_{sc}}{(e^{qV_{oc}/KT} - 1)} \tag{5.6}$$

To a very good approximation, the photon-generated current, which is equal to I_{sc}, is directly proportional to the irradiance, the intensity of illumination, to PV cell [38]. Thus, if the value, I_{sc}, is known from the datasheet, under the standard test condition, G_o=1000W/m_2 at the air mass (AM) = 1.5, then the photon generated current at any other irradiance, G(W/m_2) is given by equation 5.7

$$I_{sc}|_G = \left(\frac{G}{G_o}\right) I_{sc}|_{G_o} \tag{5.7}$$

Figure 5.5 shows that current and voltage relationship (often called as an I-V curve) of an ideal PV cell simulated by MATLAB using the simplest equivalent circuit model. The PV cell output is both limited by the cell current and the cell voltage, and it can only produce a power with any combinations of current and voltage on the I-V curve. It also shows that the cell current is proportional to the irradiance.

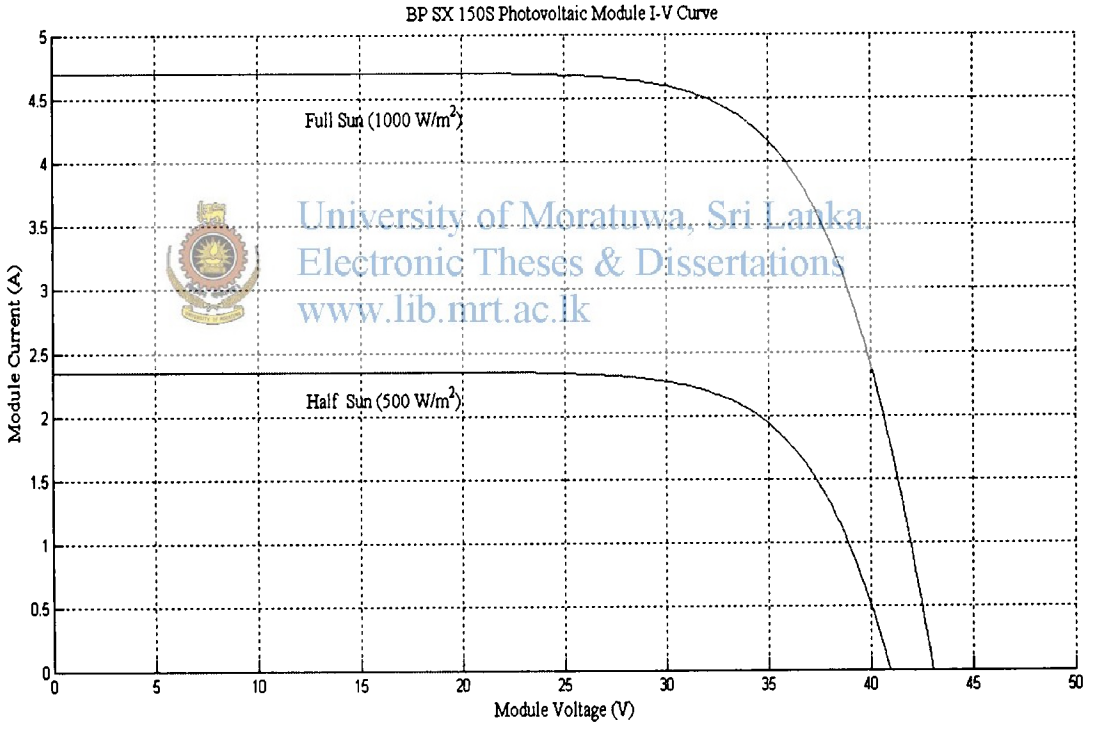

Figure 5.5: I-V plot of ideal PV cell under two different level of irradiance (25^{0}C)

5.2.2 The More Accurate Model

There are a few things that have not being taken into account in the simple model and that will affect the performance of a PV cell in practice.

a) Series Resistance

In a practical PV cell, there is a series of resistance in a current path through the semiconductor material, the metal grid, contacts, and current collecting bus [9]. These resistive losses are lumped together as a series resister (R_s). Its effect becomes very conspicuous in a PV module that consists of many series-connected cells, and the value of resistance is multiplied by the number of cells.

b) Parallel Resistance

This is also called shunt resistance. It is a loss associated with a small leakage of current through a resistive path in parallel with the basic device [9]. This can be represented by a parallel resister (R_P). Its effect is much less conspicuous in a PV module compared to the series resistance and it will only become noticeable when a number of PV modules are connected in parallel for a larger system.

c) Recombination

Recombination in the depletion region of PV cells provides non-ohmic current paths in parallel with the basic PV cell [9] [24]. As shown in Figure 5.6 this can be represented by the second diode ($D2$) in the equivalent circuit.

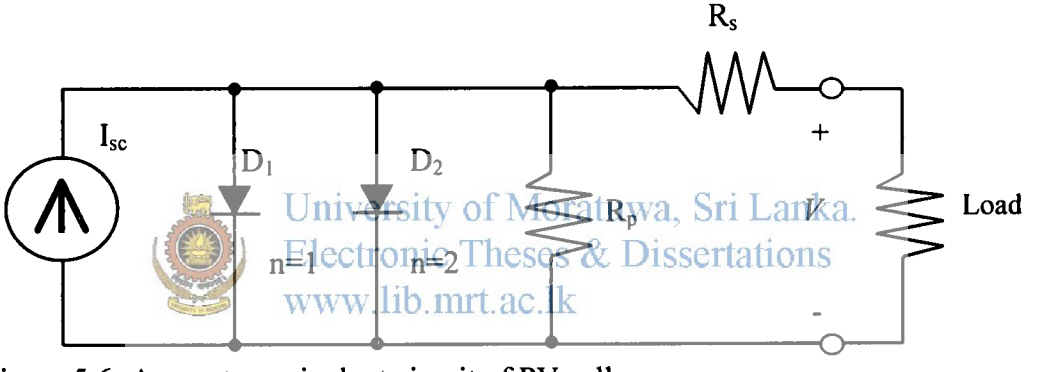

Figure 5.6: Accurate equivalent circuit of PV cell

Summarizing these effects, the current-voltage relationship of PV cell is written as equation 5.8

$$I = Isc - I_{o1}\left[e^{q\left(\frac{V+I.R_s}{KT}\right)} - 1\right] - I_{o2}\left[e^{q\left(\frac{V+I.R_s}{2KT}\right)} - 1\right] - \left(\frac{V+I.R_s}{R_p}\right) \tag{5.8}$$

It is possible to combine the first diode ($D1$) and the second diode ($D2$) and rewrite the equation (5.8) in the following form in equation 5.9.

$$I = Isc - I_o\left[e^{q\left(\frac{V+I.R_s}{nKT}\right)} - 1\right] - \left(\frac{V+I.R_s}{R_p}\right) \tag{5.9}$$

Where n is known as the "ideality factor" ("n" is sometimes denoted as "A") and takes the value between one and two [7].

5.2.3 Photovoltaic Module

A single PV cell produces an output voltage less than 1V, about 0.6V for crystallinesilicon (Si) cells, thus a number of PV cells are connected in series to archive a desired output voltage. When series-connected cells are placed in a frame, it is called as a module. Most of commercially available PV modules with crystalline-Si cells have either 36 or 72 series-connected cells. A 36-cell module provides a voltage suitable for charging a 12V battery and similarly a 72-cell module is appropriate for a 24V battery. This is because most of PV systems used to have backup batteries. However, today many PV systems do not use batteries, for example, grid-tied systems. Furthermore, the advent of high efficiency DC-DC converters has alleviated the need for modules with specific voltages. When the PV cells are wired together in series, the current output is the same as the single cell. But, the voltage output is the sum of each cell voltage, as shown in Figure 5.7.

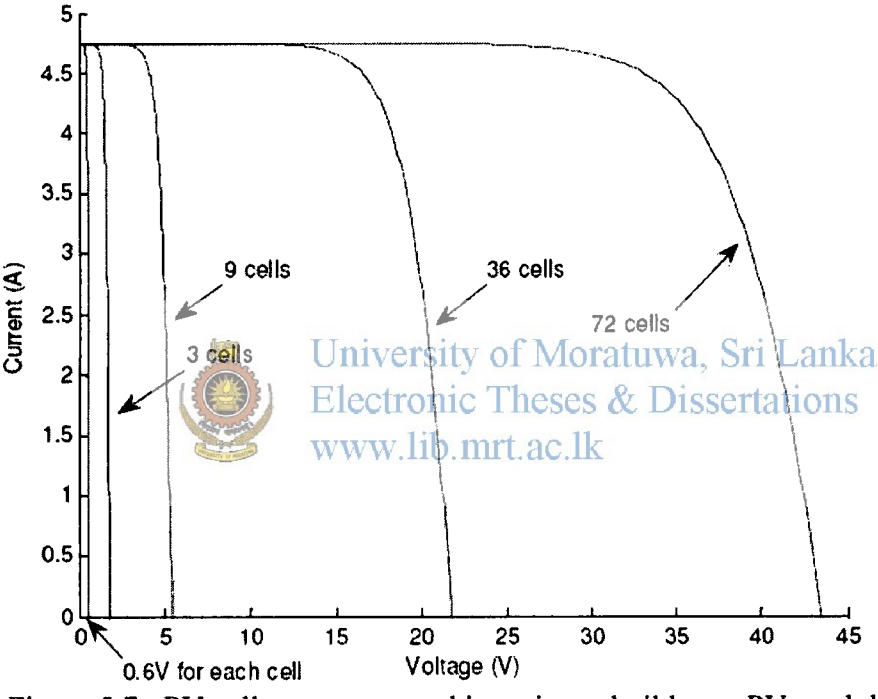

Figure 5.7: PV cells are connected in series to build up a PV module

Also, multiple modules can be wired together in series or parallel to deliver the voltage and current level needed. The group of modules is called an array.

5.3 Modeling a PV Module by MATLAB

BP Solar BP SX 150S PV module, pictured in Figure 5.8, is chosen for a MATLAB simulation model. The module is made of 72 multi-crystalline silicon solar cells in series and provides 150W of nominal maximum power [8]. Table 5.1 shows its electrical specification. The equivalent PV cell for MATHLAB simulation is as shown in Figure 5.9.

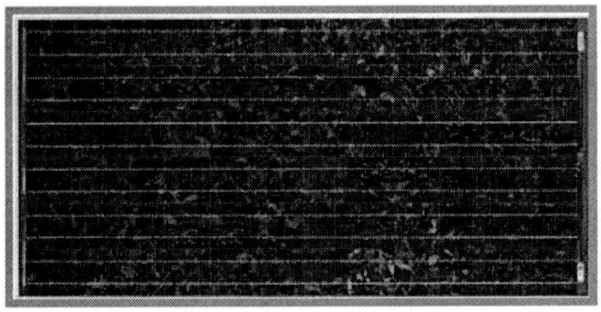

Figure 5.8: shows the 150 W PV module (BP SX 150S)

Electrical Parameters	Specifications
Maximum Power (P_{max})	150W
Voltage at P_{max} (V_{mp})	34.5V
Current at P_{max} (I_{mp})	4.35A
Open – Circuit Voltage (V_{oc})	43.5V
Short – Circuit Current (I_{sc})	4.75A
Temperature Coefficient of I_{sc}	0.065 ±0.015 %/ ^{0}C
Temperature Coefficient of V_{oc}	-160 ±20 mV/ ^{0}C
Temperature Coefficient of power	-0.5 ±0.05 % / ^{0}C
NOCT	47± 2 ^{0}C

Table 5.1: Electrical characteristics data of (BP SX 150S) PV module form the manufacture data sheet

The approach of modeling a PV module is no special from modeling a PV cell. It uses the same PV cell model. All the parameters are the same, but only a voltage parameter (such as the open-circuit voltage) is different and must be divided by the number of cells.

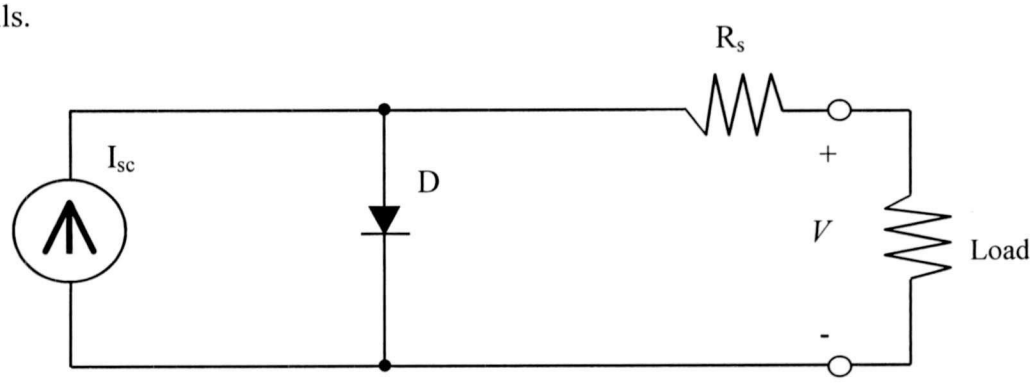

Figure 5.9: Equivalent PV cell circuit used in the MATHLAB simulations

The model consists of a current source (*Isc*), a diode (*D*), and a series resistance (*Rs*). The effect of parallel resistance (*Rp*) is very small in a single module, thus the model does not include it. To make a better model, it also includes temperature effects on the short-circuit current (*Isc*) and the reverse saturation current of diode (*Io*). It uses a single diode with the diode ideality factor (*n*) set to achieve the best *I-V* curve match. *n* is known as the "ideality factor" ("*n*" is sometimes denoted as "*A*") and takes the value between one and two(n=1 ,for the ideal diode) [27]. The diode ideality factor (*n*) is

unknown and must be predicted. After some trials with various diode ideality factors, the MATLAB model chooses the value of n = 1.62 that attains the best match with the *I-V* curve on the datasheet and Figure 5.10 shows the effect of the varying ideality factor.

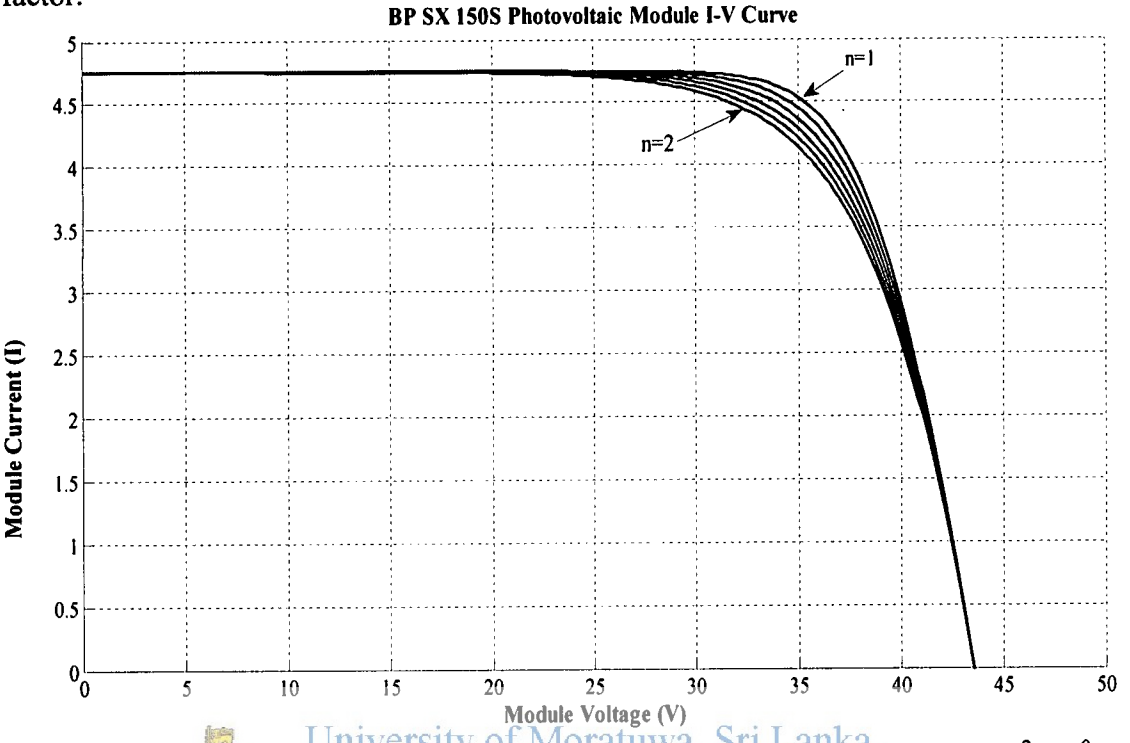

Figure 5.10: Effect of diode ideally factor by MATHLAB simulation at 1kW/m^2 ,25^{0}C

Figure 5.11. Shows the plots of *I-V* characteristics at various module temperatures simulated with the MATLAB model for BP SX 150S PV module. Data points place over on the plots are taken from the *I-V* curves on the manufacturer's specifications.

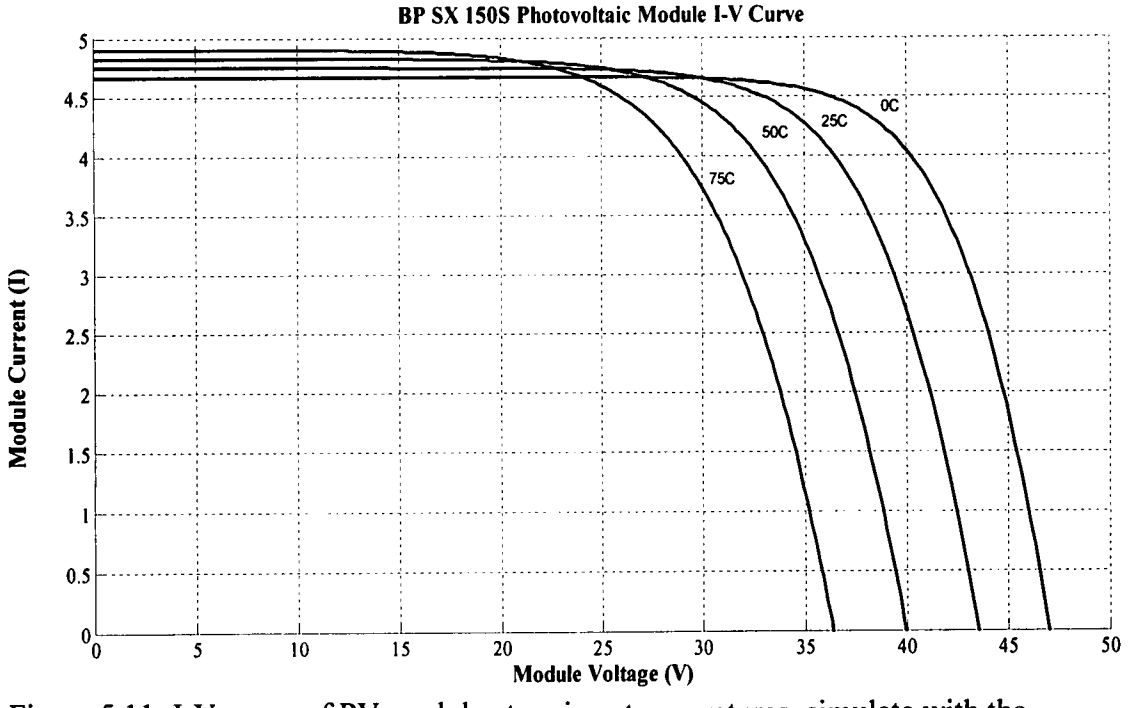

Figure 5.11: I-V curve of PV module at various temperatures, simulate with the MATHLAB (1kW/m^2 ,25^{0}C)

Chapter 6

Maximum Power Point Tracking (MPPT) of Photovoltaic Module

A PV module can generate the power at a point called an operating point anywhere on the I-V curve. There is a single point near the knee of the I-V curve called a maximum power point (MPPT) at which the module operates with the maximum efficiency and generates the maximum output power [26].

Figure 6.1 shows the *I-V* curve of the BP SX 150S PV module simulated with the MATLAB model. The coordinates of the operating point are the operating voltage and current. It is possible to visualize the location of the fitting the largest possible rectangle inside of the *I-V* curve, and its area equal to the output power which is a product of voltage and current [35].

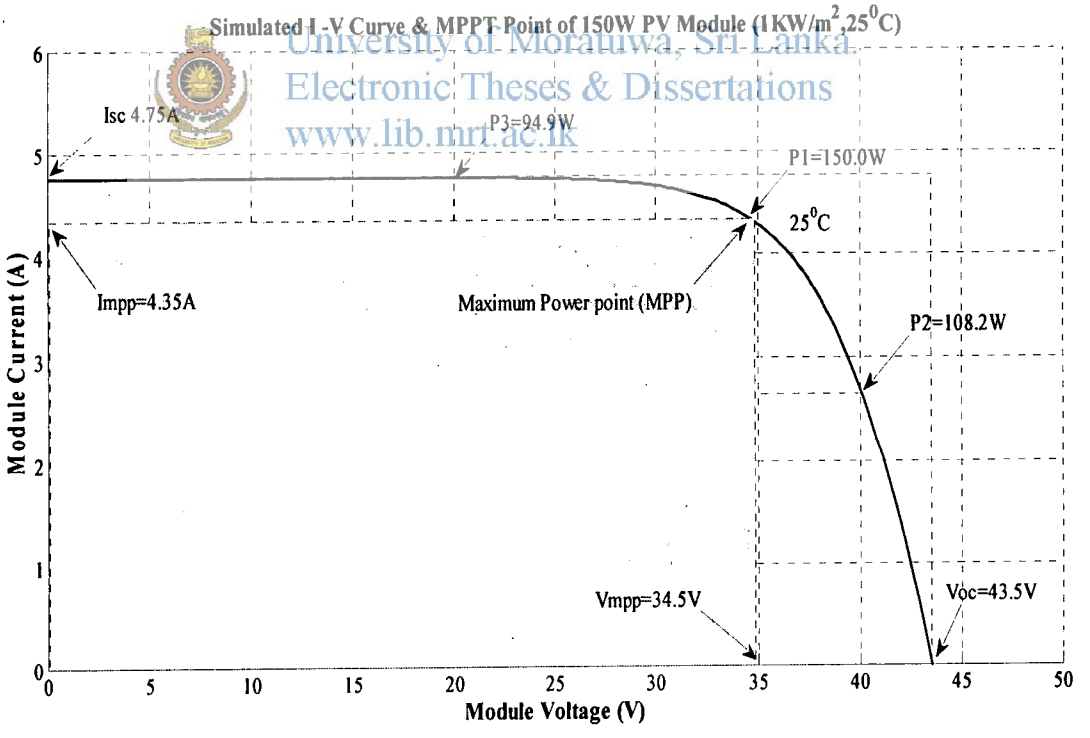

Figure 6.1 : Simulated I-V curve of 150W PV module at (1kW/m^2 , 25^{0}C)

6.1 Maximum Power Point Tracking Algorithm

The MPPT consists of two challenges to be dealt with. One of these is to find out the MPP for the current solar irradiation level and tracking it as the solar irradiations. The PV module generates different peak power points to be tracked. The second part of the problem is more likely a control problem and the objective is to operate the PV module at the MPP by managing loads and backup batteries.

The location of the MPP in the I-V plane is not known earlier and all the time changes dynamically depending on irradiance and temperature level on the PV panel. Figure 6.2 shows a set of PV I-V curves in increasing irradiance at the constant temperature (25^0C), and Figure 6.3 shows the I-V curves at the irradiance values but higher temperature (50^0C). These results show voltage shifts where the MPP occurs. Therefore the MPP needs to be positioned by tracking algorithm, which is the sensing of the MPPT controller.

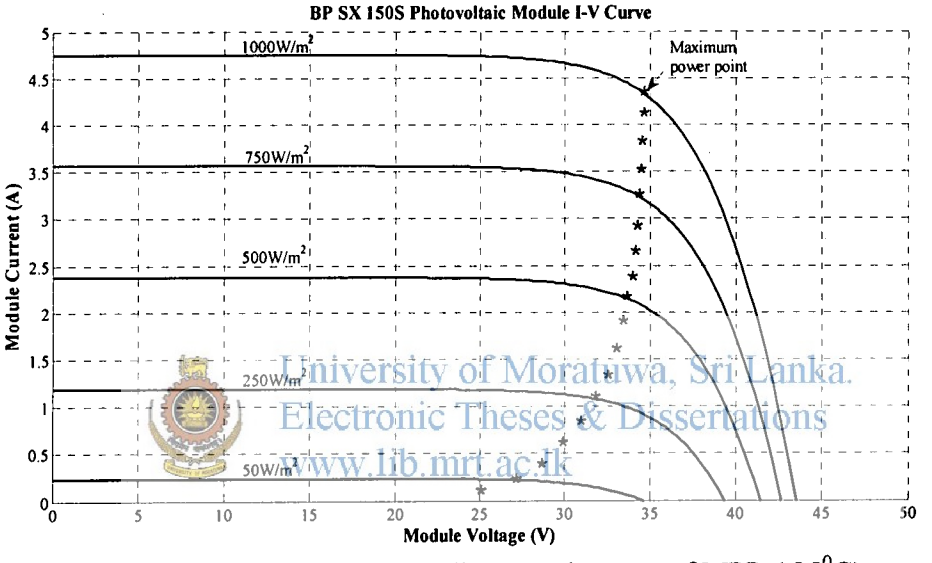

Figure 6.2: I-V curve for varying irradiance and a trace of MPPs(25^0C)

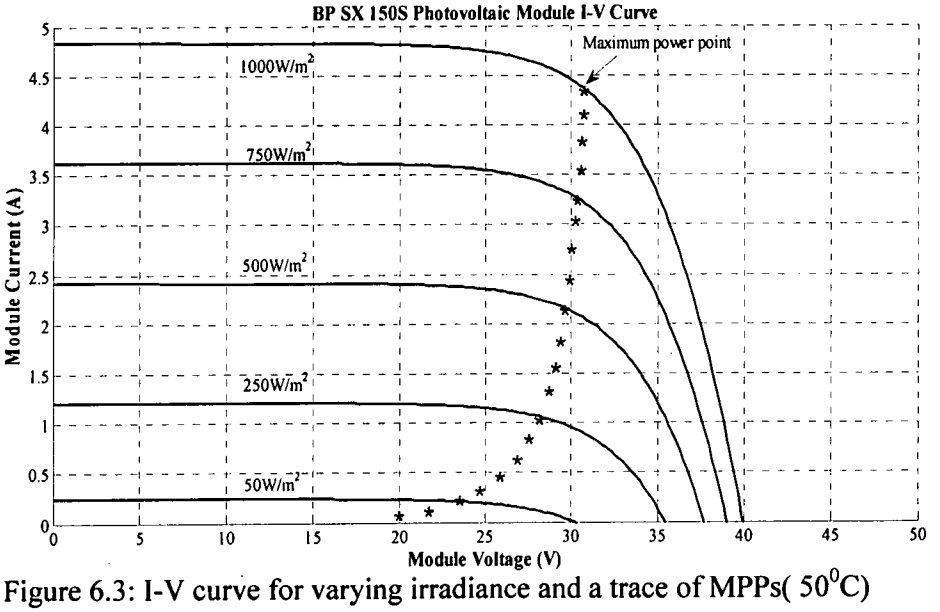

Figure 6.3: I-V curve for varying irradiance and a trace of MPPs(50^0C)

6.2 Perturbation & Observation (P&O) Algorithm

In this study the perturbation & observation (P&O) algorithm identified as the "hill climbing" method is very popular and the most frequently used in practice because of its simplicity in algorithm and the easy of implementation. Figure 6.4 shows a PV module output power curve as a function of voltage (P-V curve) at the constant irradiance and the constant module temperature condition. Assuming the PV module operates at a point which is away from the corresponding MPP. In this algorithm the operating voltage of the PV module is perturbed by a small increment, and the resulting change of power, ΔP ,is observed . If the ΔP value is positive, then it is supposed that it has move the operating point closer to the MPP. Thus, further module voltage perturbations in the same direction should move the operating point towards the MPP. If the ΔP value is negative, the operating point has moved away from the MPP, and the direction of perturbation should be reversed to back toward the MPP. Figure 6.5 shows the trace of MPPs on P-V curves at various irradiance levels and Figure 6.6 shows the flowchart of the P&O algorithm [54].

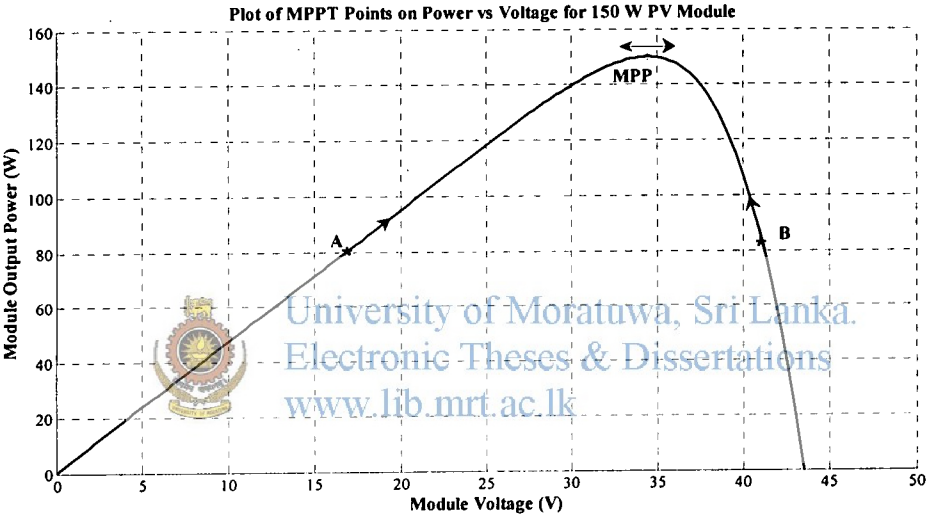

Figure 6.4 : Plot of power Vs voltage for PV module (1kW/m^2 ,25^{0}C)

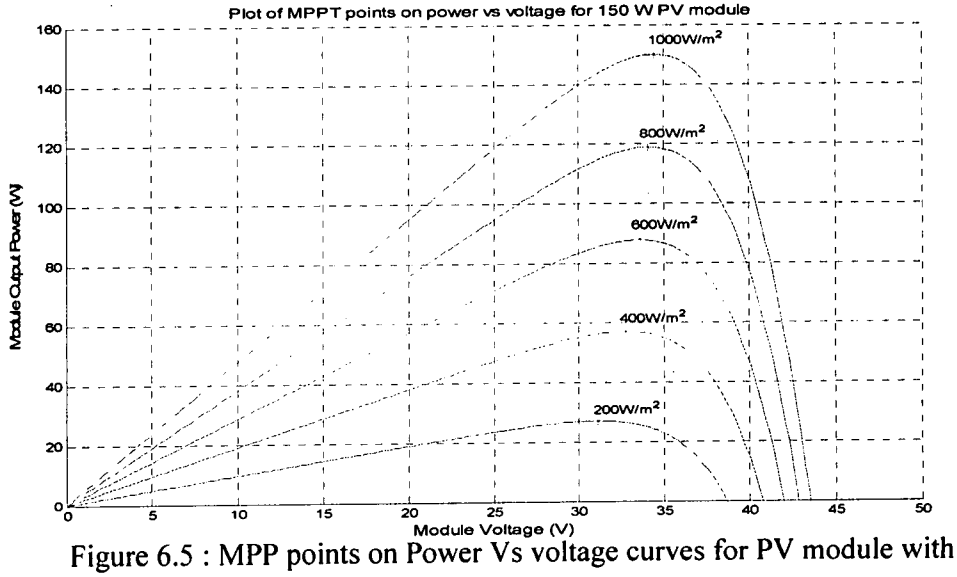

Figure 6.5 : MPP points on Power Vs voltage curves for PV module with various irradiance levels

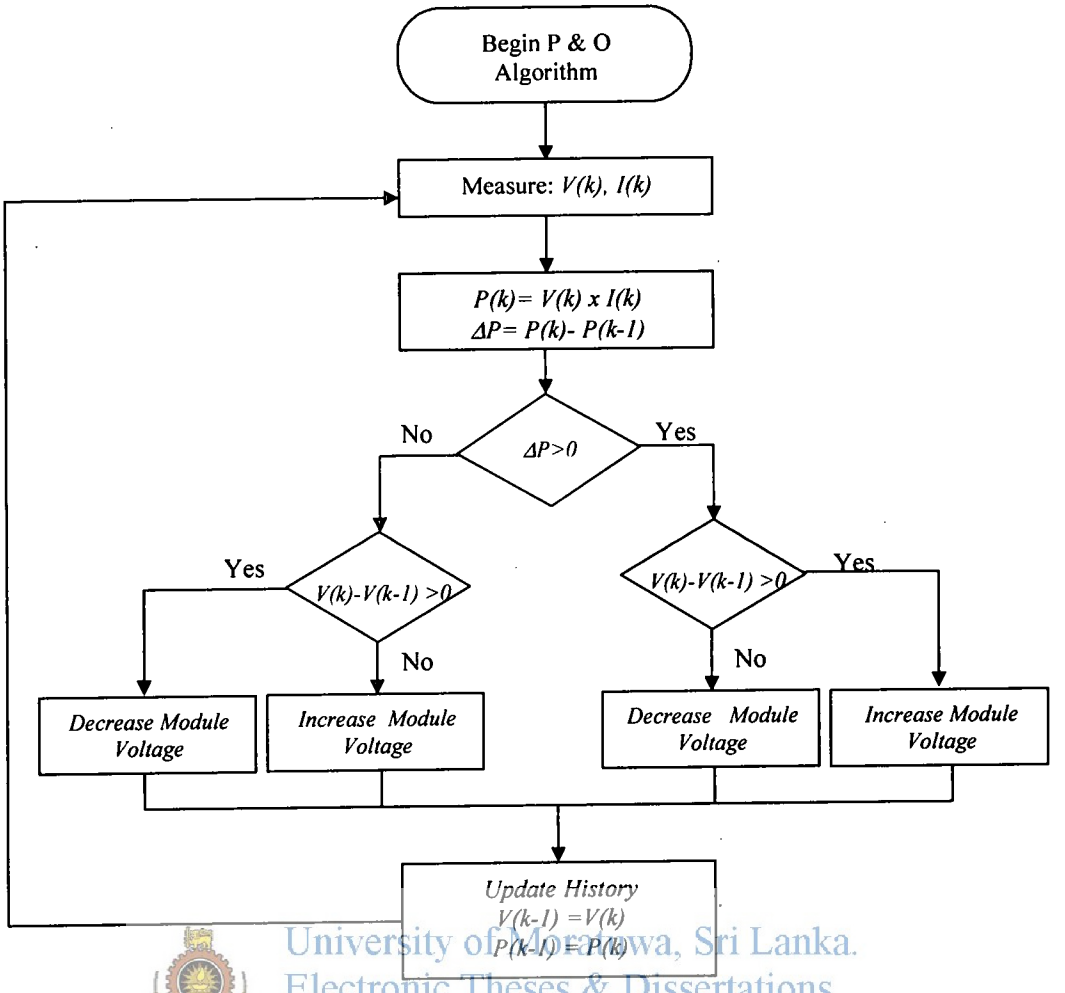

Figure 6.6 : Shows the flow chart of P & O algorithm

6.3 Simulation of the P&O Algorithm

The P&O algorithm is tested with actual irradiance data provided by [9] simulations with two set of data shown in Figure 6.7 and Figure 6.8 the first set of data was the measurements of a sunny day in September 15th 2008 and the second set of data was taken on a cloudy day October 4th 2008 at the same location. The data consists of the irradiance measurements taken every two minutes for 12 hours. Irradiance values between two data points are estimated by the cubic interpolation in MATLAB functions. The details can be referred in the MATLAB script listed in the Appendix A.1.

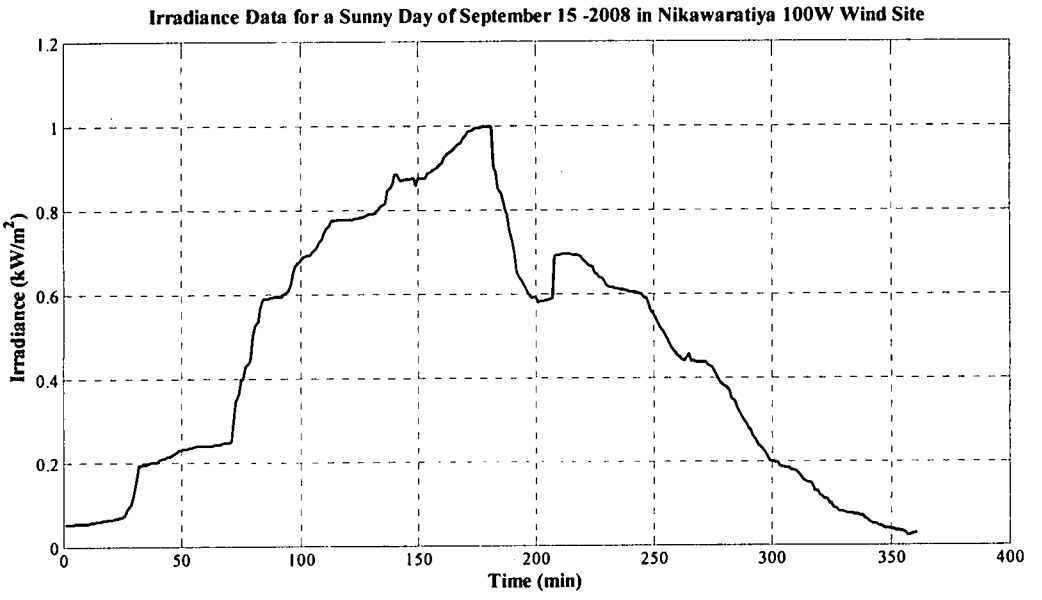

Figure 6.7: Sunny day irradiance variation in September-15th - 2008 at 100W wind turbine power generation site

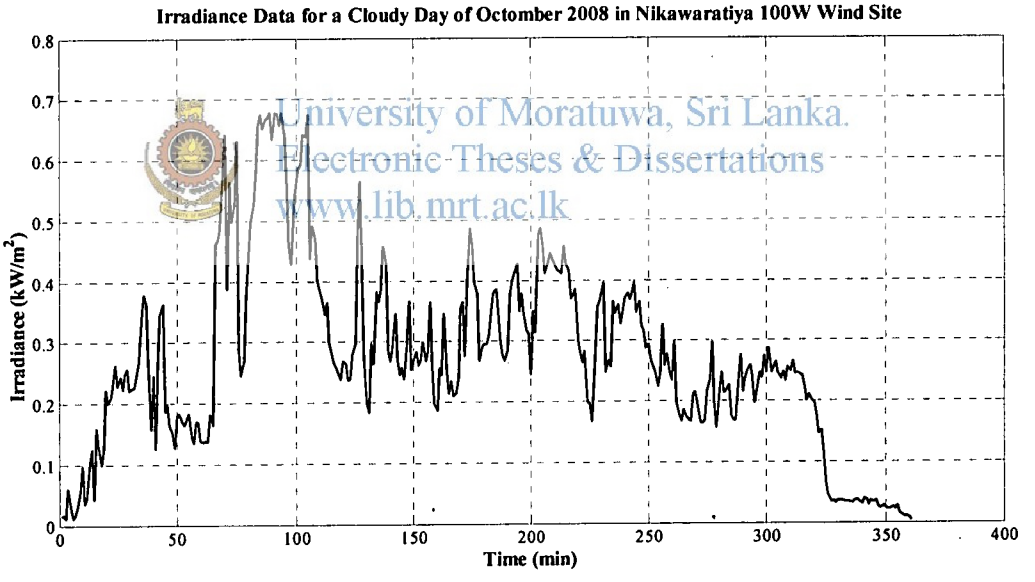

Figure 6.8: Cloudy day irradiance variation in Octomber-4th -2008 at 100W wind turbine power generation site

On a sunny day, the irradiance level changes gradually since there is no influence of cloud. MPP tracking is supposed to be easy. As shown in Figure 6.9 and Figure 6.10 algorithms locate and maintain the PV operating point very close to the MPPs without much difference in their performance.

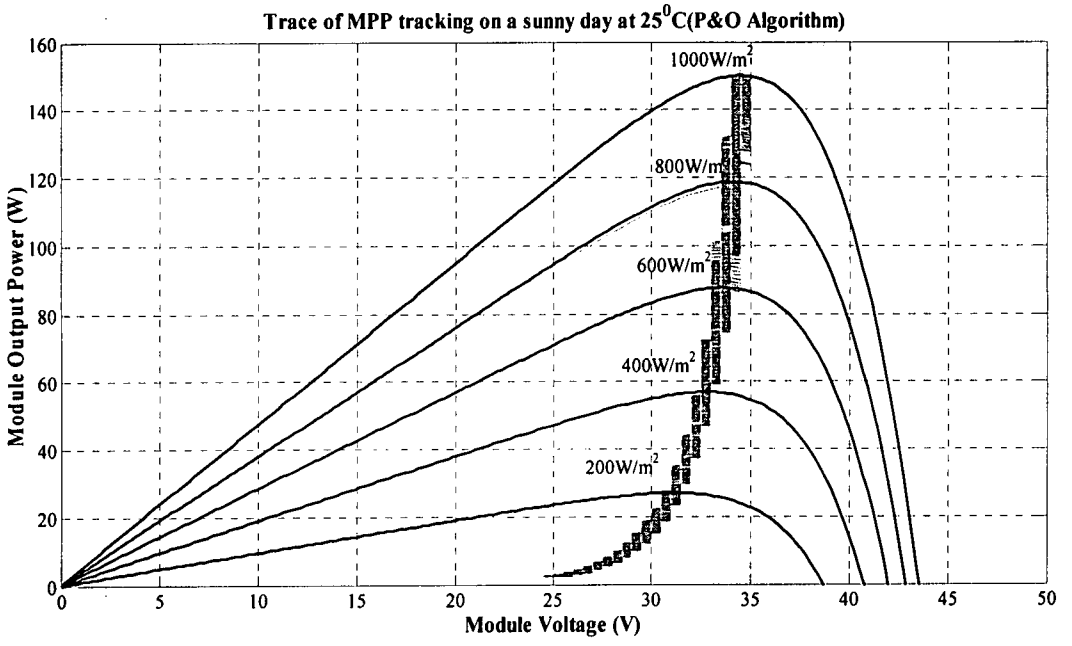

Figure 6.9: Trace of MPP tracking on a sunny day (25^{0}C)

On a cloudy day, the irradiance level changes rapidly due to passing clouds. Then, MPP tracking are supposed to be challenge [27]. Figure 6.10 shows the trace of PV operating points for P&O algorithm and deviations of operating points from the MPPs are obvious when compared to the results of a sunny day.

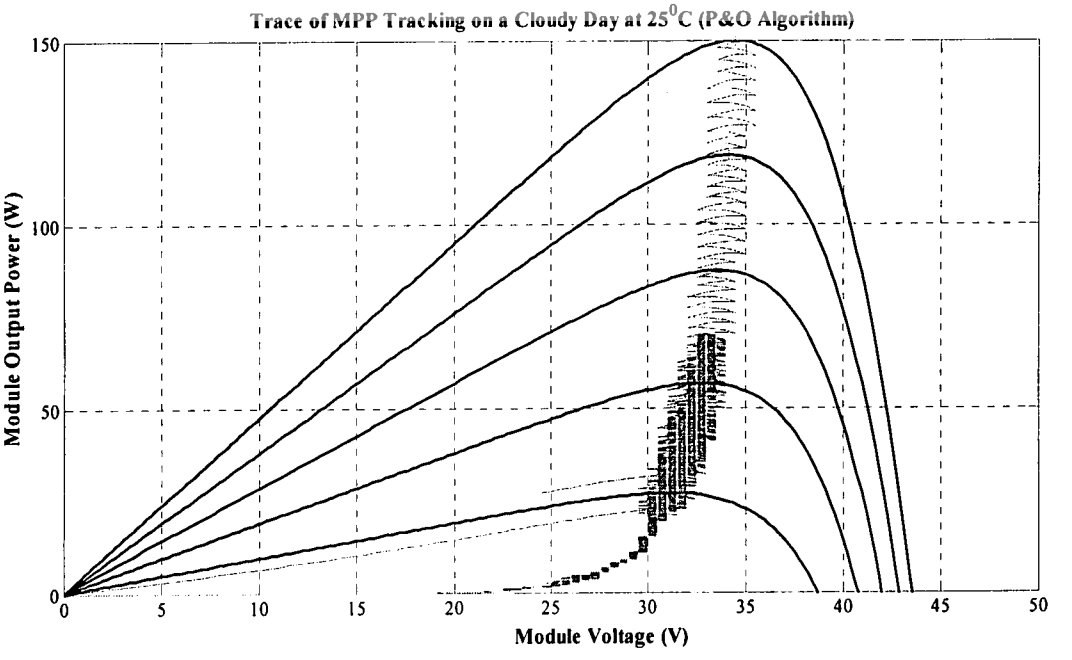

Figure 6.10: Trace of MPP tracking on a cloudy day (25^{0}C)

In order to the better evaluation, total energy produced during a 12 – hour period is calculated. The MPP tracking efficiency is obtained by [Total energy (simulation)] ÷ [Total energy (theoretical max)] x 100% an also The MPP tracking efficiency is still good in the cloudy condition for P & O algorithm. The irradiation data are only available at two minute intervals, thus they do not record a much higher rate of changes during this intervals. Also, further optimizing of algorithm and varying a testing method may provide different results. The simulation results show the efficiency of 96.2% for P & O algorithm.

Chapter 7

Lead-Acid Battery Modeling and Testing

The battery behavior prediction approaches consist of charge accumulation and empirical models. Lead – acid batteries are used commonly in stand-alone wind solar hybrid power systems. Lead – acid battery cells consist of two plates, positive and negative, immersed in a dilute sulfuric acid solution. The positive plate, or anode, is made of lead dioxide (PbO_2) and the negative plate or cathode, is made of lead (Pb) as shown in Figure 7.1. The battery model has two modes of operations, charge and discharge. The battery is in charge mode when the current into battery is positive, and discharge mode when the current is negative.

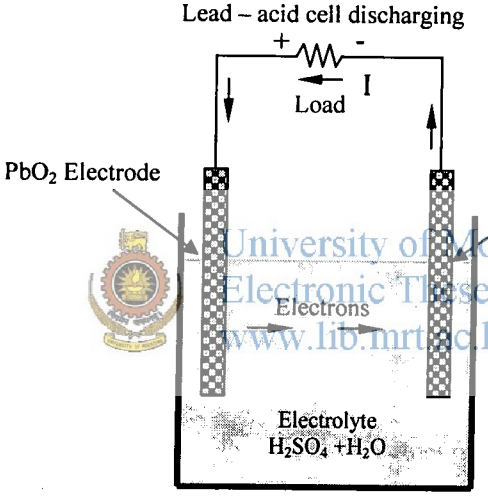

Figure 7.1 Construction of simple Lead – acid battery cell

Lead – acid battery is characterized by two indexes. They are battery state of charge (SOC) and the floating voltage (or the terminal voltage).

7.1 Battery State of Charge (SOC)

Battery SOC determination becomes gradually more important issue in all the applications that consist of a battery. A poor reliability of the SOC indication may induce undesirable situations such as not fully charged or overcharged condition.

The purpose of the battery SOC may be a problem of more or less complexity depending on the battery type and on the application in which the battery is used. The most commonly used technique the ampere hour counting method is adopted for the SOC calculation. For a just right knowledge of the real SOC of a battery, it is necessary to know the battery SOC at the starting point, the charge or discharge time and the current value [45]:

$$SOC = SOC_0 + \int_{to}^{t}\left(\frac{I_{bat}}{C_{bat}}\right)d\tau \tag{7.1}$$

Where SOC_0 is the battery SOC of the initial point, t_0 and t are the time of the initial point and the time of interest, respectively (hours), C_{bat} is the battery capacity (Ah), I_{bat} is the battery current (A). The equation 7.1 represents the calculation of battery SOC for ideal batteries. But, practically, losses occur during battery charging, discharging and also during storing periods. Taking these factors into account, the battery SOC then can be expressed by the equation 7.2.

$$SOC = SOC_0\left[1-\frac{\sigma}{24}(t-t_o)\right] + \int_{0}\left(\frac{I_{bat}\eta_{bat}}{C_{bat}}\right)d\tau \tag{7.2}$$

Where σ is the self-discharge rate which depends on the accumulated charge and the battery state of health [45], and a proposed value of 0.2%/day is recommended, η_{bat} is the battery charging and discharging efficiency. For the charging process in order to reflect the fact that only a fraction of the input energy is really stored, the average approximation of 90% is used; but for the discharging stage, 100% discharging efficiency is recommended.

Similar to the all chemical processes, the battery capacity C_{bat} is temperature dependent. It decreases with decreasing battery temperature in the range 0.5–1%/1^{0}C, caused by the temperature dependence of the kinetic parameters [47]. Normally, the battery capacity changes can usually be expressed by using the temperature coefficient δc as given in equation 7.3.

$$C_{bat} = C_{bat}(1+\delta_c(T_{bat}-298.15)) \tag{7.3}$$

where C_{bat} is the available or practical capacity of the battery when the battery temperature is T_{bat}, (Ah), C_{bat} is the nominal or rated capacity of the battery, which is the value of the capacity given by the manufacturer as the standard value that characterizes this battery usually it is specified at nominal operating conditions, δc = 0.006, a temperature coefficient of 0.6%/^{0}C, is usually used unless otherwise specified by the manufacturer.

In hybrid solar–wind system, the energy resource includes the PV module and wind turbine, they work together with the battery to cover load demand if the cable losses in the system are neglected, then the battery current I_{bat} can be simply described by the equitation 7.4[42] [28].

$$I_{bat} = \frac{P_{solar} + P_{wind}\eta_{rectifer} - P_{load}/\eta_{inverter}}{V_{bat}} \tag{7.4}$$

Where P_{Solar}, P_{Wind}, and P_{Load} are the power of the PV wind hybrid system and load respectively. V_{bat} is the battery voltage. The rectifier is used to convert the AC power from the wind turbine to DC power of constant voltage, and the rectifier efficiency $\eta_{rectifier}$ is considered as constant, 95%, in this analysis. The inverter efficiency $\eta_{inverter}$ is

considered as 92% according to the load profile of the system and the specifications of the inverter [25].

7.2 Lead – Acid battery Model by MATLAB

Dynamic modeling of Lead- acid battery is much complex due to changing non liner parameters during charging and discharging process and unpredicted parameter changes when chemical reactions occur[10] [11]. As shown in Figure 7.2, the Battery block implements a generic dynamic model parameterized to represent most popular types of rechargeable batteries [40].

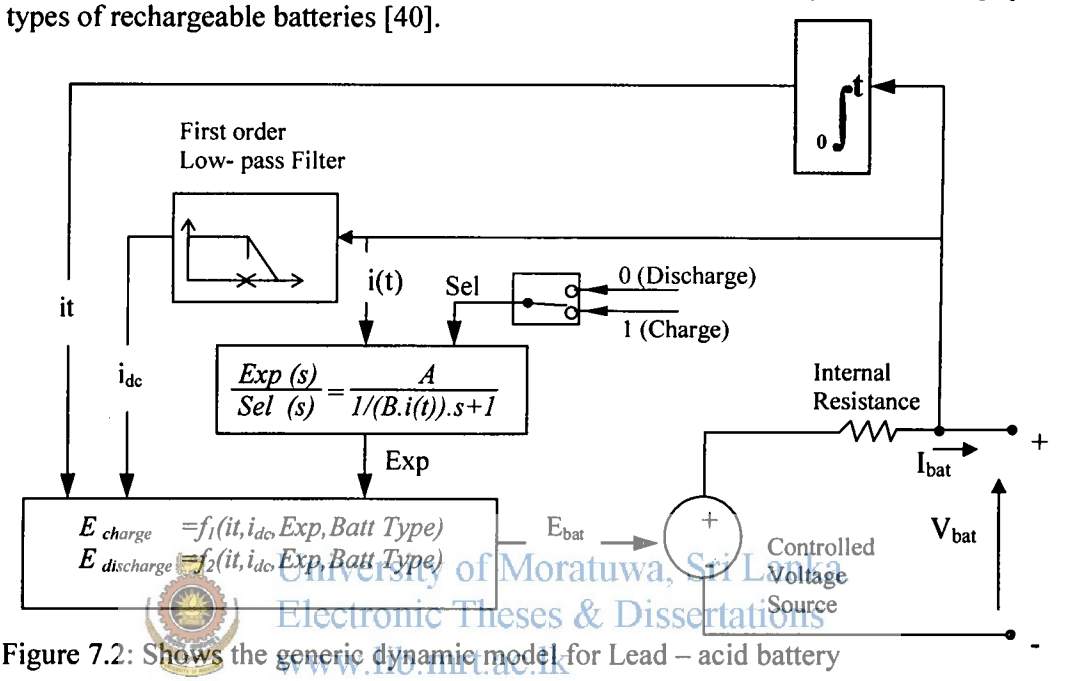

Figure 7.2: Shows the generic dynamic model for Lead – acid battery

Lead-Acid Model

Discharge model ($i_{dc} > 0$) given in equation 7.5

$$f_1(it, i_{dc}, i, Exp) = E_0 - K\frac{Q}{Q - it} i_{dc} - K\frac{Q}{Q - it} it + Laplace^{-1}\left(\frac{Exp(s)}{Sel(s)} x0\right) \quad (7.5)$$

Charge Model ($i_{dc} < 0$) given in equation 7.6

$$f_2(it, i_{dc}, i, Exp) = E_0 - K\frac{Q}{it + 0.1Q} i_{dc} - K\frac{Q}{Q - it} it + Laplace^{-1}\left(\frac{Exp(s)}{Sel(s)} x\frac{1}{s}\right) \quad (7.6)$$

Where,

E_{Batt} = Nonlinear voltage (V)

E_0 = Constant voltage (V)

Exp(s) = Exponential zone dynamics (V)

Sel(s) = Represents the battery mode. Sel(s) = 0 during battery discharge, Sel(s) = 1 during battery charging.

K = Polarization constant (Ah^{-1}) or Polarization resistance (Ohms)

i_{dc} = Low frequency current dynamics (A)

i = Battery current (A)

it = Extracted capacity (Ah)

Q = Maximum battery capacity (Ah)

A = Exponential voltage (V)

B = Exponential capacity $(Ah)^{-1}$

The Simulink Simpower system software tool box is utilized to simulate discharging behavior of Lead – acid battery as shown in Figure 7.3. The parameters of the equivalent circuit can be modified to represent a particular battery type based on its discharge characteristics as shown in Figure 7.4. The simulation parameters change in a battery block as follows.

Battery Type	- Lead – Acid
Nominal Voltage (V)	- 12 V
Rated Capacity (Ah)	- 70 Ah
Initial State of Charge	- 100 %
Discharge Current (A)	- 3.5 A

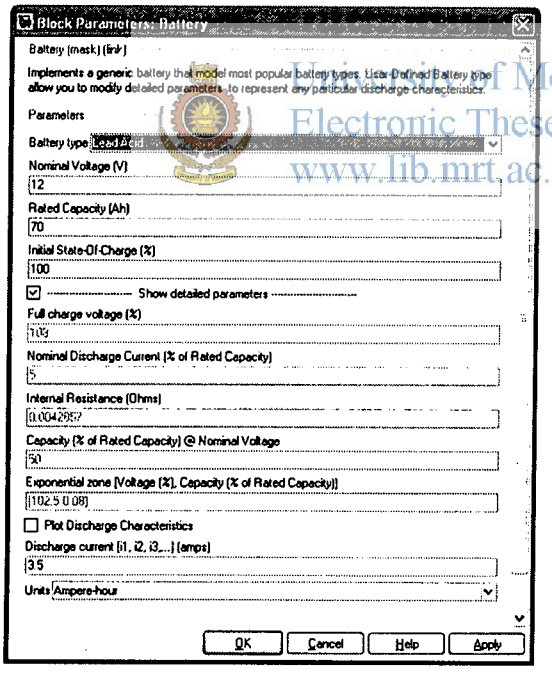

Figure 7.4: Block parameters of Simulink Simpower system Battery model

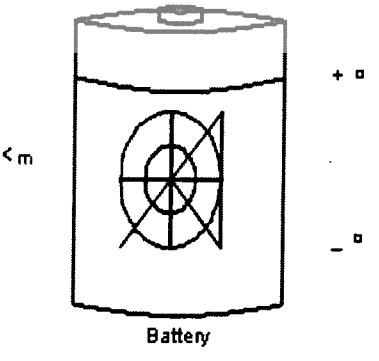

Figure 7.3: Simulink Simpower system Lead – Acid Battery.

A typical discharge curve is composed of three sections, as shown in the Figure 7.5

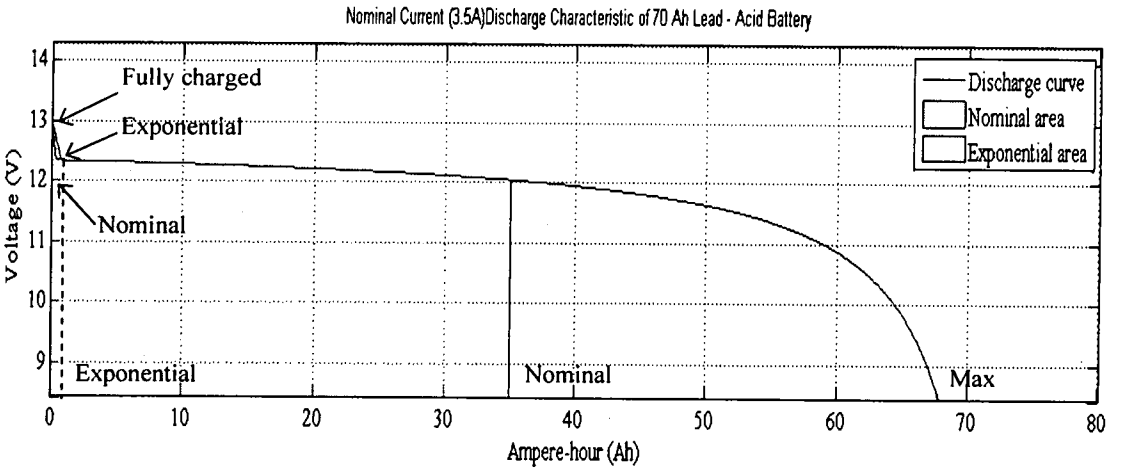

Figure 7.5: Discharge characteristic of 70 Ah Lead – Acid Battery

The first section represents the exponential voltage drop when the battery is charged. Depending on the battery type, this area is more or less wide. The second section represents the charge that can be extracted from the battery until the voltage drops below the battery nominal voltage. Finally, the third section represents the total discharge of the battery when the voltage drops rapidly.

With further developing of the dynamic model to simulate lead – acid battery, the battery model has the following input parameters.

A. Initial stage of charge: SOC1 (%) , indicating available charger.
B. Maximum state of charge: SOCm (Wh), maximum battery capacity.
(Note: battery capacity depends on charge or discharge rate)

C. Number of 2V cells in series: ns
D. Charge / discharge battery efficency : K (unitless)
E. Battery eslf – discharging rate: D (h^{-1})
Note: parameters D and E are empirical constant that depends on the battery characteristics.

The state of charge (in %) has a very linear relationship to the open – circuit terminal voltage of the battery. SOC1 can be estimated based on the current open – circuit terminal voltage of the battery. The relationship can be estimated using Table 7.1.

Voltage	State of Charge (%)
12.63	100
12.54	90
12.45	80
12.39	75
12.27	60
12.18	50
11.97	25
11.76	Completely discharge

Table 7.1 shows the relationship of battery voltage and state of charge

The terminal voltage of the battery is given by equation 7.7

$$V_{bat} = V1 + I_{bat} \, x \, R1 \tag{7.7}$$

Where V_1 and R_1 are governed by a different set of equation depending on which mode of operation the battery is in. values for the battery current (I_{bat}) are positive when the battery is in charge mode and negative when the battery is in discharge mode. The equivalent battery model is shown in Figure 7.6 [14].

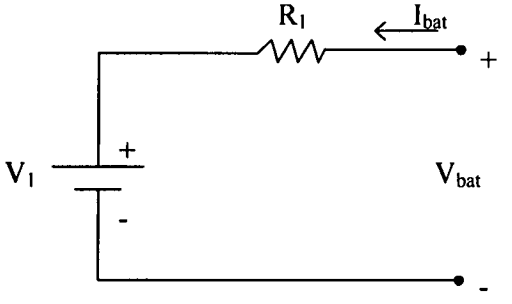

Figure 7.6: Shows the equitant circuit of battery model

Charge Mode voltage and resistance given in equation 7.8 and equation 7.9 respectively

$$V_{ch} = [2 + 0.148xSOC(t)]xns \tag{7.8}$$

$$P_{ch} = \frac{0.758 + 0.1309 /[1.06 - SOC(t)]xns}{SOC_m} \tag{7.9}$$

SOC (t) is the current state of charge (%).

Discharge Mode voltage and resistance are given in equation 7.10 and equation 7.11 respectively

$$V_{dch} = [1.926 + 0.124xSOC(t)]xns \tag{7.10}$$

$$P_{dch} = \frac{0.19 + 0.1309 /[SOC(t) - 0.14]xns}{SOC_m} \tag{7.11}$$

The most difficult part of the battery model is estimating a value of SOC (t) accurately. The estimation of the model is described by the following equation 7.12

$$SOC(t+dt) = SOC(t) * [1-D*dt/3600]+k*[V_{bat}*I_{bat}-RI*I_{bat}^2]*dt/3600 \tag{7.12}$$

This is basically the energy balance equitation computing the value of the SOC increment as the energy increment in a differential of time taking into account self-discharge and charge efficiency. For this equitation, time is assumed to have unit of seconds. So, some terms must be divided by 3600 so that SOC is in Wh. This value can

be altered to compensate for time unit of minutes (60), hours (1), or any other increment (divisions/ hour).
This equation can be further simplified by substituting V_{bat} as a function of V_1as given in equation 7.13

$$SOC(t+dt) = SOC(t) * [1-D*dt/60]+[k*V_1*I_{bat}]*dt/60 \quad (7.13)$$

It is necessary to use integration to solve for SOC (t)

Here, *t* is as the number of time units. Since SOC (0) = SOC1= initial stage of charge, SOC(1) can be found , and by looping the results with Simulink and estimate the current value of SOC(t) for any time . MATHLAB Simulik simulation block diagram shown in Figure 7.7.

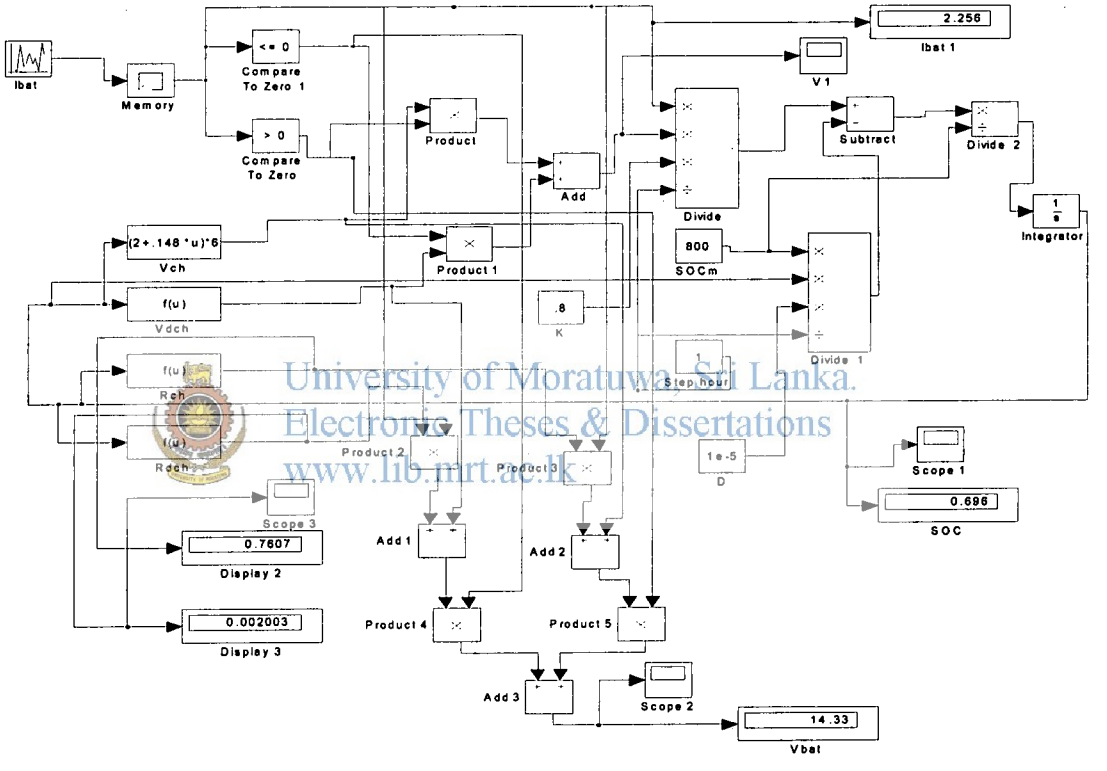

Figure 7.7 : Shows the Simulink Simulation diagram of Lead – Acid battery

Lead- acid battery simulation Simulink program has being run at 200 second sampling period with I_{bat} current values. Positive I_{bat} values as input parameter for battery charging current and negative I_{bat} values are battery discharging current. Figure 7.8 shows the battery charging / discharging voltage (V_1) variation and Figure 7.9 shows battery voltage condition during simulation period. This simulation study has being done by the 70 Ah capacity lead – acid battery. The battery fully charge (SOC at100%) means that battery reached 70 Ah capacity. The battery SOC variation characteristic is represent during the simulation period as shown in Figure 7.10.

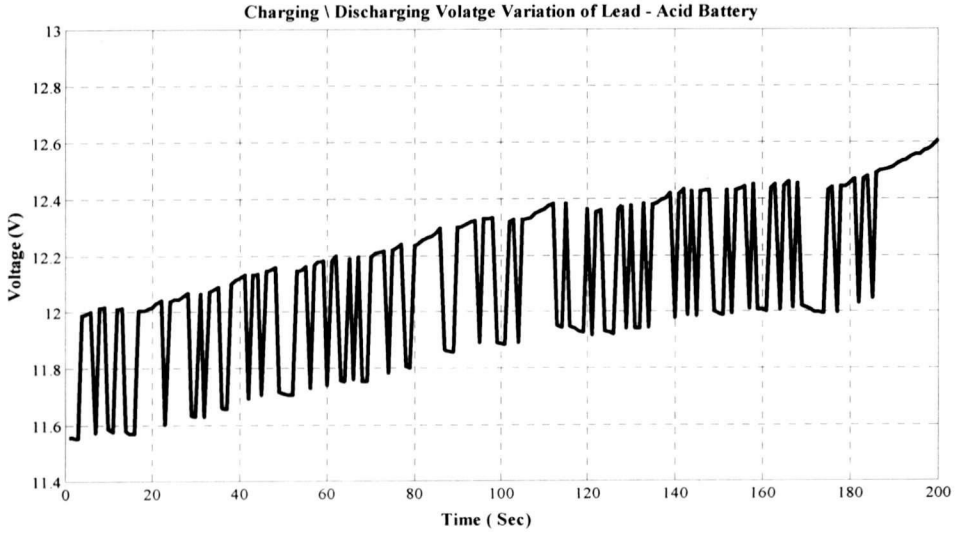

Figure 7.8: Charging \ Discharging Voltage variation of 70 Ah lead – acid battery

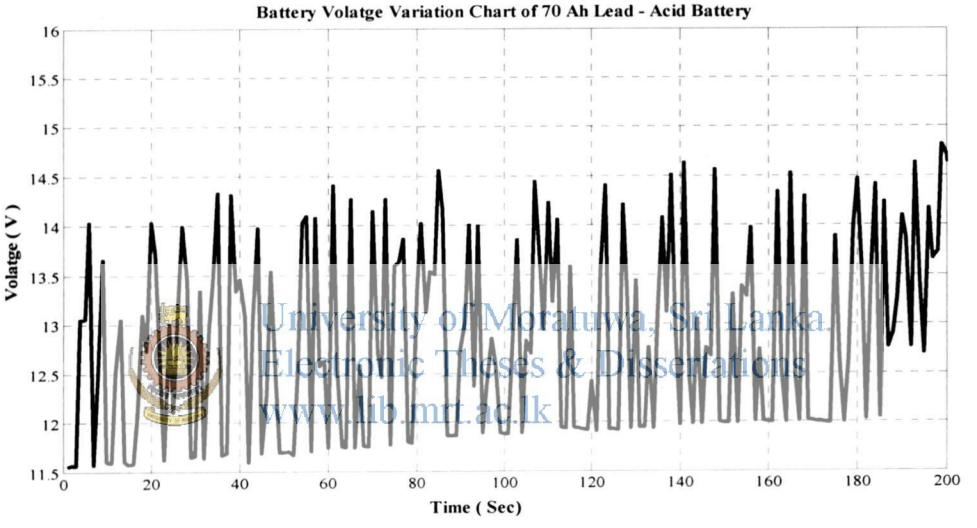

Figure 7.9: Battery Voltage variation of 70 Ah lead – acid battery

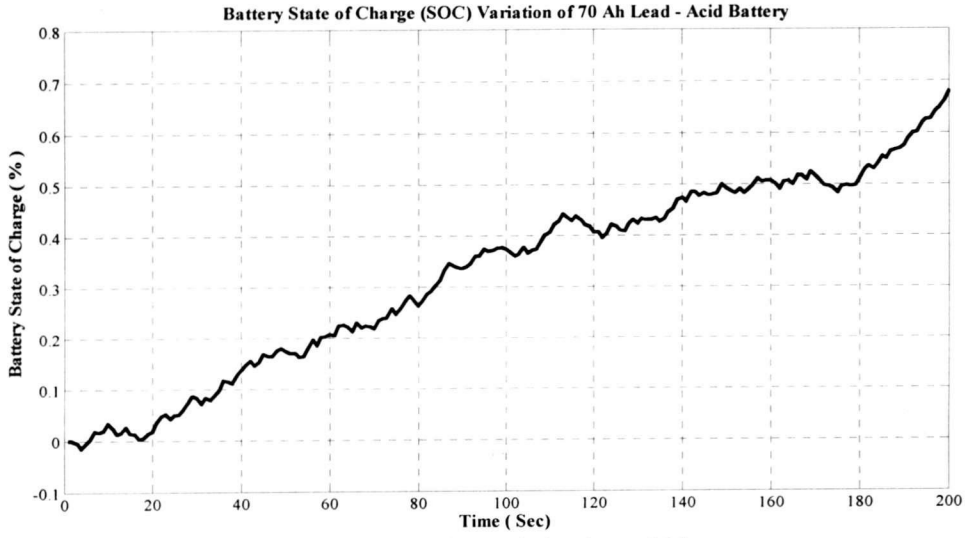

Figure 7.10: Battery SOC variation of 70 Ah lead – acid battery

7.3 Laboratory Testing of Lead – Acid Battery

The 70Ah lead – acid batteries used in this experiment and the same type as used in the hybrid solar–wind power generation project. There are some automobile lead–acid batteries commonly used for rural renewable energy applications with a capacity of 70 Ah - 100 Ah, rated at 10 h discharge time. To get the battery voltage response under different battery currents, the SLS 1126 test procedures have being followed and the testing was done in NERDC battery testing levorotary of electrical engineering department.

First, the battery was charged with a constant charging current I_{charge} to the overcharge-protection voltage (recommended by the customer manual and battery testing standard), and then held at this voltage for 20h rate. According to the customer manual, the battery can be considered as fully charged because the battery voltage does not change during this certain period of time. Figure 7.11 shows the battery charging process under laboratory condition.

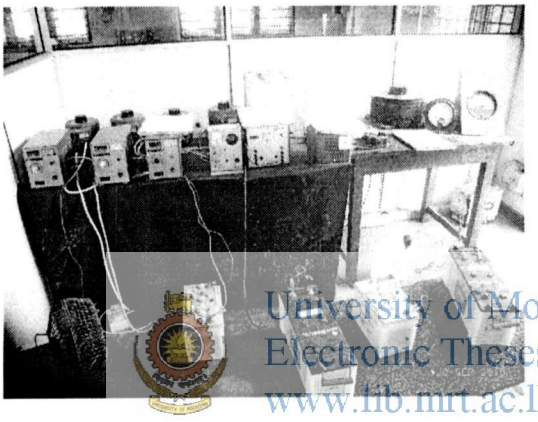

Figure 7.11: Battery charging process under the laboratory condition

Figure 7.12: Electronic load connect to the battery discharging process

Secondly, the battery was then discharged at a constant discharging current $I_{discharge}$ until the battery voltage drops to the deep-discharge protection point (10.5V is recommended by the customer manual and battery testing standard) as shown in Figure 7.13. A testing cycle constitutes these two steps [32].

During the whole experiment cycles (five cycles), the battery voltage variations were recorded every 30 min intervals. The battery voltage variations measured under charging and discharging currents has no interference of external load (charging period) or power supply (discharging period). The battery voltage curves for constant (3.5A) current rates are found to be dramatically increased to 15.8V~16V. Thereafter the battery gets in to the overcharge condition which implies that the battery is almost full and begins to decrease the charge acceptance. As a result, the battery voltage will climb up quickly until it reaches the saturation area where the battery voltage is maximized and the battery cannot accept any more energy. Therefore it can be observed that the lead–acid battery operates within a narrow voltage margin under charging conditions.

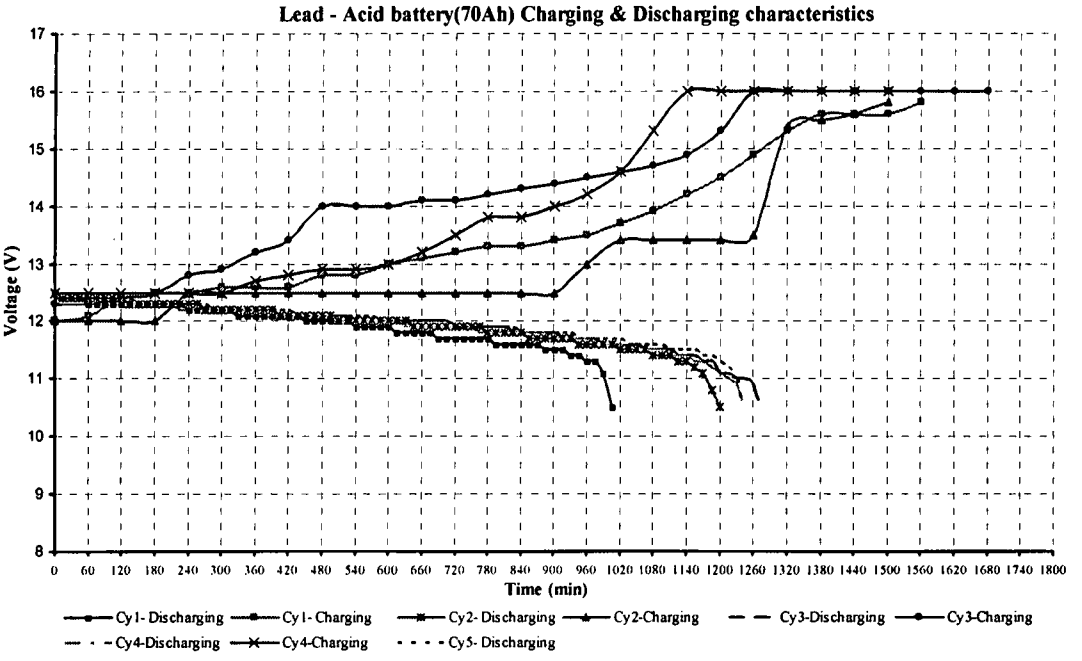

Figure 7.13: Lead – acid battery (70Ah) Charging & Discharging Characteristics

Similar situation occurs during the discharging tests as shown in Figure7.13. The battery voltages are detected to be rapidly decreased and then it provides a steady electrical discharge until it reaches the over-discharge zone where the battery voltage will decrease quickly owing to the nonlinear effects of electrochemical reactions in the battery. Also battery electrolyte temperature and Sp. gravity were measured during charging discharging process of 70 Ah battery every 30 minute intervals. The battery electrolyte temperature and Sp. gravity variation was ploted as shown in Figure 7.14.

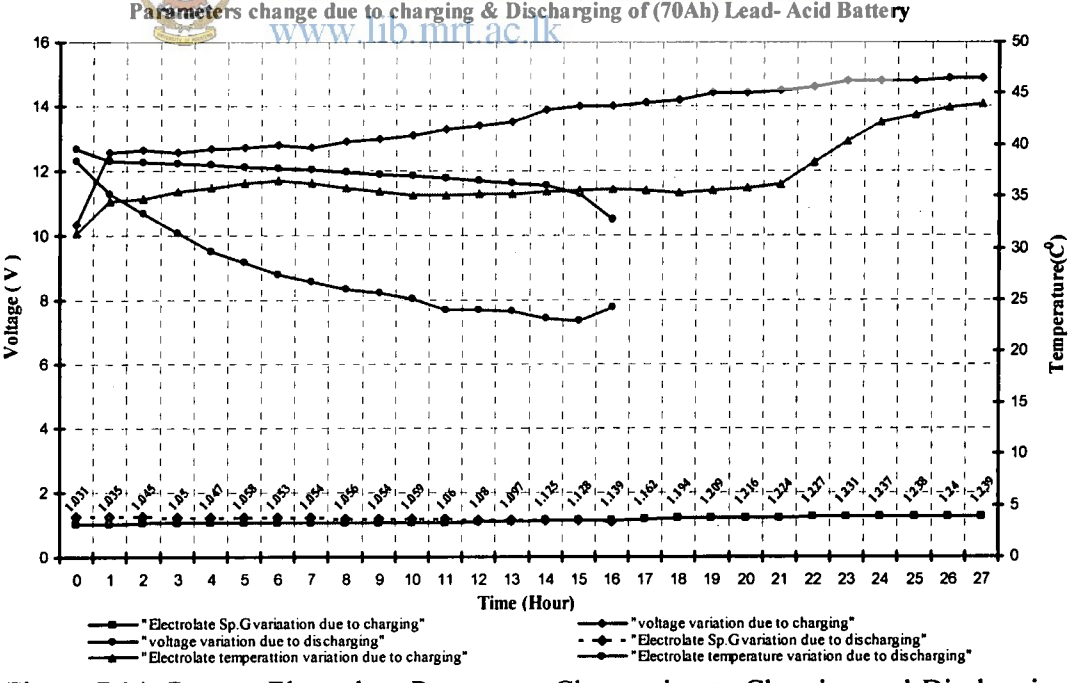

Figure 7.14: Battery Electrolyte Parameters Change due to Charging and Discharging

The 70 Ah Lead – acid battery electrolyte Sp. gravity variation was measured by using digital Hygrometer (SBS - 2500) as shown in Figure 7.15. The temperature changes are measured by a sensitive digital thermometer (TECPEL 322-K type) with 'K' type temperature probe inserting the electrolyte filling port of the battery as shown in Figure 7.16. The standard battery testing procedures and laboratory conditions are followed during testing the battery.

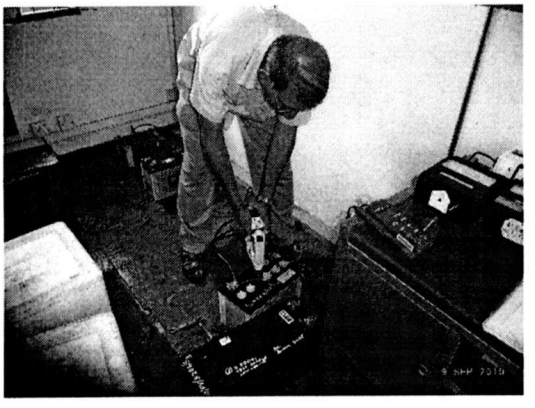

Figure 7.15: Battery electrolyte Sp. Gravity measurement

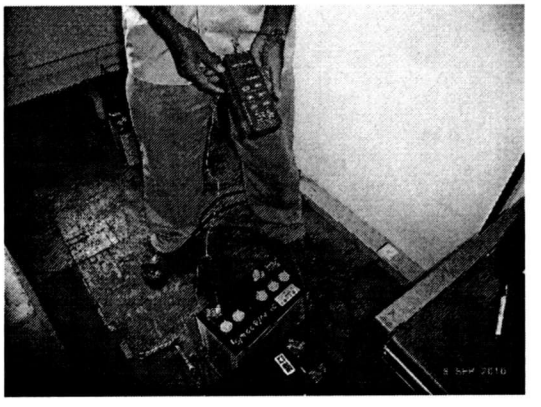

Figure 7.16: Battery electrolyte Temperature measurement

Chapter 8

Wind Solar Hybrid System & Optimization

A typical hybrid solar–wind power generation system includes a PV array, wind turbine, storage batteries and regulator, load and system controls [29]. The battery works in assistance with the PV array and wind turbine to satisfy the load demand. When the energy sources (solar and wind energy) are abundant, the generated power, after fulfilling the load demand, will be supplied to feed the battery. When the battery is fully charged, the extra energy will be dumped by disconnecting the PV module to cut off the solar energy generations. Even if extra energy generation exists after PV module is cut off means the power generation of the wind turbine is higher than the load demand and the battery is fully charged at the same time. Then the dump load (electric heater) will be turned on to discard the energy from the wind turbine. Figure 8.1 shows the proposed centralized DC bus hybrid architecture [52].

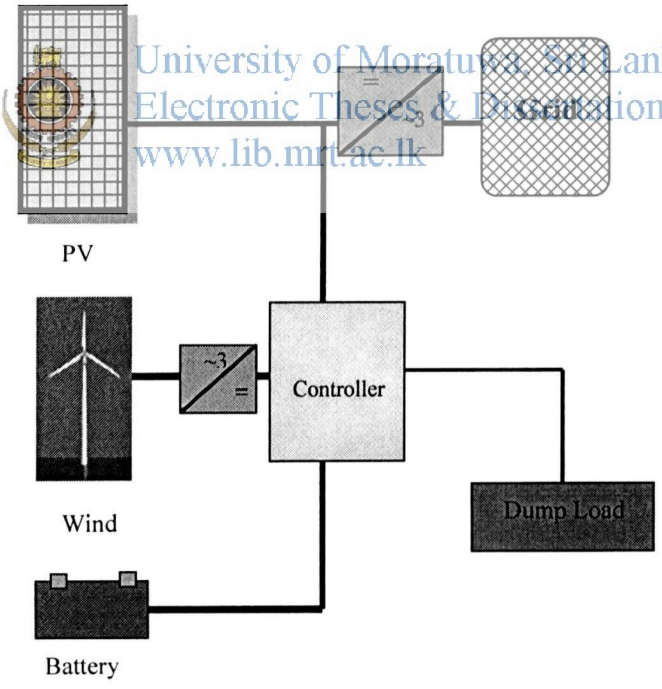

Figure 8.1: Shows the centralized DC bus Wind Solar hybrid architecture.

8.1 System Optimization

In order to utilize the renewable energy resources efficiently and economically, an optimum match design sizing method is necessary. The sizing optimization method can help assure the lowest investment with full use of the PV array, wind turbine and battery bank, so that the hybrid system can work at the optimum condition in terms of investment and system reliability requirement [19] [56].

8.1.1 Simulation and Optimization Software

Simulation programs are the most common tools for evaluating performance of the hybrid solar–wind systems. By using computer simulation, the optimum configuration can be found by comparing the performance and energy production cost of different system configurations. Several software tools are available for designing of hybrid systems, such as HOMER, HYBRID2, HOGA and HYBRIDS.

The Hybrid Optimization Model for Electric Renewables (HOMER), public domain software produced by National Renewable Energy Laboratory, uses hourly simulations for arriving at optimum target. It is a time-step simulator using hourly load and environmental data inputs for renewable energy system assessment, it facilitates the optimization of renewable energy systems based on Net Present Cost for a given set of constraints and sensitivity variables.

HOMER has being used extensively in previous renewable energy system case studies [31-58] and in renewable energy system validation tests [18]. Although simulations can take a long time, depending on the number of variables used, its operation is simple and straightforward. The program's limitation is that it does not enable the user to intuitively select the appropriate components for a system, as algorithms and calculations are not visible or accessible. Figure 8.2. shows the HOMER hybrid architecture for simulation study.

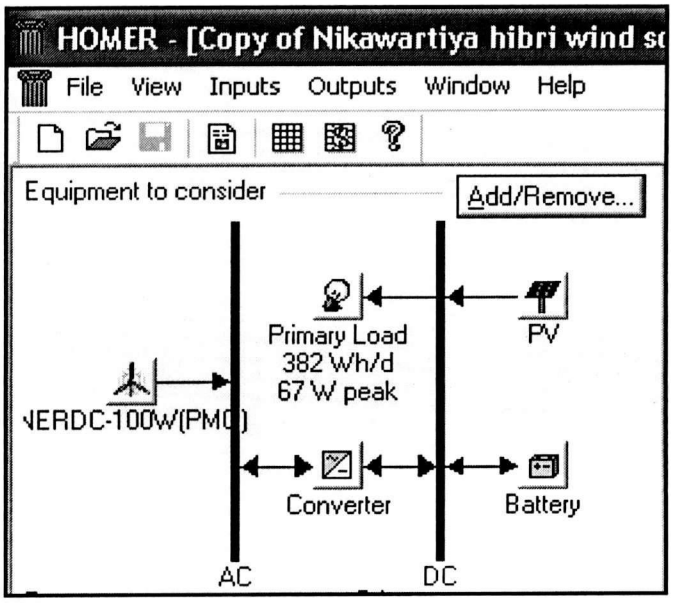

Figure 8.2 : shows the HOMER hybrid architecture for simulation study.

8.2 Components details of Hybrid system

NERDC 100W wind turbine details are given as Figure 8.3 and the input wind turbine date for the HOMER simulation and data was entered at least one size (150W) and cost value in the cost table in photovoltaic input. It search for the optimal system including modeling, mounting hardware and installation. HOMER considers each PV array capacity in the size to consider table show in Figure 8.4 . Battery type and capacity (70Ah) used in hybrid system are selected and the data is entered to the system. HOMER considers each battery quantity in the sizes to consider table as shown in Figure 8.5.

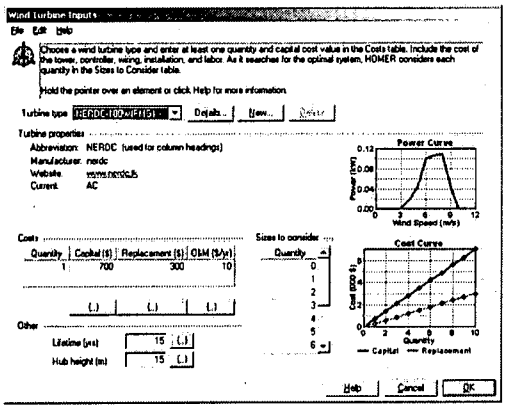

Figure 8.3 Shows the NERDC 100W Wind turbine data given as input data for HOMER simulation

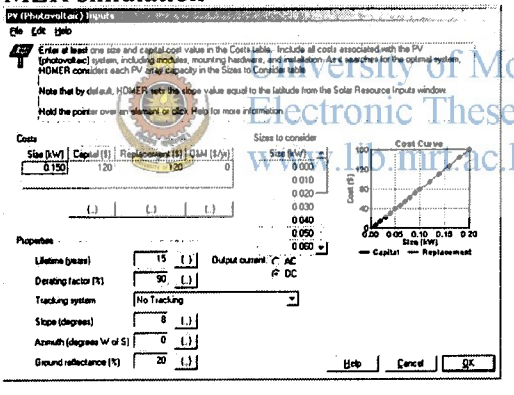

Figure 8.4 : shows the HOMER considers each PV array capacity in the size to consider table.

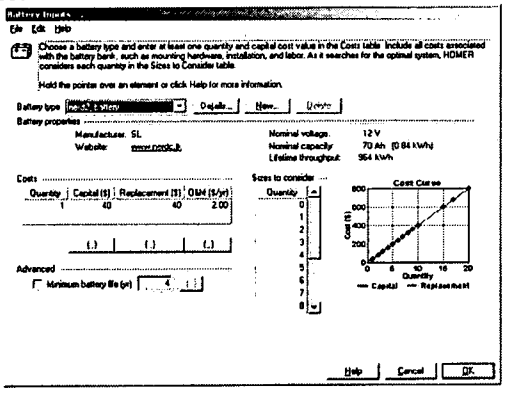

Figure 8.5: Sows the (70Ah) battery details used for simulation

Hybrid system is used AC/DC converter in capacity of 300W and 95% efficiency. The Primary load 382 Wh/day was connected to DC bus of the HOMER hybrid system.

8.3 Resources Details of Hybrid System

Annual wind speed *V (m/s)* and solar irradiation data *(W/m²)* is basic energy resources of this hybrid system. Wind and solar energy are renewable energies that need not analyze emission and cost optimization. Annual wind speed *V (m/s)* variation at 10m height as shown in Figure 8.6 and solar irradiation data shown in Figure 8.7 was used as metrological data measured from Nikawaratiya [X(m)120471,Y(m) 283682] 100W wind turbine site in year 2008.

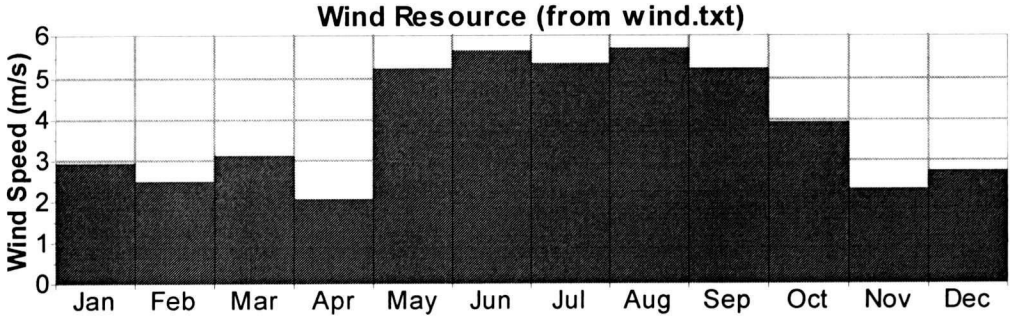

Figure 8.6: Monthly average wing speed variation at Nikawaratiya 100 W wind turbine site

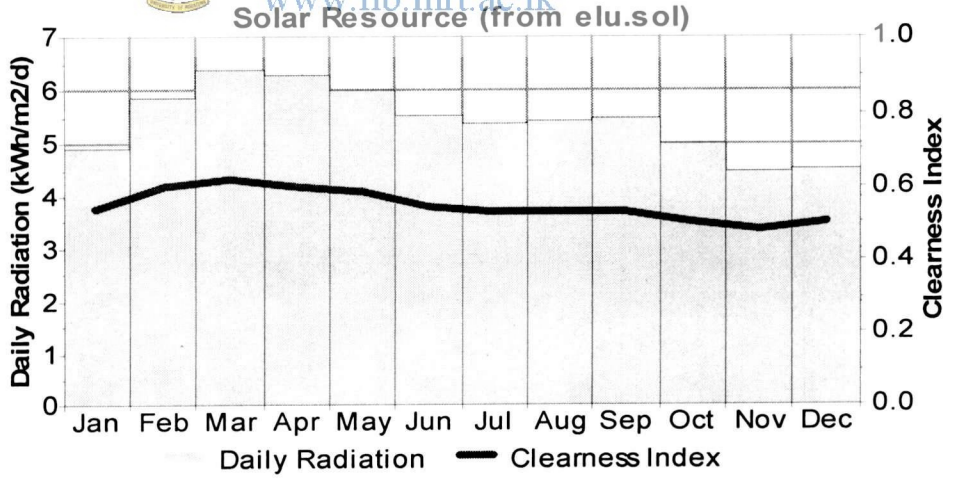

Figure 8.7: Monthly average solar irradiation at Nikawaratiya 100 W wind turbine site

8.4 Simulation of Hybrid System

In the optimization process the HOMER has being used for simulation of Hybrid system. Based on a variety of design parameters such as PV size, wind turbine capacity and storage lead – acid battery capacity have being estimated. Annual average wind speed of 3.92 m/s and annual average solar potential is 5.44 kWh/m^2/day of year 2008 at Nikavaratiya. 100W wind turbine site have being used for simulation study. Primary load scaled average of 0.382 kWh/day and annual DC primary electric load served are 139 kWh. Figure 8.8 shows the monthly average electric production of the wind PV hybrid system [53].

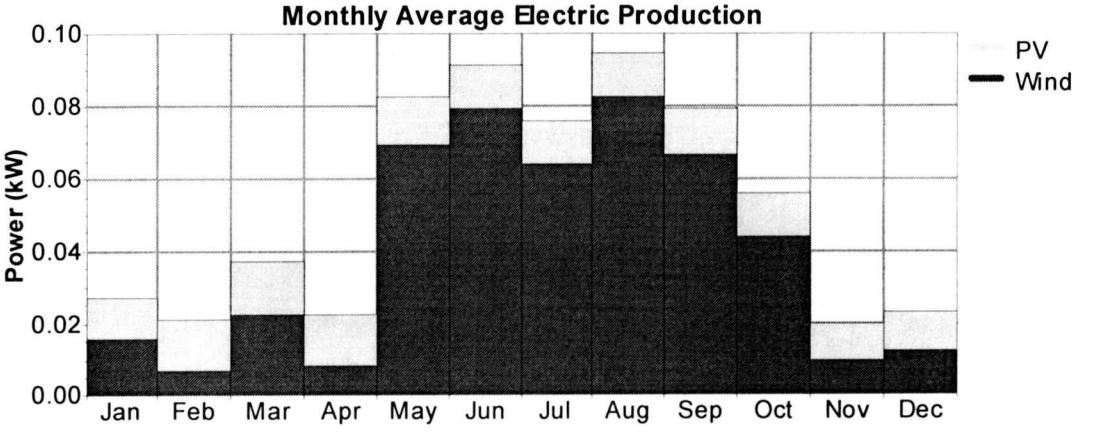

Figure 8.8: Shows the monthly average electric production of the wind PV hybrid system.

The NERDC wind turbine is already installed at a site, hence one wind turbine is set as a constraint of optimization with HOMER. Evaluation of optimization results of the hybrid system by HOMER 60 W photovoltaic panel is optimal to fulfill the rural home energy requirement with one 70Ah Lead – acid battery. Table 8.1 shows the HOMER optimized solution for the wind solar hybrid system. Plant capacity factor of solar array and wind turbine are 20.5% and 36.9% respectively.

Component	Size	Average output	Max. Output	Min. output	Capacity factor	Hours of operation
PV Array	60W	0.296 kWh/d	0.0975kW	0.000102 kW	20.5%	4,610hr/yr
Wind Turbine	100W	0.0405 kW	0.110 kW	0.000 kW	36.9 %	5,763hr/yr

Table 8.1: shows the HOMER optimized solution for the wind solar hybrid system.

The energy production of six months, May to October of year 2008 is drastically high than the other six months. The main reason for this situation is higher wind speed potential of the site and excess energy production during that period is also higher. Table 8.2.and Figure 8.9 show simulation results of annual power generation from wind, solar hybrid system and excess energy generation paten during year 2008.

Component /Description	Production (kWh/yr)	Fraction
PV array	108	23%
Wind Turbine	355	77%
Total production	463	100%
Excess electricity	297	64%
Capacity shortage	0	0%

Table 8.2: Shows Energy production of Hybrid system during year 2008

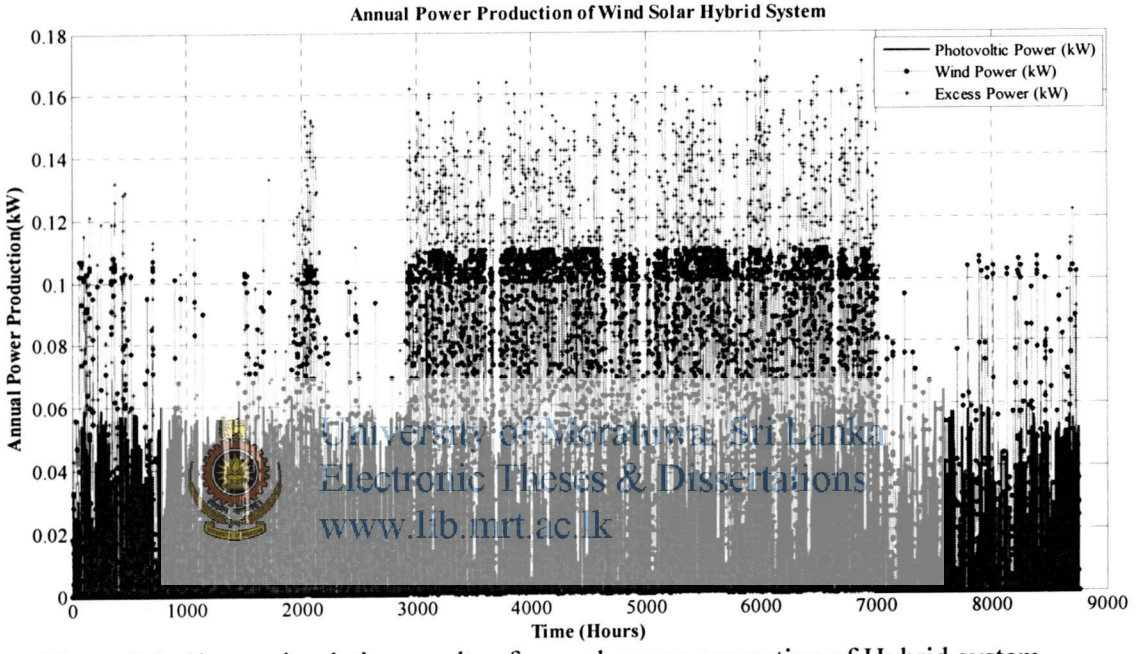

Figure 8.9: Shows simulation results of annual power generation of Hybrid system

8.5 Sensitivity analysis

HOMER can perform a sensitivity analysis by accepting multiple values for a particular input variable such as the average load. For simplicity of analysis, the load profile was not modified as the load was increased. But, the shape and scale in size could be kept constant. The sensitivity analysis was performed with 0.3 kWh/d. Further analysis is required to determine the effect of changes in the load shape.

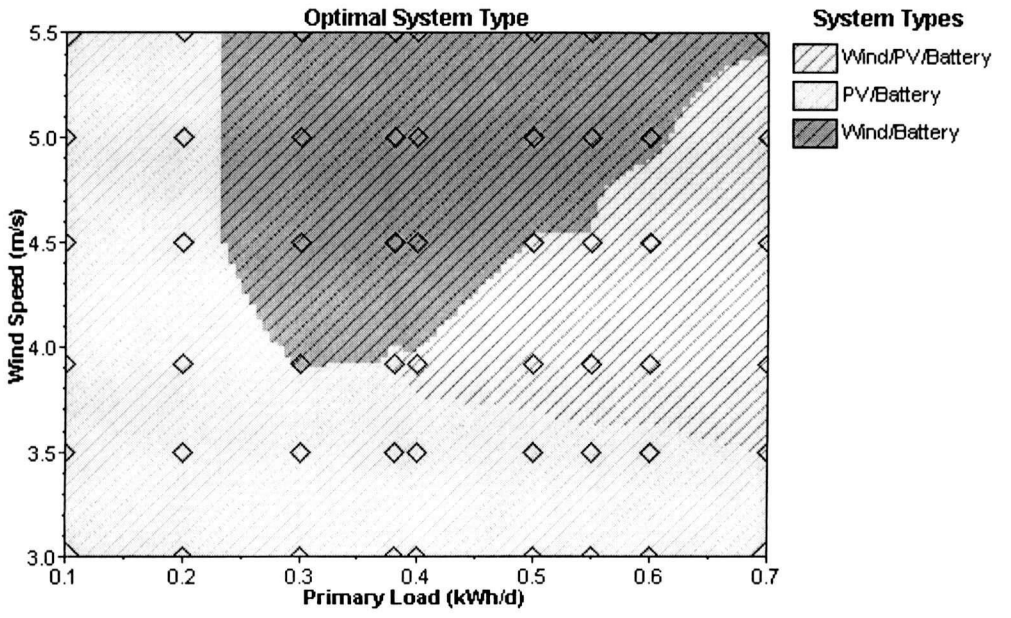

Figure 8.10: Sensitivity analysis of primary load with wind speed variation

8.6 Condition of Battery State of Charge

The stand – lone hybrid system relies on solar and wind energy as the primary power resources and it is backed up by the batteries. Lead – acid batteries used in hybrid solar – wind power generation systems operate under very specific conditions and it is often very difficult to predict when the energy will be extracted from or supplied to the battery. Several factors that affect the battery behaviors have being taken into account, such as the current rate, charging efficiency, the self – discharge rate, as well as the battery capacity. Battery state of charge (SOC) has being statistically analyzed by using HOMER optimizing software environment and the results have shown the battery working states in the wind – solar hybrid power generation system. Hybrid system optimal results shows the one 70 Ah lead – acid battery. Figure 8.11 shows the simulation results of 70 Ah lead – acid battery SOC conditions with wind solar hybrid system during one year period

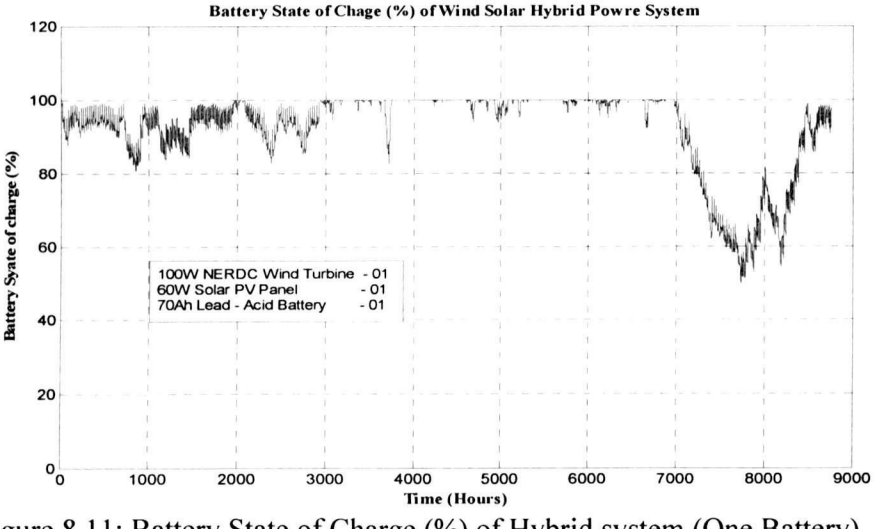

Figure 8.11: Battery State of Charge (%) of Hybrid system (One Battery)

When considering energy production of the hybrid system during one year period, May to October, six months, shows excess energy production. The excess energy absorb by means of additional battery bank is more efficient and the hybrid system was simulating with adding number of batteries with HOMER and simulation results as show in Figures 8.12 – 8.18.

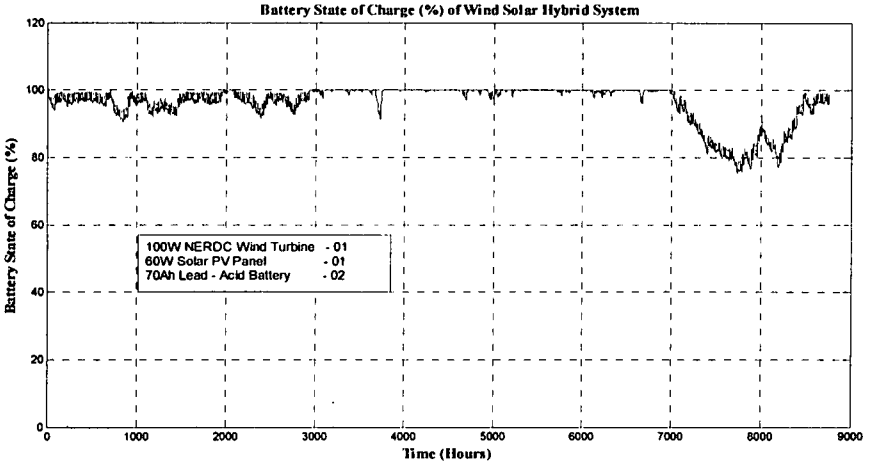

Figure 8.12: Battery State of Charge (%) of Hybrid system (Two Battery)

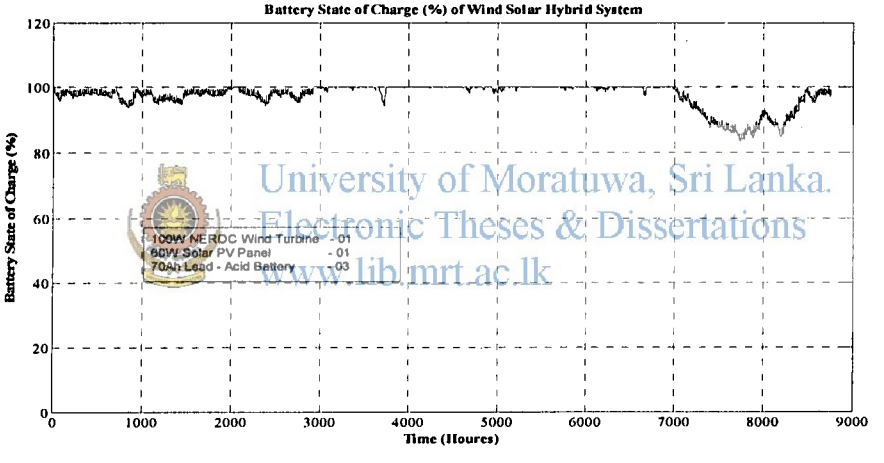

Figure 8.13: Battery State of Charge (%) of Hybrid system (Three Battery)

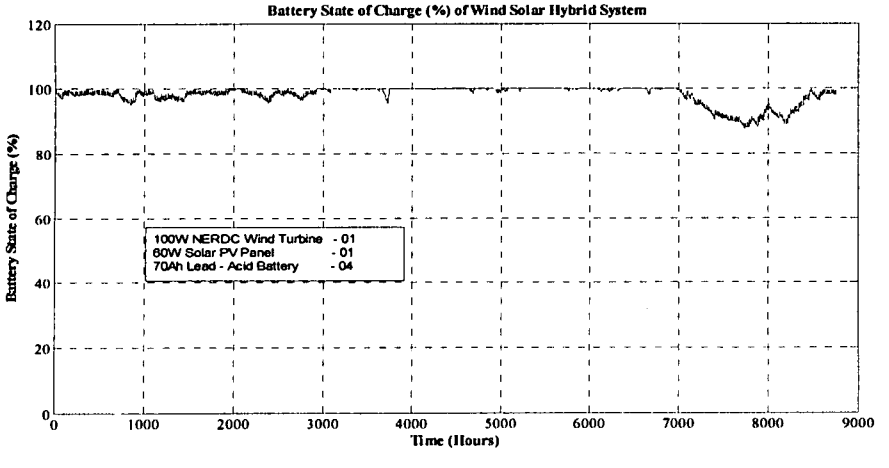

Figure 8.14: Battery State of Charge (%) of Hybrid system (Four Battery)

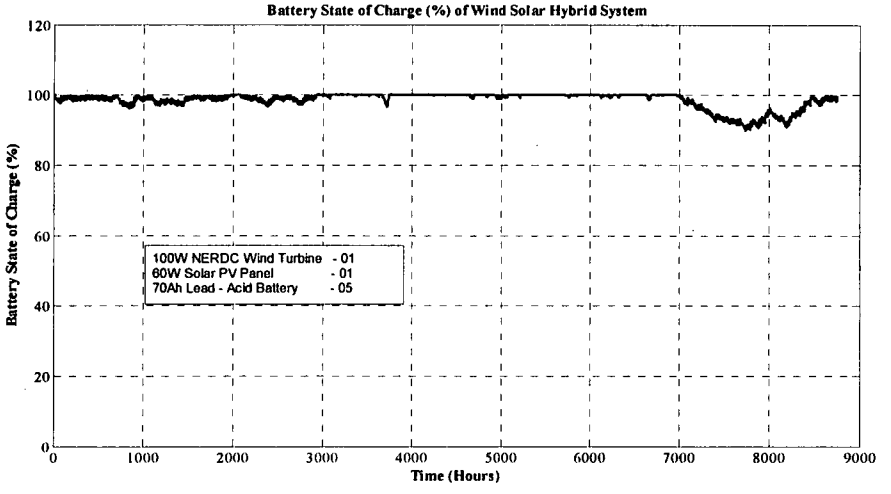

Figure 8.15: Battery State of Charge (%) of Hybrid system (Five Battery)

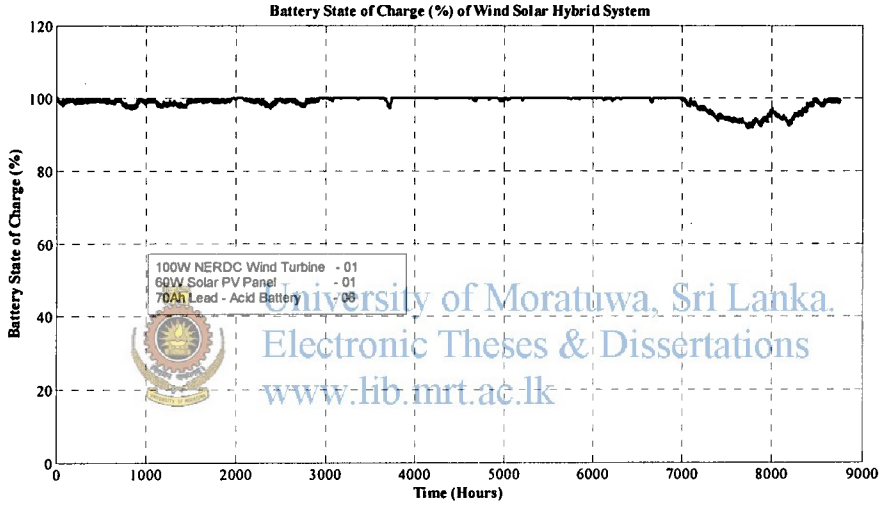

Figure 8.16: Battery State of Charge (%) of Hybrid system (Six Battery)

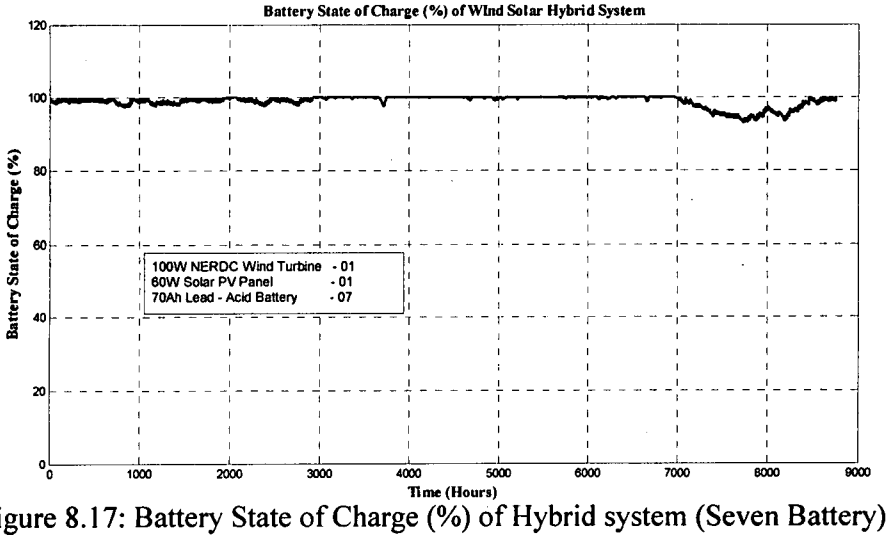

Figure 8.17: Battery State of Charge (%) of Hybrid system (Seven Battery)

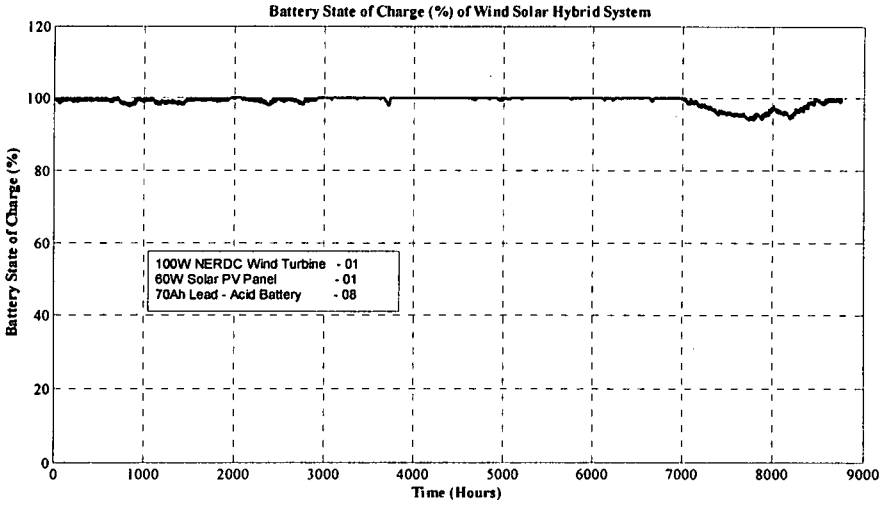

Figure 8.18: Battery State of Charge (%) of Hybrid system (Eight Battery)

The SOC behavior with one 70 Ah battery and the battery SOC level fluctuate rapidly. The main reason for this fluctuation is whether pattern distribution throughout the year. Six months of the year (May to October) show best battery SOC behavior close to the 100% and in this period it generates excess energy. For absorb this excess energy generate from the hybrid system extra 70 Ah batteries have to be added. Larger number of battery arrangement is not feasible with wind - solar hybrid home power systems. Installation cost and proper battery maintenance are the critical problems associated with rural home power battery charging wind solar hybrid systems [6] [5].

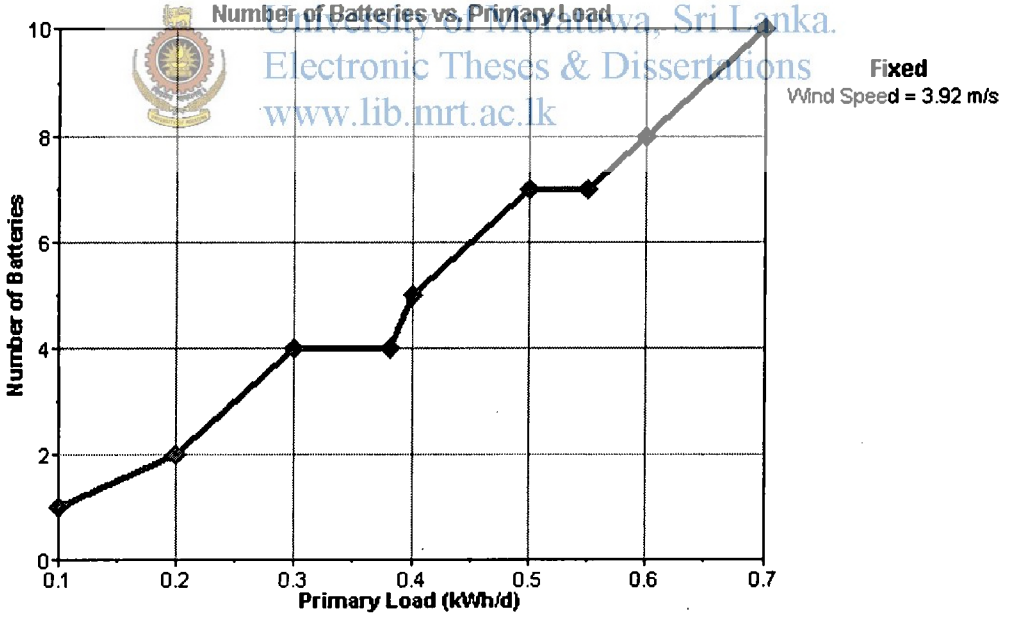

Figure 8.19: Number of Batteries Vs Primary load Characteristics plot

The primary load of the hybrid system is 0.382 kWh/d. According to the Figure 8.19 four number of 70 Ah battery bank is suitable for feeding required energy to the system. When considering the Figure 8. 14, battery SOC level is closed to the 100 % region minimizing fluctuation battery charging level.

Chapter 9

Results and Analysis

A case study was attempted at a place called Nikavaratiya ($7^0$44" 26.28"N 80^0 06" 53.79" E), in Kurunagala district, Sri Lanka. Four number of 100W wind turbines have being installed in Nikavaratiya area as wind home systems and these four locations were selected as best wind speed and feasible places. After commissioning the wind turbines the generated power was not enough to fulfill the electricity requirement of the house. Part of this study energy requirement for a rural house was evaluated and total electric net power requirement is around 264Wh/day. If average efficiency of electrical equipment is 69%, the daily gross electric energy requirement is 382Wh and monthly gross electric energy requirement is approximately 11.5 kWh for a rural house in Sri Lanka.

A 100W battery charging wind turbine can fulfill the electric requirement for about six month period of the year and the case of the other six month is lack of required wind speed (6 m/s) for due to monsoon wind Patten and direction changes. Therefore, in order to obtain maximum output power from the turbine, it is necessary to drive it at an optimal rotor speed for a particular wind speed. NERDC 100W wind turbine has being designed for variable wind conditions with constant pitch as a passive controlled machine and the variable – speed fixed approach is becoming more popular for low cost construction and is the most common scheme for small wind turbines. In this scheme, a MPPT control mechanism is used to control the restoring torque of the electrical generator for optimum operation of the wind turbine system.

A small wind turbine designed at the National Engineering Research & Development Centre (NERDC) in Sri Lanka was simulated in MATHLAB / Simulink using measured wind speed data in a turbulent wind conditions. Simulated results show that, system with Fuzzy Logic controller performs better than that with fixed voltage system. With the given wind speed data, energy output over 1000 s period is 1673.95 J with Fuzzy controller and 593.73 J with a fixed voltage controller. Figure 4.18 shows that 35% more energy can be generated by the system with a Fuzzy controller.

In this study it is used the perturb & observe (P&O) algorithm, also identified as the "hill climbing" method and it is very popular and the most frequently used in practice to searching MPPT because of its simplicity in algorithm and the ease of implementation for the PV power generation.

The MPPT algorithm was simulated with MATHLAB platform and Simulations use two sets of data on a sunny day, the irradiance level changes gradually since there is no influence of cloud. MPP tracking is supposed to be easy; algorithms locate and maintain the PV operating point very close to the MPPs without much difference in their performance. On a cloudy day, the irradiance level changes rapidly because of

passing clouds and MPP tracking is supposed to be challenging. In order to the better evaluation, total energy produced during a 12 – hour period is calculated. The simulation result shows the efficiency of 96.2% for the P & O algorithm.

Normally 70 Ah – 100Ah lead – acid batteries are used for wind solar hybrid system power generation. Develop and simulate with Simulink dynamic model for the 70Ah lead – acid and the laboratory testing have already being done according to the SLS 1126 test procedures. Main issues of using lead – acid batteries are identified as cyclic charging and discharging, overcharging of the battery and poor battery maintenance at site.

In the optimization process the HOMER has being used for simulation of Hybrid system. Base on the variety of design parameters such as PV size, wind turbine capacity and storage lead – acid battery capacity has being estimated. Annual average wind speed of 3.92 m/s and annual average solar potential is 5.44 kWh/m^2/day of year 2008 at Nikavaratiya 100W wind turbine site has being used for simulation study. Primary load scaled average of 0.382 kWh/day and annual DC primary electric load served is 139 kWh.
Simulation results show that the 100W NERDC wind turbine produce maximum Output 0.110kW and 0 kW as minimum power out put and 0.0405kW is average output. The capacity factor is 36.9% and total operation hours are 5,763 hr/yr. The 60W PV array produces Max. Output 0.0975kW and 0.000102 kW as minimum power out put and 0.296kW is average output. The capacity factor is 20.5% and total operation hours are 4,610 hr/yr.

The SOC behavior with one 70 Ah battery and the battery SOC level fluctuate rapidly. The main reason for this fluctuation is weather pattern distribute throughout the year. Six month of the year (May to October) shows best battery SOC behavior close to the 100% and this period generates excess energy. To absorb this excess energy generated the hybrid system was added extra 70 Ah batteries. Larger number of battery arrangements is not feasible with wind solar hybrid home power systems. Installation cost and proper battery maintenance are the critical problems associated with rural home power battery charging wind solar hybrid systems.

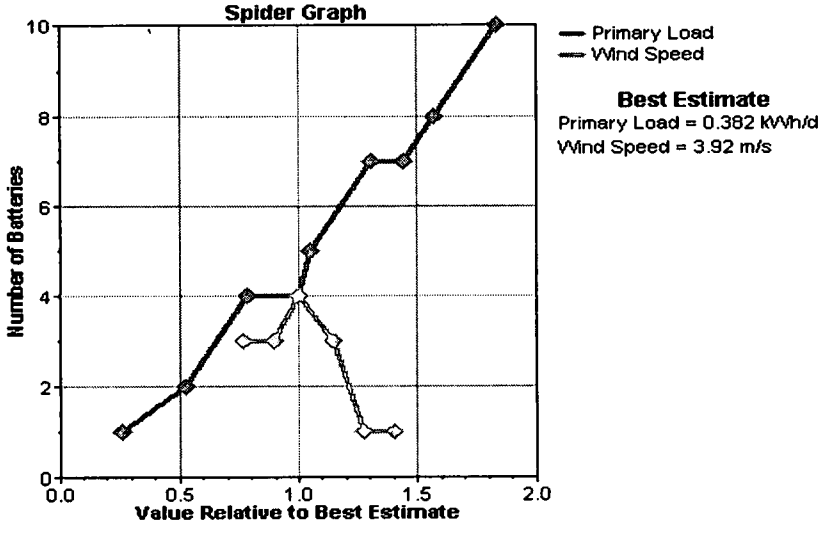

Figure 9.1 shows the relative best estimation results of the power system.

Figure 9.1 shows the relative best estimation result with number of batteries used in the hybrid system. A Hybrid system with four batteries can be utilized as shown in Figure 9.2 to get optimal solution for energy absorb from the system and maintain SOC level close to the 100 present. According to the analysis renewable energy requirement to fulfill the optimum system for energy demand of 400 Wh/day is as shown in Table 9.1.

Average Wind Speed	Optimum system
< 3.5 m/s	Solar Home System
3.5 m/s – 4.5 m/s	100W Wind turbine with Solar Hybrid system
> 4.5 m/s	100W Wind turbine

Table 9.1: Optimal Renewable Energy Requirement for Generate 400 Wh/day

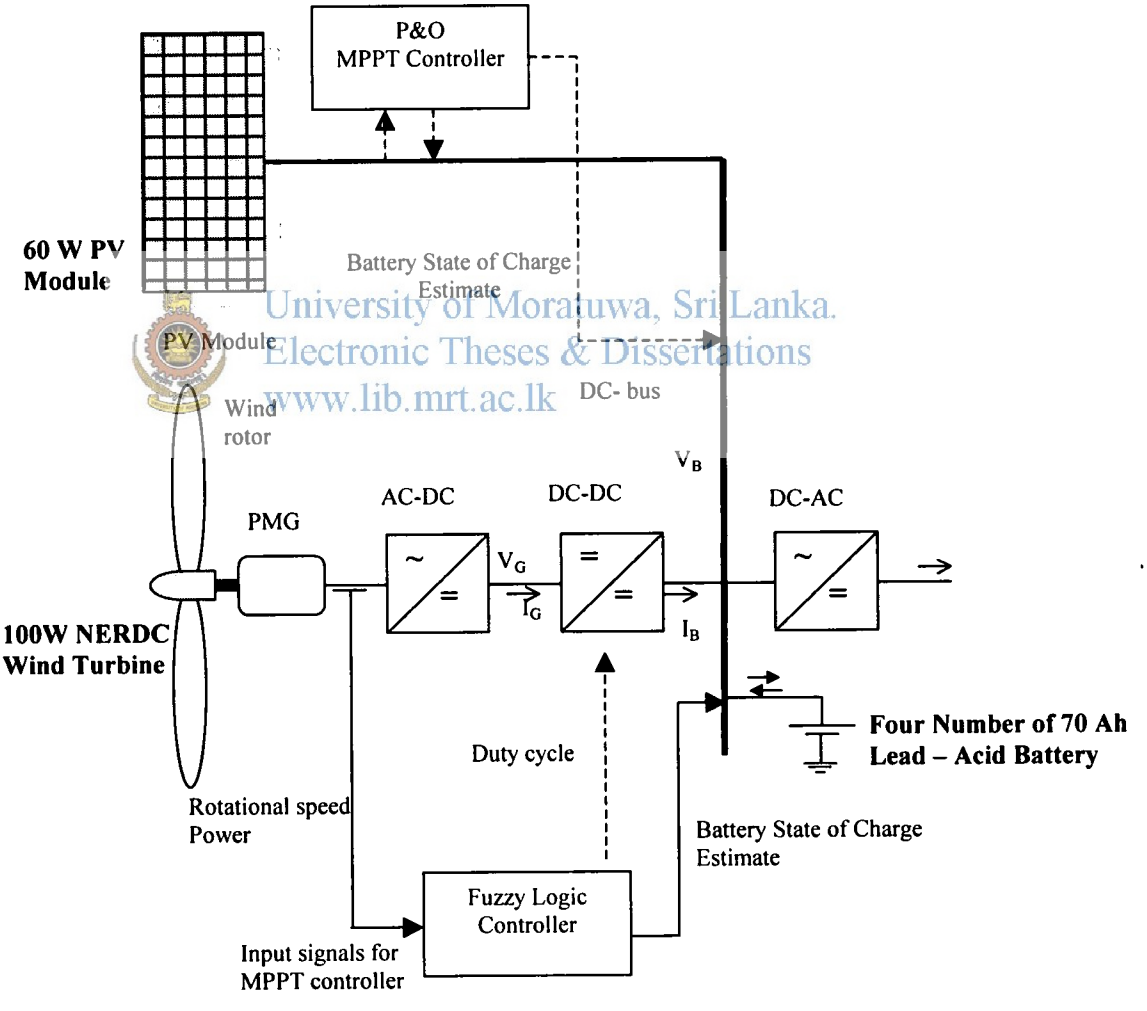

Figure 9.2: Shows the optimal power generation Hybrid architecture for Nikavaratiya 100W wind turbine generation site

Chapter 10

Conclusions

10.1 Summary

The critical issues due to weather changes and controlling of battery charging at a site conditions, of 100W NERDC wind turbines, as a stand – alone home power generation system, have being identified. Techniques that employ wind speed sensors are relatively expensive but they perform well with speed variations, particularly with the control systems of large-scale wind turbines. However, in practice it is difficult to measure wind speed accurately by an anemometer installed with the wind turbine, since the wind turbine experience different forces due to wake rotation.

Therefore, it is useful to enhance a sensor less control strategy for small wind turbine systems that operate without predetermined turbine characteristics. "Perturbation & observation searching method" operates without knowledge of system parameters. In this analysis, fuzzy logic based MPPT control system is introduced for small wind turbines. Fuzzy set and fuzzy rules were developed considering the qualitative and quantitative parameters of wind turbine outputs to track optimum operating points of the system. Research outcome shows that the proposed Fuzzy controller performs better than conventional controller.

This study has being done in a simple but efficient manner for photovoltaic power generation system. Each PV module component of the system is modeled and simulated using MATLAB software. The result shows that the PV model using the equivalent circuit in moderate complexity provides good matching with the real PV modules. Simulations perform for the P&O MPPT algorithms using actual irradiance data in the two different weather conditions, which are sunny day and cloudy day. The proposed P&O algorithm shows better performance of irradiation levels for both sunny day and cloudy day.

Automobile Lead – acid batteries are commonly used for wind solar hybrid systems due to low cost and availability. But deep cycle batteries are more suitable for hybrid power systems.

In the optimization process, the HOMER has being use for simulation of Hybrid system. Based on a variety of design parameters such as PV size, wind turbine capacity and storage lead – acid battery capacity has being estimated.

A MPPT controlling algorithm based wind solar hybrid system is essential to generate electricity with according to the weather changes.

10.2 Difficulties and Future Research

However, it is difficult to acquire optimum operating points from outputs of the wind turbine, as mechanically stored energy is interlaced with the aerodynamic power of wind rotor.
Correct modeling of the dynamic and non-linear systems is an important area of the study, but various difficulties remain in the current study. Some approaches of analysis are limited with use of commonly available simulation software. As an example of this study HOMER does not have the facility of optimized hybrid systems with MPPT algorithms.

Physical implementation of the system with power electronics remains for future research. It may involve implementation of a DSP or a microcontroller, a method of supplying power to the controller, signal conditioning circuits for A/D converters and a driving circuit. It may also involve performance analysis on the actual Hybrid system and comparisons with simulations.

10.3 Concluding Remarks

Issues of energy and global warming are the biggest challenges for the human kind in the 21st century. Energy is very important for everyone and in fact, taking control of the world's supply of oil is one of the most important challenges.

Especially, wind and PV have a powerful demand since it produces electric energy in an efficient manner as sustainable sources.

Finally, the author wishes that this thesis hand round the benefit to other students who are interested in power electronics for hybrid applications and provides encouragement towards more advanced sophisticated project or master's thesis research.

References

[1] Ackermann Thomas, Wind power in power system. John Wiley & Sons press;2005

[2] American wind Energy Association (AWEA). Roadmap: A 20- year industry plan for small wind turbine technology, American wind Energy Association ,122 C Street. NW, Site 380, Washington, DC 2001, June 2002,

[3] Armenta C. Prediction of battery behavior in SAPV applications. Renew Energy 2003; 28(11): 1671 – 84.

[4] Bansal, R.C., 2003. Bibliography on the Fuzzy set Theory applications in Power Systems (1994 – 2001)'', IEEE Trans. Energy Conversion , 18: 1291 – 1299.

[5] Berndt D. Maintenance – free batteries. England Willey;1994.

[6] Bogdon S.Borowy, Ziyad M. Salameh. 1996. Methodology for optimally sizing the combination of a battery bank and PV array in a wind-PV hybrid system. IEEE Transactions on energy conversion. 11(2): 367-375.

[7] Borowy BS, Salameh ZM. Methodology for optimally sizing the combination of a battery bank and PV array in a wind/PV hybrid system. IEEE Trans Energy Converse 1996;11(2):367–73.

[8] BP Solar BP SX150 - 150W Multi-crystalline Photovoltaic Module Datasheet, 2010

[9] Castañer, Luis & Santiago Silvestre Modelling Photovoltaic Systems, Using PSpice John Wiley & Sons Ltd, 2002

[10] Catherino HA, Burgel JF.et al. Modeling and simulation of lead – acid battery charging. J power sources 2001;96(1):113 – 20.

[11] Ceraolo, M., 2000. New dynamical models of lead–acid batteries. IEEE Trans. Power Syst. 15 (4), 1184–1190.

[12] Chan TF, Lai LL. An axial-flux permanent-magnet synchronous energy for a direct-coupled wind turbine system. IEEE Trans Energy Convers 2007; 22(1).

[13] Chapin, D. M., C. S. Fuller, & G. L. Pearson, Bell Telephone Laboratories, Inc., Murray Hill, New Jersey "A New Silicon p-n Junction Photocell for Converting Solar Radiation into Electrical Power" Journal of Applied Physics, Volume 25, Issue5, May 1954, page 676-677

[14] Copetti JB, Chenlo F, Lorenzo E. A general battery model for PV systemsimulation. Prog Photovoltaics Res Appl 1993;1:283–92

[15] Cox, E., Fuzzy fundamentals, IEEE Spectrum, vol. 29, pp. 58-61, October 1992.

[16] Dang, Thuy Lam A Digitally-controlled Power Tracker, Master's Thesis, California Polytechnic State University, Pomona, 1990

[17] D Le. Gourieres, 1982, Wind Power Plants Theory and Design, Oxford: Pergamon press, pp76-120.

[18] Dufo-López R, Bernal-Agustín JL. Design and control strategies of PV–diesel systems using genetic algorithms. Solar Energy 2005;79(1):33–46.

[19] Ekren O, Ekren BY, Ozerdem B. Break-evenanalysis and size optimization of a PV/wind hybrid energy conversion system with battery storage - A case study. Applied Energy; In Press, Corrected Proof.

[20] E. Koutroulis, K. Kalaitzakis, April 2006, "Design of a Maximum Power Tracking System for Wind- Energy-Conversion Application", IEEE Transaction on Industrial Electronics, Vol.53, No.2, pp486-494.

[21] Ellition,D. ,Schwartz, M., Scott,G., Haymes,S.,Heimiller, D., George, R., Wind Energy Resource Atlas of Sri Lanka and the Maldives, National Renewable Energy Laborotory USA.

[22] E. Muljadi, K. Pierce, P. Migliore, 2000, "Softcontrol control for variable-speed stall-regulated wind turbines", Wind Engineering, Vol.85, pp277-291.

[23] Francois Giraud and Zyiad M. Salmaeh.2001.Steady – state performance of a gri – connected rooftop hybrid wind – photovoltaic power system with battery storage. IEEE Transaction of energy conversion. Vol .16,pp.1-6.

[24] Green, Martin A. Solar Cells; Operating Principles, Technology, and System Applications Prentice Hall Inc., 1982

[25] Guash D, Silvester S. Dynamic battery model for photovoltaic applications. Prog photovoltaic Res Appl 2003;11:193 – 206.

[26] Hohm, D. P. & M. E. Ropp "Comparative Study of Maximum Power Point Tracking Algorithms" Progress in Photovoltaics: Research and Applications November 2002, page 47-62

[27] Hussein, K. H., I. Muta, T. Hoshino, & M. Osakada "Maximum Photovoltaic Power Tracking: an Algorithm for Rapidly Changing Atmospheric Conditions" IEE Proceedings – Generation, Transmission and Distribution – v. 142 January 1995, page 59-64

[28] Jossen, A., Garche, J., Sauer, D.U., 2004. Operation conditions of batteries in PV applications. Solar Energy 76, 759–769.

[29] Kellogg WD, et al. Generation unit sizing and cost analysis for standalone wind, photovoltaic and hybrid wind/PV systems. IEEE Trans Energy Convers 1998;13(1):70–5.

[30] Kerr MJ, Cuevas A, Generalized analysis of the illumination intensity Vs, open – circuit voltage of PV modules . Solar energy 2003; 76(1-3): 263 – 7.

[31] Khan MJ, Iqbal MT. Pre-feasibility study of stand-alone hybrid energy systems for applications in Newfoundland. Renew Energy 2005;30(6):835–54.

[32] Kim, S.C., Hong, W.H., 1999. Analysis of the discharge performance of a looded lead/acid cell using mathematical modeling. J. Power Sources 77, 74–82.

[33] K. Tan, S. Islam, June 2004, "Optimum Control Strategies in Energy Conversion of PMSG Wind Turbine System without Mechanical Sensors", IEEE Transaction on Energy Conversion Vol.19, No.2, pp392-399.

[34] Lavanya V, Gounden N Ammasai, Rao Polimera Malleswara. A simple controller using line commutated inverter with maximum power tracking for wind-driven grid-connected permanent magnet synchronous generators. In: Proceedings of IEEE PEDES; 2006. p. 1–6.

[35] Lee Dong-Yun, Noh Hyeong-Ju, Hyun Dong-Seok, Choy Ick. An improved MPPT converter using current compensation method for small scaled PV-applications. In: IEEE Conference, vol. 3; 2003. p. 540–45.

[36] Masters, Gilbert M. Renewable and Efficient Electric Power Systems John Wiley & Sons Ltd, 2004.

[37] Md. Arifujjaman, M. T. Iqbal, J. E. Quaice, 2008, "Energy capture by a small wind-energy conversion system", Applied Energy, Vol.85, pp41-51.

[38] Messenger, Roger & Jerry Ventre Photovoltaic Systems Engineering 2nd Edition CRC Press, 2003

[39] Mick Sagrllo, Apples & Oranges 02 Technical Appendix, Home Power magazine, URL: http://wwwhomepower.com

[40] Mohmoud MM. On the storage batteries used in solar electric power systems and development of an algorithm for determining their ampere–hour capacity. Electric Power Syst Res 2004;71(1):85–9.

[41] Mohanlal Kolhe, Sunita Kolhe and Joshi J.C. 2003. Economic viability of stand-alone solar photovoltaic system in comparison with diesel-powered system for India. Energy economics. Vol. 24, pp.155-165.

[42] Muselli M, Notton G, Poggi P, Louche A. PV-hybrid power systems sizing incorporating battery storage: an analysis via simulation calculations. Renew Energy 2000;20(1):1–7.

[43] Narayana M, Putrus G, Jovanovic M , Leune P. Maximum power tracking for variable speed fixed pitch small wind turbines. Prague, 8-11 June 2009, p.0542.

[44] Ong Chee Mun. Modeling and dynamic simulation of electric machinery using Matlab/Simulink. Prentice Hall Press; 1998.

[45] Piller S. Perrn M. Jossen A. Methods for state – of – charge determination and their applications. Power sources 2001;96(1):113-20.

[46] Radziemska E, Klugmann E. Thermally affected parameters of the current–voltage characteristics of silicon photocell. Energy Convers Manage 2002;43(14):1889–900.

[47] Salameh ZM, Cassacca MA, Lynch WA. A mathematical model for lead–acid batteries. IEEE Trans Energy 1992;7(1):93–7.

[48] Simoes MG, Bose BK, Spiegel RJ. Fuzzy logic based intelligent control of a variable speed cage machine wind generation system. IEEE Trans Power Electron 1997;12(1):87–95.

[49] S. Morimoto, H. Nakayama, M. Sanada, Jan/Fab 2005, Sensorless output maximization control for variable-speedwind generation systemusing IPMSG, IEE transaction on industrial applications, Vol.41, No.1, pp60-67.

[50] Tan K, Islam S. Optimum control strategies in energy conversion of PMSG wind turbine system without mechanical sensors. IEEE Trans Energy Convers 2004;19(2):392–9.

[51] T. Tanaka, T. Toumiya, 1997, "Output control by hillclimbing method for a small scale wind power generation system", Renewable Energy,Vol.12,No.4, pp387-400.

[52] Tina G, Gagliano S, Raiti S. Hybrid solar/wind power system probabilistic modeling for long term performance assessment. Solar Energy 2006;80: 578–88.

[53] Tsai, Huan.-Liang, Tu, Ci.-Siang, Su, Yi.-Jie, 2008. Development of generalized photovoltaic model using MATLAB/SIMULINK. Proceedings of the World Congress on Engineering and Computer Science 2008. San Francisco, USA, pp. 846–851.

[54] T. Esram, P.L. Chapman, Comparison of photovoltaic array maximum power point tracking techniques, IEEE Transactions on Energy Conversion 22 (June (2)) (2007)

[55] Xinyan Zhang, Xiaobo Zhang, Peiyi Zhou, Jing Cheng, Ye Liu. Fuzzy control used in variable speed wind turbine. In: International conference on automation and logistics; 2009. p. 1194–8.

[56] Yang HX,Lu L, Zho W.A novel optimization sizing model for hybrid solar – wind power generation system. Solar energy 2007;81(1): 76-84

[57] Zadeh LA. A fuzzy-set-theoretic interpretation of linguistic hedges. Cybernet 1972;2:4–34.

[58] Zoulias EI, Lymberopoulos N. Techno-economic analysis of the integration of hydrogen energy technologies in renewable energy based stand-alone power systems. Renew Energy 2007;32(4):680–96.

APPENDIX – A : Analysis of C_{pr} Values for Each Blade Elements

A.1 C^{++} Computer program and Script

A.1.1 C^{++} Computer program for evaluate values of C_{pr} in NACA4415 Wind Rotor

This C^{++} program was developed to evaluate the values of C_{pr} (Chapter 2) for each elements in NACA 4415 wind rotor used in NERDC wind turbines.

```
#include<stdio.h>
#include<math.h>
main()
{
int j;
float sCp,Cp,sCm,Cm,Cf,sCf,R,r1,r2,b,lamda;
float chord[10],angle_beta[10],r[10],lamdao[10];
double cl,cd,h,k,G,E,eta,alpha,phi,phi1;
printf(" Radious of Wind Rotor mm =");
scanf("%f",&R);
printf("No. of blades b=");
scanf("%f",&b);
printf("No. of segment of blade=9\n");
printf("Give the width of the segment delta.r in mm=");
scanf("%f",&r2);
printf("Radious to the first segment r1 mm =");
scanf("%f",&r1);
for(j=1;j<=9;++j)
{
printf(" Chord lenth at r=%0.0f C=",r1);
scanf("%f",&chord[j]);
printf("Blade angle beta =");
scanf("%f",&angle_beta[j]);
r[j]=r1;
r1=r1+r2;
}
printf(" No.  Radious(mm)  Chord lenth(mm)  Blade Angle(degree)\n" );
printf("-----------------------------------------------------\n");
for(j=1;j<=9;++j)
printf("%d   %0.0f    %0.3f       %0.3f \n",j,r[j],chord[j],angle_beta[j]);

printf("\n Tip speed ratio=");
scanf("%f",&lamdao);
Cp=0;
Cm=0;
for (j=1;j<=9;++j)
{
alpha=-20;
 do
 {
  phi=alpha+angle_beta[j];
  phi1=phi*3.1415927/180;

/*calculation of Cl values with respect alpha angle*/
  if (alpha<-8)
  cl=-0.00017*pow(alpha,3)+0.002431*pow(alpha,2)+0.201389*alpha+0.966667;
  if(alpha>=-8 && alpha<=8)
```

```
cl=0.1*alpha+0.4;
if (alpha>8 && alpha<=15)
cl=-0.00021*pow(alpha,4)+0.009645*pow(alpha,3)-0.16968*pow(alpha,2)+1.354548*alpha-2.94;
if (alpha>15 && alpha<=24)
cl=-6.9e-6*pow(alpha,3)-0.00115*pow(alpha,2)+0.010528*alpha+1.703333;
/*Calculation of Cd values with respect Cl values*/
if (cl>=-0.95 && cl<=0.8)
cd=-2.70563e-05*pow(cl,3)+0.002625812*pow(cl,2)-0.001870671*cl+0.00682987;
if(cl>0.8 && cl<=1.6)
cd=-0.034722222*pow(cl,4)+0.15625*pow(cl,3)-0.243055556*pow(cl,2)+0.16375*cl-0.034222222;

eta=atan(cd/cl);
G=(cl*b*chord[j]*cos(phi1-eta))/(8*3.141592654*r[j]*cos(eta)*sin(phi1)*sin(phi1));
E=(cl*b*chord[j]*sin(phi1-eta))/(4*3.141592654*r[j]*sin(2*phi1)*cos(eta));

k=(1-G)/(1+G);
h=(1+E)/(1-E);
lamda=(R/r[j])*((1+k)/(1+h))/tan(phi1);
alpha=alpha+0.0001;

 }
while ((alpha<=24) && (((lamda-lamdao[j])>0.1) || ((lamda-lamdao[j])<-0.1) || (k<0) || (h<1) ||(k>1) ||
(h>2)));
sCp=r[j]*r2*pow((lamdao[j]*(r[j]/R)),2)*(1+k)*(h-1);
Cp=sCp+Cp;
sCm=(lamdao[j]*r[j]/R)*(1+k)*(h-1)*pow(r[j],2)*r2;
Cm=sCm+Cm;
sCf=r[j]*r2*(1-k*k);
Cf=sCf+Cf;
if ((lamda-lamdao[j])>0.1 || (lamda-lamdao[j])<-0.1 )
printf("\n r=%0.0f Error  Can't calculate lamda with given alpha range",r[j]);
 else
 printf("\n r=%0.0f alpha=%0.3f h=%0.3f k=%0.3f Cpr= %0.4f  Cmr=%0.4f Cfr=%0.4f",r[j],alpha-
0.0001,h,k,(pow((lamdao[j]*
(r[j]/R)),2)*(1+k)*(h-1)),(lamdao[j]*(r[j]/R)*(1+k)*(h-1)),(1-k*k));

        }
 printf("\n\n Tip speed ratio=%0.3f Cp =%f  Cm=%f
Cf=%f\n",lamdao[j],((2/(R*R))*Cp),((2/pow(R,3))*Cm),((2/(R*R))*Cf));
     return(0)
        }
```

APPENDIX – B: Analysis Characteristics of Solar PV Module

B.1 MATHLAB Functions and Script

B.1.1 MATHLAB Function for Modeling BP SX 150 PV Module

This MATHLAB function (bp_sx 150s) is to simulate with the current – voltage relationship of BP SX150S PV module and used in simulations throughout of this study.

```
function Ia = bp_sx150s(Va,G,TaC)
% function bp_sx150s.m models the BP SX 150S PV module
% calculates module current under given voltage, irradiance and
temperature
% Ia = bp_sx150s(Va,G,T)
%
% Out: Ia = Module operating current (A), vector or scalar
% In: Va = Module operating voltage (V), vector or scalar
% G = Irradiance (1G = 1000 W/m^2), scalar
% TaC = Module temperature in deg C, scalar

%////////////////////////////////////////////////////////////////////
////////
% Define constants
k = 1.381e-23; % Boltzmann's constant
q = 1.602e-19; % Electron charge
% Following constants are taken from the datasheet of PV module and
% curve fitting of I-V character (Use data for 1000W/m^2)
n = 1.62; % Diode ideality factor (n),
% 1 (ideal diode) < n < 2
Eg = 1.12; % Band gap energy; 1.12eV (Si), 1.42 (GaAs),
% 1.5 (CdTe), 1.75 (amorphous Si)
Ns = 72; % # of series connected cells (BP SX150s, 72 cells)
TrK = 298; % Reference temperature (25C) in Kelvin
Voc_TrK = 43.5 /Ns; % Voc (open circuit voltage per cell) @ temp TrK
Isc_TrK = 4.75; % Isc (short circuit current per cell) @ temp TrK
a = 0.65e-3; % Temperature coefficient of Isc (0.065%/C)
% Define variables
TaK = 273 + TaC; % Module temperature in Kelvin
Vc = Va / Ns; % Cell voltage
% Calculate short-circuit current for TaK
Isc = Isc_TrK * (1 + (a * (TaK - TrK)));
% Calculate photon generated current @ given irradiance
Iph = G * Isc;
% Define thermal potential (Vt) at temp TrK
Vt_TrK = n * k * TrK / q;
% Define b = Eg * q/(n*k);
b = Eg * q /(n * k);
% Calculate reverse saturation current for given temperature
Ir_TrK = Isc_TrK / (exp(Voc_TrK / Vt_TrK) -1);
Ir = Ir_TrK * (TaK / TrK)^(3/n) * exp(-b * (1 / TaK -1 / TrK));
% Calculate series resistance per cell (Rs = 5.1mOhm)
dVdI_Voc = -1.0/Ns; % Take dV/dI @ Voc from I-V curve of datasheet
Xv = Ir_TrK / Vt_TrK * exp(Voc_TrK / Vt_TrK);
Rs = - dVdI_Voc - 1/Xv;
% Define thermal potential (Vt) at temp Ta
Vt_Ta = n * k * TaK / q;
% Ia = Iph - Ir * (exp((Vc + Ia * Rs) / Vt_Ta) -1)
% f(Ia) = Iph - Ia - Ir * ( exp((Vc + Ia * Rs) / Vt_Ta) -1) = 0
% Solve for Ia by Newton's method: Ia2 = Ia1 - f(Ia1)/f'(Ia1)
```

```
Ia=zeros(size(Vc)); % Initialize Ia with zeros
% Perform 5 iterations
for j=1:5;
Ia = Ia - (Iph - Ia - Ir .* ( exp((Vc + Ia .* Rs) ./ Vt_Ta) -1))...
./ (-1 - Ir * (Rs ./ Vt_Ta) .* exp((Vc + Ia .* Rs) ./ Vt_Ta));
End
```

B.1.2 MATLAB Script to Draw PV, I-V Graphs

The following MATLAB script is used for Figure 2-12 to draw the *I-V* characteristics of various module temperatures. Other plots showing PV characteristics are done in similar ways using MATLAB environment.

```
% plot_iv_temp.m - Script file to draw i-v curves of pv module
% with variable temp (0C, 25C, 50C, 75C)

%////////////////////////////////////////////////////////////////
clear;
% Define constant
G = 1;
% Functions to plot
figure
hold on
for TaC=0:25:75
Va = linspace (0, 48-TaC/8, 200);
Ia = bp_sx150s(Va, G, TaC);
plot(Va, Ia)
end
title('BP SX 150S Photovoltaic Module I-V Curve')
xlabel('Module Voltage (V)')
ylabel('Module Current (A)')
axis([0 50 0 5])
gtext('0C')
gtext('25C')
gtext('50C')
gtext('75C')
hold off
```


B.1.3 MATLAB Function to Find the MPP

This MATLAB function is to find the power, voltage, and current at the MPP of BP SX 150S PV module under the given irradiance and module temperature.

```
function [Pa_max, Imp, Vmp] = find_mpp(G, TaC)
% find_mpp: function to find a maximum power point of pv module
% [Pa_max, Imp, Vmp] = find_mpp(G, TaC)
% in: G (irradiance, KW/m^2), TaC (temp, deg C)
% out: Pa_max (maximum power), Imp, Vmp

%////////////////////////////////////////////////////////////////
% Define variables and initialize
Va = 12;
Pa_max = 0;
% Start process
while Va < 48-TaC/8
Ia = bp_sx150s(Va,G,TaC);
Pa_new = Ia * Va;
if Pa_new > Pa_max
Pa_max = Pa_new;
```

```
Imp = Ia;
Vmp = Va;
end
Va = Va + .005;
end
```

B.1.4 MATLAB Script for P&O Algorithm

This MATLAB script is to test the P&O algorithm under the sunny weather condition in chapter 6 and Figure 6.9.

```
clear;
% Define constants
TaC = 25; % Cell temperature (deg C)
C = 0.5; % Step size for ref voltage change (V)
% Define variables with initial conditions
G = 0.028; % Irradiance (1G = 1000W/m^2)
Va = 24.0; % PV voltage
Ia = bp_sx150s(Va,G,TaC); % PV current
Pa = Va * Ia; % PV output power
Vref_new = Va + C; % New reference voltage
% Set up arrays storing data for plots
Va_array = [];
Pa_array = [];
% Load irradiance data
load irrad; % Irradiance data of a sunny day
x = irrad(:,1)'; % Read time data (second)
y = irrad(:,2)'; % Read irradiance data
xi = 15.4e+3:230.6e+3; % Set points for interpolation
yi = interp1(x,y,xi,'cubic'); % Do cubic interpolation
% Take 43200 samples (12 hours)
for Sample = 1:43.2e+3
   % Read irradiance value
G = yi(Sample);
% Take new measurements
Va_new = Vref_new;
Ia_new = bp_sx150s(Vref_new,G,TaC);
% Calculate new Pa
Pa_new = Va_new * Ia_new;
deltaPa = Pa_new - Pa;
% P&O Algorithm starts here
if deltaPa > 0
if Va_new > Va
Vref_new = Va_new + C; % Increase Vref
else
Vref_new = Va_new - C; % Decrease Vref
end
elseif deltaPa < 0
if Va_new > Va
Vref_new = Va_new - C; % Decrease Vref
else
Vref_new = Va_new + C; %Increase Vref
end
else
Vref_new = Va_new; % No change
end
% Update history
Va = Va_new;
Pa = Pa_new;
% Store data in arrays for pl
```

```
Va_array = [Va_array Va];
Pa_array = [Pa_array Pa];
end
% Plot result
figure
plot (Va_array, Pa_array, 'g')
% Overlay with P-I curves and MPP
Va = linspace (0, 45, 200);
hold on
for G=.2:.2:1
Ia = bp_sx150s(Va, G, TaC);
Pa = Ia.*Va;
plot(Va, Pa)
[Pa_max, Imp, Vmp] = find_mpp(G, TaC);
plot(Vmp, Pa_max, 'r*')
end
title('P&O Algorithm')
xlabel('Module Voltage (V)')
ylabel('Module Output Power (W)')
axis([0 50 0 160])
%gtext('1000W/m^2')
%gtext('800W/m^2')
%gtext('600W/m^2')
%gtext('400W/m^2')
%gtext('200W/m^2')
hold off
```

This MATLAB script is to test the P&O algorithm under the sunny weather condition in chapter 6 and Figure 6.10.


```
clear;
% Define constants
TaC = 25; % Cell temperature (deg C)
C = 0.5; % Step size for ref voltage change (V)
% Define variables with initial conditions
G = 0.028; % Irradiance (1G = 1000W/m^2)
Va = 24.0; % PV voltage
Ia = bp_sx150s(Va,G,TaC); % PV current
Pa = Va * Ia; % PV output power
Vref_new = Va + C; % New reference voltage
% Set up arrays storing data for plots
Va_array = [];
Pa_array = [];
% Load irradiance data
load cloud; % Irradiance data of a sunny day
X = cloud(:,1)'; % Read time data (second)
Y = cloud(:,2)'; % Read irradiance data
Xi = 19.8e+3: 450e+3; % Set points for interpolation
Yi = interp1(X,Y,Xi,'cubic'); % Do cubic interpolation
% Take 43200 samples (12 hours)
for Sample = 1:43.2e+3
   % Read irradiance value
G = Yi(Sample);
% Take new measurements
Va_new = Vref_new;
Ia_new = bp_sx150s(Vref_new,G,TaC);
% Calculate new Pa
Pa_new = Va_new * Ia_new;
deltaPa = Pa_new - Pa;
% P&O Algorithm starts here
```

```
if deltaPa > 0
if Va_new > Va
Vref_new = Va_new + C; % Increase Vref
else
Vref_new = Va_new - C; % Decrease Vref
end
elseif deltaPa < 0
if Va_new > Va
Vref_new = Va_new - C; % Decrease Vref
else
Vref_new = Va_new + C; %Increase Vref
end
else
Vref_new = Va_new; % No change
end
% Update history
Va = Va_new;
Pa = Pa_new;
% Store data in arrays for pl
Va_array = [Va_array Va];
Pa_array = [Pa_array Pa];
end
% Plot result
figure
plot (Va_array, Pa_array, 'g')
% Overlay with P-I curves and MPP
Va = linspace (0, 45, 200);
hold on
for G=.2:.2:1
Ia = bp_sx150s(Va, G, TaC);
Pa = Ia.*Va;
plot(Va, Pa)
[Pa_max, Imp, Vmp] = find_mpp(G, TaC);
plot(Vmp, Pa_max, 'r*')
end
title('P&O Algorithm')
xlabel('Module Voltage (V)')
ylabel('Module Output Power (W)')
axis([0 50 0 150])
%gtext('1000W/m^2')
%gtext('800W/m^2')
%gtext('600W/m^2')
%gtext('400W/m^2')
%gtext('200W/m^2')
hold off
```